

Force Modeling for Oblique Cutting on Non-Planar Surfaces

Submitted in partial fulfillment of the requirements of the degree of
Bachelor & Master of Technology

by

Ayush Bandil (12D100033)

Under the guidance of

Prof. Anirban Guha

&

Prof. Asim Tewari



Department of Mechanical Engineering

INDIAN INSTITUTE OF TECHNOLOGY BOMBAY

(2017)

REPORT APPROVAL SHEET

This report entitled as "**Force Modeling for Oblique Cutting on Non-Planar Surfaces**" by **Ayush Bandil** (12D100033) has been approved as a DDP Phase II submission

Supervisors

Prof. Anirban Guha

Anirban Guha

Prof. Asim Tewari

Asim Tewari

Internal Examiners

Prof. S. S. Joshi

S. S. Joshi
22.06.17

Prof. Sushil Mishra

Sushil Mishra

External Examiner

Prof. Prita Pant

Prita Pant

DECLARATION

I declare that this written submission represents my ideas in my own words and where others ideas or words have been used, I have adequately cited, quoted and referenced the original sources. I also declare that I have adhered to all principles of academic honesty and integrity and have not misrepresented or fabricated or falsified any idea/data/fact/source in my submission. I understand that any violation of any of the above will be cause for disciplinary action by the Institute and also evoke penal action from the sources which have thus not been properly cited or from whom proper permission has not been taken when needed



Ayush
22/6/18

Date:

Ayush Bandil

Roll No. 12D100033

ACKNOWLEDGEMENT

I would like to gratefully acknowledge the support provided for this work by National Centre for Aerospace Innovation and Research (NCAIR) at Indian Institute of Technology Bombay (IIT Bombay), a Department of Science and Technology - Government of India, The Boeing Company and IIT Bombay collaboration. I would also like to express my gratitude to my guide Prof. Anirban Guha and co-guide Prof. Asim Tewari for their constant support and guidance.

ABSTRACT

Precision machining is one of the most important and widely used manufacturing processes these days. A very tight tolerance limit over free form surfaces is required in some industries like aerospace and defense. This can be achieved by introducing two more degrees of freedom (the lead and tilt angles) to the conventional 3-axis milling process in order to reduce cutting forces. This report focuses on the development of a methodology to predict cutting forces and the torque generated during multi-axis generic profile milling processes. This report focuses on development of three different models. The first model is developed assuming a planar workpiece and a ball-end cutting tool having only horizontal feed of tool. The second model is developed for ball-end mill on planar surfaces having vertical feed along with the horizontal feed. Finally, the third model is for general milling having cutting edge wrapped around the tool envelope. Later the third model is extended to incorporate different kinds of workpiece profiles. All these models are based on the mechanistic approach in which basic orthogonal cutting parameters of the shear-zone are determined by using a regression curve fitting of several experimental results. The Orthogonal Cutting Database (OCD), which converts orthogonal cutting parameters to oblique cutting parameters is developed for Titanium alloy. The methodology follows a modular approach to model the forces. The tool surface is discretized into smaller elements first and then the forces are calculated considering each element undergoing the orthogonal cutting process. The elemental forces are added up to give the net force experienced by the cutting tool. To validate the results, the results are benchmarked against data in published literature. The maximum force is calculated using the given values of lead and tilt angles. Furthermore, lead and tilt angles are determined to minimize the maximum cutting force at any angular position of the tool. These lead and tilt angles will result in the most precise machining process. The model can be further used for selection of other machining parameters and several aspects of machining processes from tool-geometry design which will reduce the cutting forces and torque on the cutting tool.

Table of Contents

<i>DECLARATION</i>	<i>ii</i>
<i>ACKNOWLEDGEMENT</i>	<i>iii</i>
<i>ABSTRACT</i>	<i>iv</i>
<i>List of Figures</i>	<i>viii</i>
<i>List of Symbols</i>	<i>xi</i>
<i>INTRODUCTION</i>	1
1.1 <i>Introduction</i>	1
1.2 <i>Motivation</i>	2
1.3 <i>Project Objectives and Scope</i>	3
<i>LITERATURE REVIEW</i>	5
2.1 <i>Coordinate Systems</i>	5
2.2 <i>Declaration of the Tool Envelope</i>	5
2.2.1 <i>Case 1: Ball-End Geometry [2]</i>	5
2.2.1.1 <i>Cutting Edge Parameters [2]</i>	6
2.2.2 <i>Case 2: General Milling Tool Geometry [12]</i>	8
2.3 <i>Chip Dimensions [7]</i>	12
2.3.1 <i>Chip Thickness</i>	12
2.3.2 <i>Chip Width</i>	13
2.3.3 <i>Chip Length</i>	13
2.4 <i>Force Coefficients [3]</i>	14
2.4.1 <i>Edge Force Coefficients</i>	14
2.4.2 <i>Cutting Force Coefficients</i>	14
2.4.2.1 <i>Orthogonal Cutting Database</i>	15
2.4.2.2 <i>Oblique Cutting</i>	15
2.5 <i>Force Equation</i>	16
2.5.1 <i>Force Transformation to TCS</i>	16
2.5.2 <i>Force Transformation to FCN</i>	18
<i>MODEL DEVELOPMENT</i>	19
3.1 <i>Calculation Overview</i>	19
i. <i>Declaration of the Tool Envelope</i>	19
ii. <i>Discretization of Surface Points</i>	19

iii.	<i>Determination of the Engagement Region</i>	19
iv.	<i>Defining chip dimensions</i>	20
v.	<i>Calculation of force</i>	20
vi.	<i>Determination of Optimal Value of Lead and Tilt Angles</i>	21
3.2	<i>Different Types of Models</i>	21
3.2.1	<i>Model 1: Ball-End Mill Cutting Planar Surface having only Horizontal Feed</i>	22
3.2.1.1	<i>Discretization of tool geometry</i>	22
3.2.1.2	<i>Determination of the Engagement Region</i>	23
3.2.1.3	<i>Model Assumptions and Limitations</i>	25
3.2.2	<i>Model 2: Ball-End Mill Cutting Planar Surface</i>	25
3.2.2.1	<i>Determination of Engagement region</i>	26
3.2.2.2	<i>Defining Chip Dimensions</i>	28
3.2.3	<i>Model 3: General Milling Tool Cutting Planar Surface</i>	29
3.2.3.1	<i>Constraints of surface parameters</i>	29
3.2.3.2	<i>Discretization of the Surface Points</i>	31
3.2.3.3	<i>Determination of the engagement region</i>	32
3.2.3.4	<i>Defining chip dimensions</i>	33
3.3	<i>Determination of engagement region for non-planar surfaces</i>	34
3.3.1	<i>Slope</i>	34
3.3.1.1	<i>Case 1: Tool is going inside the slope</i>	34
3.3.1.2	<i>Case 2: Tool is moving parallel to the slope</i>	35
3.3.2	<i>Edge</i>	35
3.3.3	<i>Step</i>	36
3.3.4	<i>Corner</i>	36
3.3.5	<i>User Defined Surface</i>	37
3.4	<i>Step Over and Surface Roughness</i>	37
	RESULTS AND VALIDATION.....	40
4.1	<i>Results Based on Model 1</i>	40
4.1.1	<i>Case 1: Force Simulation for $N_f = 1$, lead = tilt = 0</i>	40
4.1.2	<i>Case 2: Force Simulation for $N_f = 2$, lead = 300, tilt = 300</i>	41
4.1.3	<i>Case 3: Force Simulation for $N_f = 2$, lead = 150, tilt = 00</i>	43
4.1.4	<i>Case 4: Force Simulation for $N_f = 3$, lead = 200, tilt = 100</i>	44
4.1.5	<i>Case 5: Lead and Tilt optimization for $N_f = 2$, depth of cut = 2.5mm</i>	47
4.1.6	<i>Case 6: Lead and Tilt optimization for $N_f = 2$, depth of cut = 5mm</i>	47

4.1.7	<i>Reason for Abruptness in Plots.....</i>	48
4.2	<i>Results Based on Model 2.....</i>	50
4.2.1	<i>Case 1: depth of cut = 10mm, feed = -100k mm/min.....</i>	50
4.2.2	<i>Case 2: depth of cut = 0mm, feed = -100k mm/min</i>	52
4.2.3	<i>Case 3: depth of cut = 0mm, feed = 100i – 100k mm/min</i>	54
4.3	<i>Results Based on Model 3.....</i>	56
4.3.1	<i>Case 1: Tool → Cylindrical End Mill.....</i>	56
4.3.2	<i>Case 2: Tool → Bull Nose End Mill.....</i>	58
4.3.3	<i>Case 3: Tool → Taper End Mill.....</i>	59
4.3.4	<i>Case 4: Tool → Taper Ball End Mill.....</i>	61
4.3.5	<i>Case 5: Tool → General End Mill</i>	62
4.3.6	<i>Case 6: Tool → Cone End Mill.....</i>	64
4.3.7	<i>Case 7: Tool → Rounded End Mill.....</i>	65
4.3.8	<i>Case 8: Tool → Inverted Cone End Mill.....</i>	67
4.3.9	<i>Case 9: Surface → Slope, Tool is Moving Inside the Slope.....</i>	68
4.3.10	<i>Case 10: Surface → Slope, Tool is Moving Parallel the Slope.....</i>	70
4.3.11	<i>Case 11: Surface → Edge.....</i>	72
4.3.12	<i>Case 12: Surface → Step.....</i>	73
4.3.13	<i>Case 13: Surface → Corner</i>	75
4.3.14	<i>Case 14: Surface → Custom Surface.....</i>	77
4.3.15	<i>Case 15: Following Cut, Step Over =10, lead = 0, tilt = 0</i>	79
4.3.16	<i>Case 16: Following Cut, Step Over =10, lead = 00, tilt = 700</i>	81
CONCLUSIONS AND PLAN FOR FUTURE WORK.....		83
5.1	<i>Shortcomings of the Current Model.....</i>	83
5.2	<i>Conclusions.....</i>	84
5.3	<i>Future Scope</i>	85
REFERENCES		87

List of Figures

<i>Figure 1: Helical cutting edge on ball end mill envelope, i) Orthogonal view ii) Top view.....</i>	6
<i>Figure 2: Geometry of Ball-end tool</i>	7
<i>Figure 3: Geometry of Ball-end in top view.....</i>	7
<i>Figure 4:General tool geometry</i>	8
<i>Figure 5: Different end Mill shapes</i>	9
<i>Figure 6: Radial and axial offsets representation.....</i>	10
<i>Figure 7: Chip thickness representation</i>	12
<i>Figure 8: Chip width representation.....</i>	13
<i>Figure 9: Chip length representation.....</i>	13
<i>Figure 10: Cutting depth correction</i>	20
<i>Figure 11: x and y coordinates in TCS.....</i>	23
<i>Figure 12: Discretized points in FCN coordinate system</i>	23
<i>Figure 13: Discretized points below the cutting depth for 20⁰ lead 30⁰ tilt.....</i>	24
<i>Figure 14: Discretized points in the cutting zone for 20⁰ lead 30⁰ tilt</i>	24
<i>Figure 15: Engagement Zone</i>	27
<i>Figure 16: Check for normal vector for Engagement Region</i>	27
<i>Figure 17: Chip thickness representation</i>	28
<i>Figure 18:General tool geometric parameters.....</i>	30
<i>Figure 19: General tool offset parameters.....</i>	30
<i>Figure 20: Tool discretization</i>	32
<i>Figure 21: Determination of Engagement Region for general milling tool.....</i>	32
<i>Figure 22: Chip thickness for general milling tool</i>	33
<i>Figure 23: Engagement region for non-planar surfaces</i>	34
<i>Figure 24: Geometry - slope</i>	35
<i>Figure 25: Geometry - slope</i>	35
<i>Figure 26: Geometry - edge.....</i>	36
<i>Figure 27: Geometry - step.....</i>	36
<i>Figure 28: Geometry - corner</i>	37
<i>Figure 29: Geometry - custom surface</i>	37
<i>Figure 30: Step over representation</i>	38
<i>Figure 31: Published result for case 1 [4]</i>	41
<i>Figure 32: Simulated forces for case 1</i>	41
<i>Figure 33: Simulated torque for case 1</i>	41
<i>Figure 34: Published result for case 2 [10]</i>	42
<i>Figure 35: Simulated forces for case 2</i>	42
<i>Figure 36: Simulated Touque for case 2</i>	43
<i>Figure 37: Published result for case 3 [10]</i>	43
<i>Figure 38: Simulated cutting force for case 3.....</i>	44
<i>Figure 39: Simulated torque for case 3</i>	44
<i>Figure 40: Ball-end cutting tool profile for 20⁰ lead, 10⁰ Tilt angle.....</i>	45
<i>Figure 41: Discretized point profile for cutting tool (a) below depth of cut & (b) cutting zone</i>	45

<i>Figure 42: Cutting force in FCN coordinate system</i>	46
<i>Figure 43: Cutting force in FCN coordinate system</i>	46
<i>Figure 44: cutting tool discretized point profile lying in cutting zone</i>	46
<i>Figure 45: Variation of $F_{xy\ max}$ with lead and tilt angles for case 5.....</i>	47
<i>Figure 46: Variation of $F_{xy\ max}$ with lead and tilt angles for case 6.....</i>	48
<i>Figure 47: Representation of abrupt entry and exit into the cutting zone.....</i>	49
<i>Figure 48: Cutting forces for 20 axial divisions.....</i>	49
<i>Figure 49: Cutting forces for 50 axial divisions.....</i>	50
<i>Figure 50: Engagement zone at different instances for case 1</i>	50
<i>Figure 51: Forces in GCS for case 1.....</i>	51
<i>Figure 52: Torque in TCS for case 1</i>	51
<i>Figure 53: Engagement zone at different instances for case 2</i>	52
<i>Figure 54:Forces in GCS for case 2.....</i>	53
<i>Figure 55: Torque in TCS for case 2</i>	53
<i>Figure 56: Engagement zone at different instances for case 3</i>	54
<i>Figure 57:Forces in GCS for case 3.....</i>	55
<i>Figure 58: Torque in TCS for case</i>	55
<i>Figure 59: Engagement region for case 1</i>	56
<i>Figure 60: Forces in GCS for case 1.....</i>	57
<i>Figure 61: Torque in TCS for case 1</i>	57
<i>Figure 62: Engagement region for case 2</i>	58
<i>Figure 63: Forces in GCS for case 2.....</i>	58
<i>Figure 64: Torque in TCS for case 2</i>	59
<i>Figure 65: Engagement region for case 3</i>	59
<i>Figure 66 : Forces in GCS for case 3.....</i>	60
<i>Figure 67 : Torque in TCS for case 3</i>	60
<i>Figure 68: Engagement region for case 4</i>	61
<i>Figure 69: Forces in GCS for case 4.....</i>	61
<i>Figure 70: Torque in TCS for case 4</i>	62
<i>Figure 71: Engagement region for case 5</i>	62
<i>Figure 72: Forces in GCS for case 5.....</i>	63
<i>Figure 73: Torque in TCS for case 5</i>	63
<i>Figure 74 : Engagement region for case 6.....</i>	64
<i>Figure 75 : Forces in GCS for case 6.....</i>	64
<i>Figure 76 : Torque in TCS for case 6</i>	65
<i>Figure 77: Engagement region for case 7</i>	65
<i>Figure 78: Forces in GCS for case 7.....</i>	66
<i>Figure 79: Torque in TCS for case 7</i>	66
<i>Figure 80: Engagement region for case 8</i>	67
<i>Figure 81 : Forces in GCS for case 8.....</i>	67
<i>Figure 82: Torque in TCS for case 8</i>	68
<i>Figure 83: Engagement zone at different instances for case 9</i>	69
<i>Figure 84: Forces in GCS for case 9.....</i>	69

<i>Figure 85: Torque in TCS for case 9</i>	70
<i>Figure 86: Engagement region for case 10</i>	70
<i>Figure 87: Forces in GCS for case 10.....</i>	71
<i>Figure 88: Torque in TCS for case 10</i>	71
<i>Figure 89: Engagement region for case 11</i>	72
<i>Figure 90: Forces in GCS for case 11.....</i>	72
<i>Figure 91: Torque in TCS for case 11</i>	73
<i>Figure 92: Engagement zone at different instances for case 12</i>	74
<i>Figure 93: Forces in GCS for case 12.....</i>	74
<i>Figure 94: Torque in TCS for case 12</i>	75
<i>Figure 95; Engagement zone at different instances for case 13</i>	76
<i>Figure 96: Forces in GCS for case 13.....</i>	76
<i>Figure 97: Torque in TCS for case 13</i>	77
<i>Figure 98: Custom surface as a function of piecewise linear functions.....</i>	77
<i>Figure 99; Engagement region for case 14 (a) front view (b) top view.....</i>	78
<i>Figure 100: Forces in GCS for case 14.....</i>	78
<i>Figure 101: Torque in TCS for case 14</i>	79
<i>Figure 102: Engagement region for slotting</i>	79
<i>Figure 103: Engagement region for following cut for step over = 10 mm</i>	80
<i>Figure 104 : Forces in GCS for case 15.....</i>	80
<i>Figure 105: Torque in TCS for case 15</i>	81
<i>Figure 106: Engagement region for following cut with step over 10 mm and non-zero tilt</i>	81
<i>Figure 107: Forces in GCS for case 16.....</i>	82
<i>Figure 108: Torque in TCS for case 16</i>	82
<i>Figure 109: Discretization of cutting tool.....</i>	84

List of Symbols

FCN	Feed coordinate system
TCS	Tool coordinate system
GCS	Global coordinate system
LCS	Local coordinate system
N_f	Number of cutting edges (flutes)
Z	Axial distance from tool tip
$r(z)$	Local radius of the ball end mill
κ	Radial immersion angle
Θ	Tool rotational angle
Φ	Radial immersion angle
i_o	Helix angle at ball shank interface
Φp	Pitch angle
$xx_{tcs}(z)$	X coordinates in TCS coordinates system
$yy_{tcs}(z)$	Y coordinates in TCS coordinates system
$zz_{tcs}(z)$	Z coordinates in TCS coordinates system
$d\theta$	Angular increment
dz	Axial increment
K_p	Angular integration points
L_p	Axial integration points
T	Transformation matrix from TCS to FCN coordinates
Lead	Lead angle
Tilt	Tilt angle
St	Feed per cutting edge
tn	Chip thickness
db	Chip width
ds	Chip length
R	Chip compression ratio/cutting ratio
$[T]$	Transformation matrix from TCS to FCN
$[A]$	Transformation matrix from LCS to TCS

CHAPTER 1

INTRODUCTION

1.1 Introduction

We see technology driven changes in the manufacturing processes everyday across the globe. As technology has been continuously evolving over the last few decades, the demand and importance of lowering the tolerance limit in various industries has been increasing. Industries like aerospace, automotive and die mold machining, are demanding a very high quality of the component which essentially leads to a demand for extremely tight tolerance limit in the manufacturing processes [1].

Milling process is one of the most extensively used manufacturing processes when it comes to precision machining. Advancements in factors like reduction in manufacturing cost, lowering manufacturing time and improvement of quality taken alone or in combination may give a binary switch to the manufacturers in industries like aerospace. This makes the machining process a crucial subject of study. Also, introduction of new and superior materials imposes more challenges to the existing manufacturing processes.

Turbine blades and aircraft structural components are made up of advance composites containing nickel, aluminium and titanium [2]. These composites exhibit magnificent mechanical properties but conventional 3-axis milling process does not meet the required tolerance limit. This happens because the tool undergoes deflection due to high forces while cutting. Tool wear over time reduces the tool life significantly, and it essentially governs the duration for which the given tool can be used without compromising the quality (or surface roughness) and accuracy (or deviation from desired surface profile) of the machined part. Apart from tool deflection and tool wear, tool accessibility is also an important concern in free form surfaces manufacturing. All of these shortcomings can be solved by taking the conventional milling process to the next level, by introducing two more degrees of freedom the lead and tilt angles. Lead and tilt angles determine the orientation of the cutting tool. Cutting forces

experienced by the tool can be significantly reduced by the selection of appropriate lead and tilt angles under certain machining conditions. It also gives us more accessibility to cut complex shapes.

1.2 Motivation

Many models have been developed for the prediction of cutting forces in 5-axis milling process. These models can be broadly classified as:

- 1) **Empirical Models:** Models are often used in practice. It requires gathering of large databases of the cutting forces under different cutting conditions and then preparing a final regression model to be used. Work of Lazoglu, 2003; Gradisek et al., 2006 was completely experimental. [2]
- 2) **Analytical Models:** These are based on various assumptions and do not essentially lead to correct results. The work of Shatla and Atlan, 2000, was completely analytical. [3]
- 3) **Numerical Models:** FEM has become the main tool for the simulation of cutting forces. FEM simulations are very time consuming and accuracy is always a concern.

All the available methods are not very generic in nature and their results are based on some specific cases of workpiece material and tool geometry. The orthogonal cutting data was developed only for a particular workpiece material (Ti6Al4V) in the paper published by P. Lee and Y. Altintas [5]. The orthogonal cutting data obtained for cutting force constants by E. Budak and Y. Altintas [6] is also only valid for the same workpiece material. This report focuses on development of a generic model which can be used for any tool geometry, workpiece surface geometry and workpiece material. The motivation for this study comes from the fact that being a very crucial subject of study, there exists a literature and experimental gap between the research required in precision machining and research which has been done till date.

The main aim of this project is to develop and generalize the methodology to predict the cutting forces and torque experienced by the tool during the 5-axis milling process. These forces are dependent on various factors such as 1) tool geometry 2) machining parameters like tool orientation, feed, speed, cutting depth and 3) workpiece material characteristics.

Based on the geometry and other machining parameters, forces and torque are calculated using a physics based mechanistic approach which deals with the complete geometry and kinematics of the cutting process. It also involves some empirical based results, for instance, basic orthogonal cutting parameters are estimated using a regression curve fitting model on several measured cutting force test results.

1.3 Project Objectives and Scope

This report focuses on computation of cutting force and torque generated in multi-axis machining processes using methodology which is based on mechanistic approach and a physics based mathematical approach. A constitutive material *traction* model is developed for user-specified machining process parameters, which essentially involves an integration of the geometric, process and the material models. This mechanistic *traction* model utilizes basic orthogonal cutting parameters which are determined by using a regression curve fitting of several experimental results.

Forces experienced by the cutting tool depend on various factors mentioned below:

- i. **Cutting tool geometry:** The model in this report deals with ball-end cutting tool having helical cutting edge. This model can be further extended to other tool geometries and cutting edge curves.
- ii. **Cutting tool material:** Orthogonal cutting data is developed for Titanium alloys (Ti6Al4V). The empirical relations developed between orthogonal cutting parameters and oblique cutting parameters are only valid for the Titanium alloy.
- iii. **Workpiece surface:** Initial model is developed for flat workpiece surface undergoing a straight slot milling operation, later the model has been extended to incorporate non-planer surfaces having feed in any direction.

The methodology follows a modular approach in order to model the forces. The tool surface is discretized initially and forces are calculated for each of the elements undergoing orthogonal cutting. The elemental forces are added up to give the net force experienced by the cutting tool. The maximum net force is determined for different angular positions of the cutting tool and subsequently minimized by selecting values of lead and tilt angles which will result in minimum deflection of the cutting tool. Surface roughness parameter can be optimized with

changing tilt and step over in order to optimize the machining time. The model can also be used to predict other machining parameters for the optimization of the cutting process such as precision, cutting depth, feed rate and time required to finish the job. A variety of end mill tools are used for different purposes: Ball end mills are widely used in machining sculptured die and aerospace part surfaces. Tapered helical end mills are used in machining of jet engine compressors using five-axis machining [11]. The model is developed that can be used to analyze any geometry of the cutting tool.

CHAPTER 2

LITERATURE REVIEW

2.1 Coordinate Systems

Four coordinate systems are required in order to define the angular position and orientation of the tool with respect to the workpiece and also for the calculations for the forces. They coordinate systems are [2]:

Feed Coordinate System (FCN): axes are defined along the three dimensions; Feed, Cross feed and Normal to the workpiece. Note the FCN are defined using right hand thumb rule i.e. $\vec{F} \times \vec{C}$ points in the same direction as \vec{N} .

Tool Coordinate System (TCS): axes are defined as x, y and z directions. Tool axis is along z-axis, and other two axes are in the transversal directions of the cutting tool.

Local Coordinate System (LCS): axes are along radial, tangential and axial directions on an individual cutting element.

Global Coordinate System (GCS): axes are defined as x, y and z directions of the workpiece. The axes of GCS are along axes of FCN coordinate system (assuming feed is only horizontal) but origin of GCS is stationary whereas origin of FCN coordinate system is attached to the tool tip

These coordinate systems are interconvertible given the required parameters. Refer section 2.4.1 and 2.4.2 regarding conversion of one coordinate system to another.

2.2 Declaration of the Tool Envelope

2.2.1 Case 1: Ball-End Geometry [2]

The bottom on the ball-end cutting tool is considered as a hemispherical surface of radius R_0 . The cutting edges are lying on the hemispherical surface in a helical fashion. The flutes

have a helix angle i_0 , which dictates the geography of the cutting edges on the surface. The expression for the hemispherical envelope of surface is given as [2]:

$$x^2 + y^2 + (R_0 - z)^2 = R_0^2$$

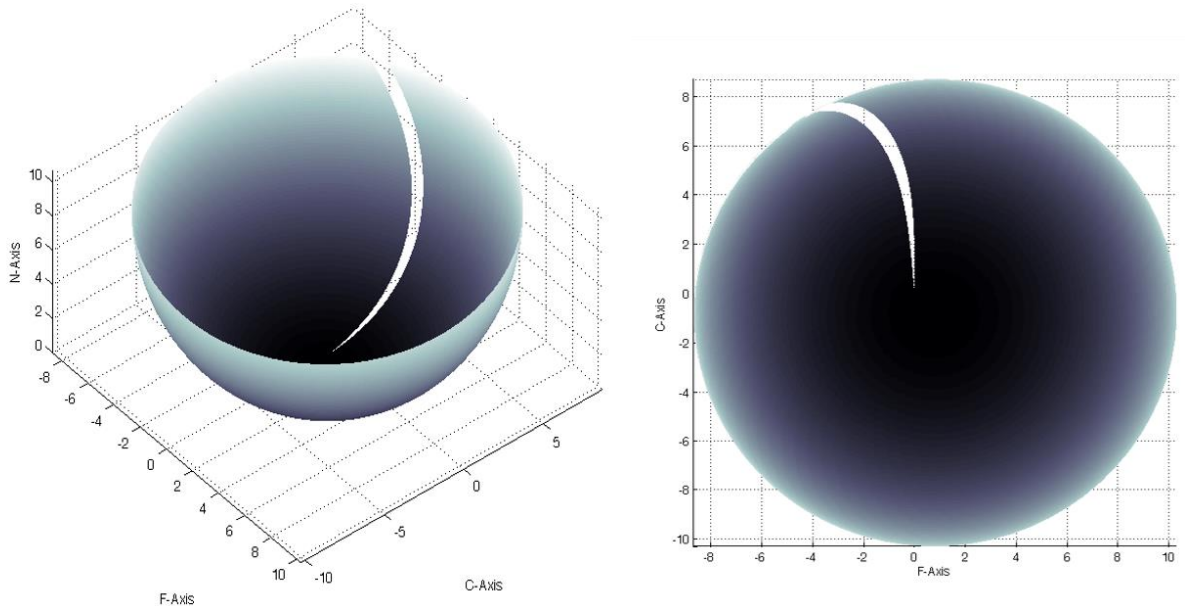


Figure 1: Helical cutting edge on ball end mill envelope, i) Orthogonal view ii) Top view

2.2.1.1 Cutting Edge Parameters [2]

As mentioned above a single flute (or cutting edge) is segmented into various infinitesimal cutting elements. To model each element of the cutting edge, following five parameters needed to be defined [2]:

- i. **Distance from tool tip along tool-axis (Z):** z coordinate of any cutting element is measured taking tool tip as origin.
- ii. **Local radius $r(z)$:** Local radius is a function of z-coordinate of a cutting element. Since each cutting element lies on the hemispherical envelope, expression for $r(x)$ is given as:

$$r(z) = \sqrt{R_0^2 - (R_0 - z)^2}$$

- iii. **Axial immersion angle (K):** The axial immersion angle is defined as the angle between the tool axis (taken as z-axis in TCS) and the vector joining cutting point and center of the hemisphere.

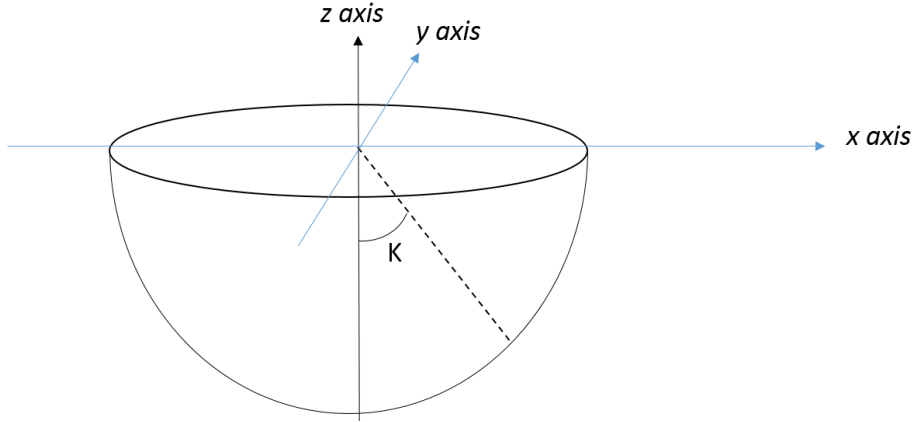


Figure 2: Geometry of Ball-end tool

- iv. **Lag angle Ψ :** Lag angle is defined as the angle on x-y plane in TCS between the line which connects the cutting point to the tool tip. It can be expressed as:

$$\Psi(z) = \frac{z}{R_0} \tan i_0$$

- v. **Radial Immersion angle (Φ):** It is defined as the angular position of the infinitesimal point in x-y plane measured from +y axis. For j^{th} flute of the tool, radial immersion angle is expressed as:

$$\Phi_j(z) = \theta + (j - 1)\Phi_p - \Psi_j(z)$$

Here, Φ_p is the pitch angle between the cutting edges

$$\Phi_p = 2\pi/N_f,$$

Where, N_f is the number of flutes.

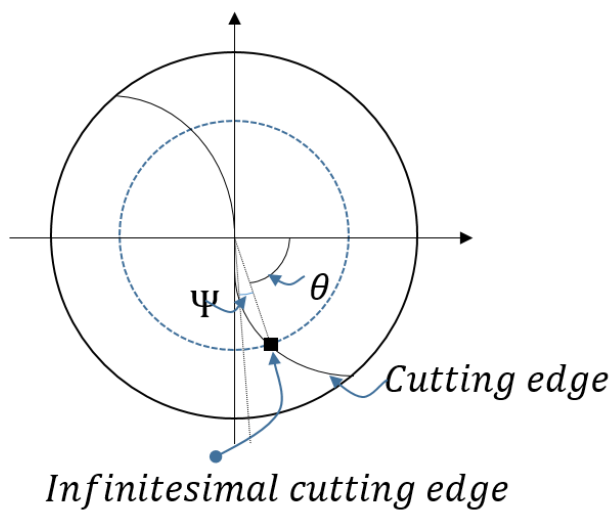


Figure 3: Geometry of Ball-end in top view

2.2.2 Case 2: General Milling Tool Geometry [12]

Any tool geometry can be visualized as a combination of three regions. The envelope of milling cutters can be defined using 7 parameters: $R, R_r, R_z, \alpha, \beta, h$ and D

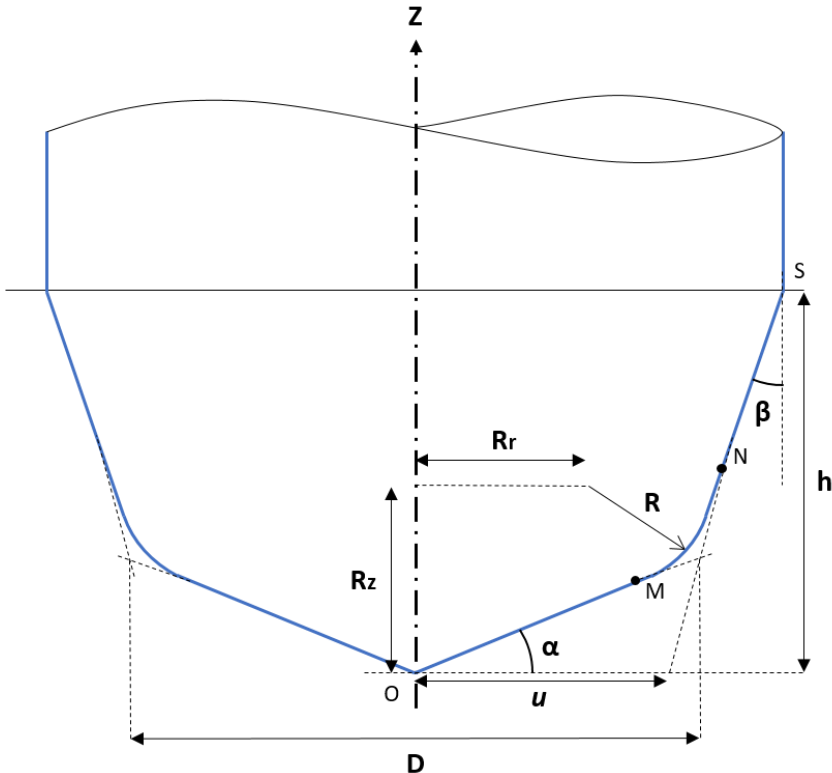


Figure 4:General tool geometry

These seven parameters are independent of each other. Variety of tools can be developed by different combinations of these parameters but in order to make it physically possible there are some constraints which have to be followed as discussed in section 3.2.3.1. On the tool envelope, a helical shaped cutting edge is wrapped around it.

The periphery of the tool can be divided into three segments: two Linear taper zones and an Arc zone. The radii of each zone can be determined as:

$$r(z) = \begin{cases} \frac{z}{\tan \alpha} & \text{for zone } OM \\ \sqrt{R^2 - (R_z - z)^2} + R_r & \text{for zone } MN \\ u + z \tan \beta, \text{ where } u = \frac{D}{2}(1 - \tan \alpha \tan \beta) & \text{for zone } NS \end{cases}$$

Where $r(z)$ is the radius of the cutter at an elevation of z and u the distance between the cutter tip and the point at which the NS line intersects the XY plane as shown in the figure 6.

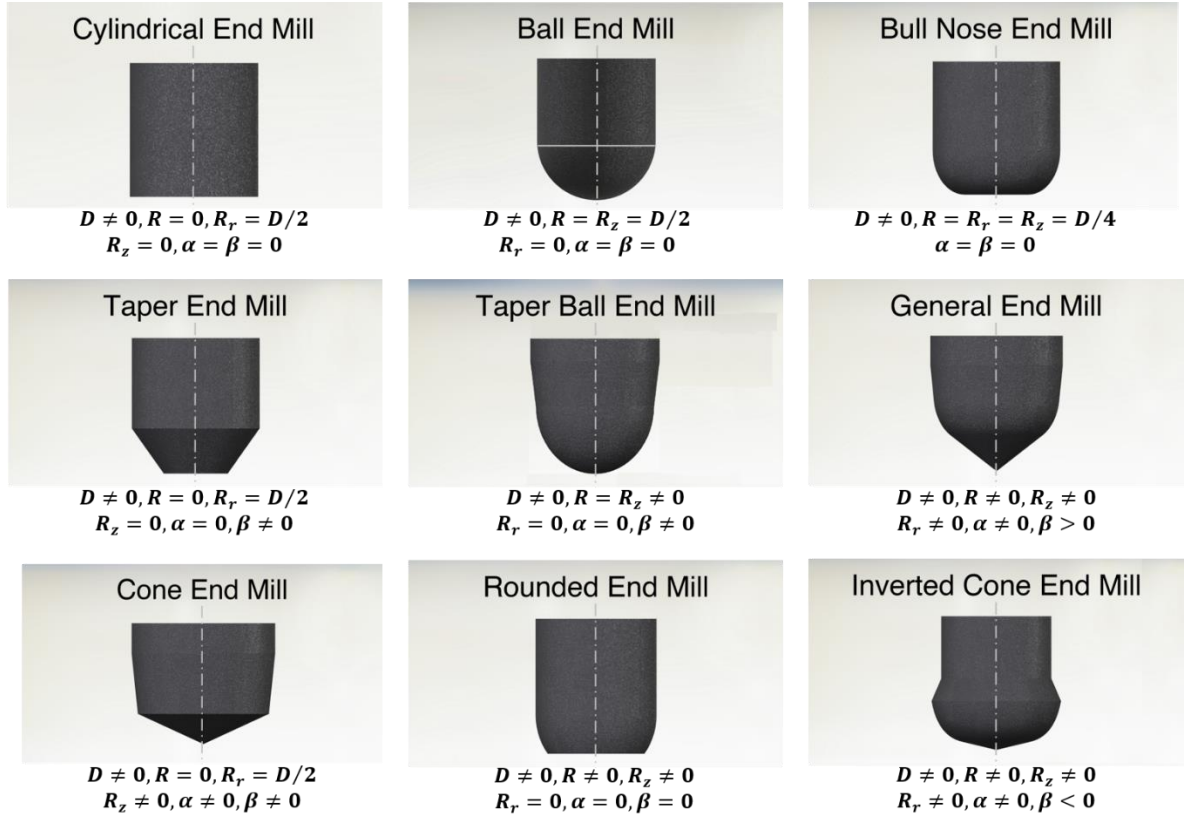


Figure 5: Different end Mill shapes

Point M and N are the starting and finishing point of the arc zone i.e. where the taper zone and the arc zone intersects starts. The should be noted the randomly chosen values of seven parameters do not ensure that the tapered segments are tangent to the arc segment. The lines OM and SN are not necessary tangent to the arc section at points M and N. Even though for the geometry to be mathematically realizable, tangency is not a necessary condition, but for practical purposes tangency is ensured for smoother finish and less wear of the tool. This can be ensured by putting additional tangency constraints the to the given parameters. The radial and axial offsets of points M and N are as:

$$\begin{cases} M_r = \frac{R_z \tan \alpha + R_r + \sqrt{(R^2 - R_r^2) \tan^2 \alpha + 2R_r R_z \tan \alpha - R_z^2 + R^2}}{\tan^2 \alpha + 1} \\ M_z = M_r \tan \alpha \end{cases} \quad \text{for } 0 \leq \alpha < 90^\circ$$

and

$$\begin{cases} N_z = \frac{(R_r - u) \tan \beta + R_z + \sqrt{(R^2 - R_z^2) \tan^2 \beta + 2R_z(R_r - u) \tan \beta - (R_r - u)^2 + R^2}}{\tan^2 \beta + 1} \\ N_r = u + N_z \tan \beta \end{cases} \quad \text{for } 0 \leq \alpha < 90^\circ$$

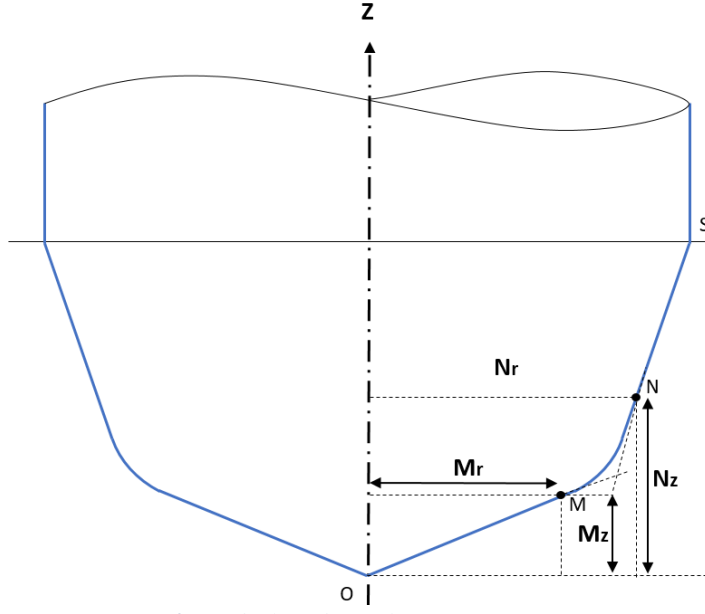


Figure 6: Radial and axial offsets representation

The axial immersion angle of $\text{Kappa}(\mathcal{K})$ in the three zones are:

$$\mathcal{K}(z) = \begin{cases} \alpha & \text{for along line } OM \\ \sin^{-1} \left(\frac{r(z) - R_r}{R} \right) & \text{for along arc } MN \\ \frac{\pi}{2} - \beta & \text{for along line } NS \end{cases}$$

Radial Immersion angle is defined as the angular position of the infinitesimal point in x-y plane measured from +y axis. For j^{th} flute of the tool, radial immersion angle is expressed as:

$$\Phi_j(z) = \theta + (j - 1)\Phi_p - \Psi_j(z)$$

Here, Φ_p is the pitch angle between the cutting edges. $\Phi_p = 2\pi/N_f$, Where, N_f is the number of flutes. To get the coordinates, the value of $\Psi_j(z)$ or the lag angle is defined for the three regions as:

Zone 1: OM ($z \leq M_z$)

$$\Psi_1(z) = \frac{\ln(z \cot \alpha) \tan i_0}{\cos \alpha} - \Psi_{1s}$$

Where Ψ_{1s} is the starting lag angle defined as:

$$\Psi_{1s} = \frac{\ln r_s \tan i_0}{\cot \alpha}, r_s = \frac{M_r}{20}$$

Zone 2: Arc zone MN ($M_z < z \leq N_z$)

$$\Psi_2(z) = \frac{(R + z - R_z) \tan i_0}{R} - \Psi_{as} + \Psi_{1e}$$

$$Where, \quad \Psi_{1e} = \frac{\ln M_r \tan i_0}{\cos \alpha} - \Psi_{1s} \quad and \quad \Psi_{as} = \frac{(R + M_z - R_z) \tan i_0}{R}$$

Zone 3: Taper zone NS ($N_z < z$)

The taper zone of the tool can either have constant lead or constant helix. The constant lead, which leads to variable helix angle along the flute, is preferred as it saves the material during re-grinding operation. However, cutting mechanics are more uniform with constant helix angle tools, which require varying lead.

Case 1: Constant helix

$$\Psi_3(z) = \begin{cases} \frac{\ln(N_r - (N_z - z) \tan \beta) \tan i_0}{\sin \beta} - \Psi_{2s} + \Psi_{ae} & if \beta \neq 0 \\ \frac{(z - N_z) \tan i_0}{N_r} - \Psi_{2s} + \Psi_{ae} & if \beta = 0 \end{cases}$$

$$Where \quad \Psi_{ae}(z) = \frac{(R + N_z - R_z) \tan i_0}{R} - \Psi_{as} + \Psi_{1e}$$

$$and \quad \Psi_{2s}(z) = \begin{cases} \frac{\ln(N_r) \tan i_0}{\sin \beta} & if \beta \neq 0 \\ \Psi_{2s}(z) = 0 & if \beta = 0 \end{cases}$$

Case 2: Constant lead

$$\Psi_3(z) = \frac{(z - N_z) \tan i_s}{N_r} + \Psi_{ae} \quad for \quad N_z \leq z \leq h$$

$$Where \quad \Psi_{ae}(z) = \frac{(R + N_z - R_z) \tan i_0}{R} - \Psi_{as} + \Psi_{1e} \quad and \quad i_s = \tan^{-1} \left[\frac{2\pi N_r}{lead \cdot \cos \beta} \right]$$

2.3 Chip Dimensions [7]

While machining, workpiece material is removed out in the form of chips. The forces generated on the tool are mainly a result of change in the geometry of workpiece material as it converts to chip, hence forces depend on the geometry of the chips formed. The dimensions of chips depend on the machining parameters like feed rate, lead and tilt angles and tool geometry (tool diameter and helix angle). The 3 main geometric parameters associated with the chips are [4]:

- i. Chip Thickness
- ii. Chip Width
- iii. Chip Length

Note that the dimensions mentioned above are NOT the dimensions of the chip actually formed while machining process. The chips formed in our case are result of infinitesimal edge (formed by the line segment joining two adjacent discretized cutting points) cutting the workpiece, and are considered for the force modeling. The actual chip dimensions are different and are a function of workpiece elasticity and various other milling conditions.

2.3.1 Chip Thickness

Chip thickness is the thickness of uncut material removed by the cutting element. Chip thickness is maximum at the infinitesimal cutting element lying in the direction of feed. It depends on cutting feed, axial immersion angle (K) and radial immersion angle (Φ) as:

$$t_n(S_t, \Phi, K) = S_t \sin \Phi \sin K$$

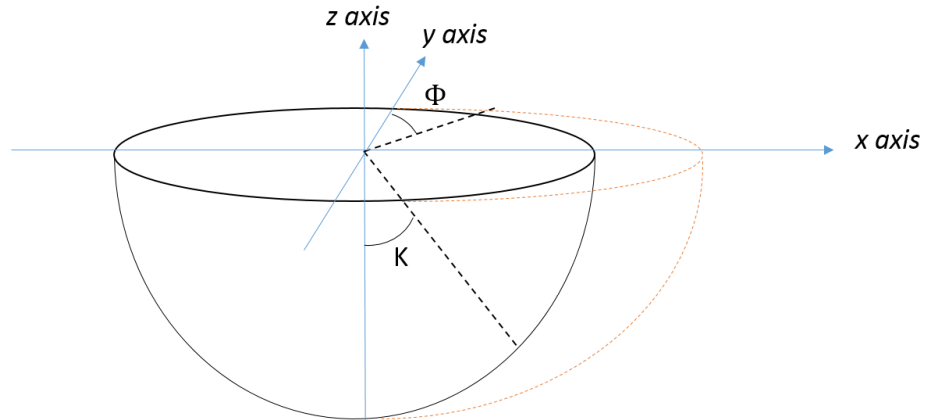


Figure 7: Chip thickness representation

2.3.2 Chip Width

Chip width is defined as the projected length of an infinitesimal cutting element in the direction of cutting velocity. It varies as the value of K decreases. Chip width is expressed as a function of axial incremental value and axial immersion angle:

$$db = \frac{dz}{\sin K}$$

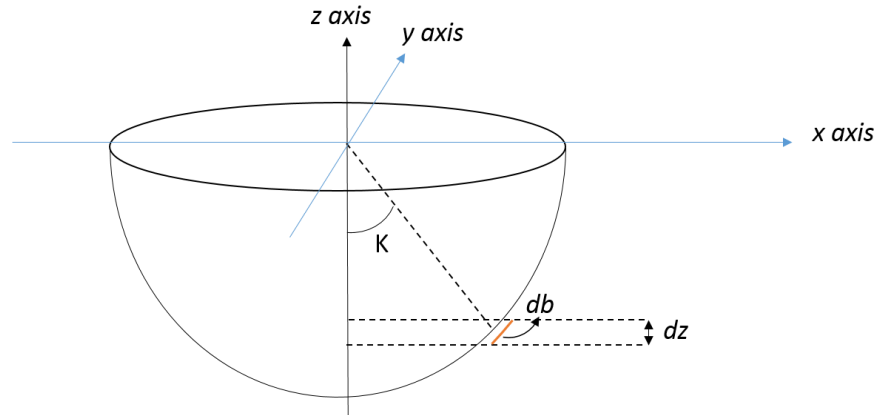


Figure 8: Chip width representation

2.3.3 Chip Length

Chip length is defined as the distance between two adjacent (along axial direction) discretized cutting points. It is expressed as:

$$ds = \sqrt{(\vec{X}(j, i) - \vec{X}(j - 1, i))^2}$$

$\vec{X}(j, i)$ and $\vec{X}(j - 1, i)$ represent position vector of two points in TCS coordinate system

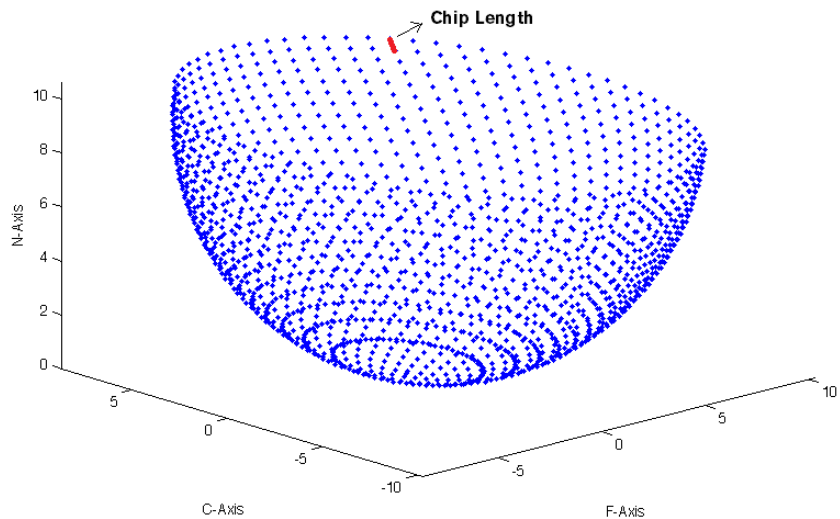


Figure 9: Chip length representation

2.4 Force Coefficients [3]

The cutting edge is divided into infinitesimal piecewise linear cutting edges; these elements are assumed to be having as oblique cutting tool to the workpiece. The overall forces experienced by the tool is calculated by adding all the forces experienced by the individual cutting elements.

Cutting forces experienced by the tool are generated due to two operations:

- i. **Edge Forces:** Rubbing of the tool against the workpiece material
- ii. **Cutting Forces:** Shearing of the workpiece material in the shear zone

2.4.1 Edge Force Coefficients

Edge cutting forces come into picture due to rubbing or ploughing of the cutting edge on the workpiece. The edge cutting coefficients are defined as force per unit length. The forces are determined after performing various experiments and finding a regression model for the same. It was found that edge forces do not vary significantly as we change rake angle and speed of the cutting edge for a specific workpiece material. The coefficients are determined for each of the three force components in LCS i.e.: along tangential K_{te} , radial K_{re} and axial K_{ae} . Forces along axial direction is very small, hence axial coefficient is taken as zero [3].

$$K_{te} = 24N/mm$$

$$K_{re} = 43N/mm$$

$$K_{ae} = 0N/mm$$

2.4.2 Cutting Force Coefficients

These force coefficients take into account the forces due to shearing of workpiece material in shear zone. These coefficients represent the cutting force per unit cross-sectional area of chip. Similar to the edge force coefficients, these coefficients are determined for each of the three force components in LCS i.e.: along tangential K_{tc} , radial K_{rc} and axial K_{ac} . They are dependent on cutting conditions and determined using Orthogonal Cutting Database (OCD).

2.4.2.1 Orthogonal Cutting Database

This database provides the empirical relationships between machining process parameters and material shearing parameters such as friction angle and shear angle [5].

$$\text{Shear stress } (\tau) = 613 \text{ MPa}$$

$$\text{Friction angle } (\beta) = 19.1 + 0.29\alpha$$

$$r = r_0 t^\alpha$$

$$r_0 = 1.755 - 0.028\alpha$$

$$\alpha = 0.331 - 0.0082\alpha$$

Where α is the rake angle.

Shear angle can be determined using the model developed for oblique cutting. Shear angle can be expressed as [6]:

$$\tan \phi = \frac{r \cos \alpha}{1 - r \sin \alpha}$$

2.4.2.2 Oblique Cutting

The results for oblique cutting are used to determine the forces along the direction of cutting velocity (F_t), along the direction of cutting feed (F_f) and along radial direction (F_r) which is perpendicular to the both axes. The cutting force coefficients are determined by dividing the expression by chip width and thickness. The cutting force coefficients are mathematically expressed as [7]:

$$\begin{cases} K_{tc} = \frac{\tau}{\sin \phi_n} \frac{\cos(\beta_n - \alpha_n) + \tan \eta_c \sin \beta_n \tan i}{c} \\ K_{rc} = \frac{\tau}{\sin \phi_n \cos i} \frac{\sin(\beta_n - \alpha_n)}{c} \\ K_{ac} = \frac{\tau}{\sin \phi_n} \frac{\cos(\beta_n - \alpha_n) \tan i - \tan \eta_c \sin \beta_n}{c} \end{cases}$$

$$\text{Where, } c = \sqrt{\cos^2(\phi_n + \beta_n - \alpha_n) + \tan^2 \eta_c \sin^2 \beta_n}$$

The following assumptions are made in order to relate orthogonal cutting mechanics to oblique cutting mechanics.

- i. Normal rake angle is taken same as orthogonal rake angle and normal shear angle in oblique cutting is taken same as orthogonal shear angle.

$$\varphi_n = \varphi_0$$

$$\alpha_n = \alpha_0$$

- ii. Friction angle and shear stress are same in both cases given the other parameters remain the same.

$$\beta_n = \beta$$

$$\tau_s = \tau$$

- iii. Chip flow angle is approximated to helix angle

$$\eta_n = i$$

2.5 Force Equation

Total forces on any cutting element is the vector sum of cutting and shear force. The elemental tangential, radial and normal force acting on the cutting edge are expressed as [5]:

$$dF_t(\theta, z) = K_{te} dS_c + K_{tc} t_{nc}(\theta, \psi, K) db_c$$

$$dF_r(\theta, z) = K_{re} dS_c + K_{rc} t_{nc}(\theta, \psi, K) db_c$$

$$dF_a(\theta, z) = K_{ta} dS_c + K_{ta} t_{nc}(\theta, \psi, K) db_c$$

Where,

$$dS_c = LG \cdot dS$$

$$db_c = LG \cdot db$$

$$t_{nc} = LG \cdot t_n$$

Logical matrix is multiplied by chip dimensions to nullify the effect of points not lying the cutting zone and only consider the points lying in the cutting zone.

2.5.1 Force Transformation to TCS

The forces calculated on every cutting element using the above expressions are defined in Local Coordinate System. They have to be transformed into Tool Coordinate System to determine the forces and torque acting on the tool using a transformation matrix A. Matrix A is

essentially considering the effect of axial immersion angle and radial immersion angle and rotating LCS two times. It is expressed as follows [8]:

$$\begin{Bmatrix} dF_x \\ dF_y \\ dF_z \end{Bmatrix}_{TCS} = [A] \begin{Bmatrix} dF_t \\ dF_r \\ dF_a \end{Bmatrix}_{LCS}$$

Where,

$$[A] = \begin{bmatrix} -\sin K \sin \phi & -\cos \phi & -\cos K \sin \phi \\ -\sin K \cos \phi & -\sin \phi & -\cos K \cos \phi \\ \cos K & 0 & -\sin K \end{bmatrix}$$

Where K is the axial immersion angle and ϕ is radial immersion angle.

Further, the elemental torque acting on each on the cutting edge is the product of the elemental tangential force and elemental instantaneous radius in TCS coordinate system. It can be expressed as:

$$dT_{TCS} = r(z) \cdot dF_t$$

The total cutting force experienced by the ball-end tool is calculated by adding up all the differential forces exerted on each elemental cutting edge. This can be mathematically expressed as follows [9]:

$$\begin{aligned} F_x(\theta) &= \sum_{j=1}^{L_p} dF_x(\theta, z) \\ F_y(\theta) &= \sum_{j=1}^{L_p} dF_y(\theta, z) \\ F_z(\theta) &= \sum_{j=1}^{L_p} dF_z(\theta, z) \end{aligned}$$

Similarly, total torque experienced by the tool along the axis can be expressed as:

$$T_{TCS}(\theta) = \sum_{j=1}^{L_p} dT_{TCS}(\theta, z)$$

Where L_p is the number of divisions along the axial direction.

2.5.2 Force Transformation to FCN

The cutting force calculated in the above section are in Tool Coordinates System (TCS). The cutting forces are transformed into FCN coordinate system using matrix T. Matrix T is essentially considering the effect of lead and tilt angles and rotating TCS two times, along ‘tilt’ direction followed by rotation along ‘lead’ direction. T can be defined as [2]:

$$[T] = \begin{bmatrix} 1 & 0 & 0 \\ 0 & \cos t & -\sin t \\ 0 & \sin t & \cos t \end{bmatrix} \begin{bmatrix} \cos l & 0 & \sin l \\ 0 & 1 & 0 \\ -\sin l & 0 & \cos l \end{bmatrix} = \begin{bmatrix} \cos l & 0 & \sin l \\ \sin t \sin l & \cos t & -\sin t \cos l \\ -\cos t \sin l & \sin t \sin l & \cos t \cos l \end{bmatrix}$$

Forces along FCN are expressed as multiplication of T with TCS coordinates:

$$\begin{Bmatrix} dF_F \\ dF_C \\ dF_N \end{Bmatrix}_{FCN} = [T] \begin{Bmatrix} dF_x \\ dF_y \\ dF_z \end{Bmatrix}_{TCS}$$

CHAPTER 3

MODEL DEVELOPMENT

3.1 Calculation Overview

Computational code of the entire model is written in C# using IDE Microsoft Visual Basic Studio. Various tool geometric parameters, machining process parameters, tool orientation parameters, axial and radial division parameters and material specific parameters are taken as input.

The steps involved in the development of different kind of models (section 3.2) are given below:

i. Declaration of the Tool Envelope

Various kind of tools have different kind of profiles. The first step is to identify the tool shape. The cutting edge is wrapped around the tool envelope depending on the helix angle.

ii. Discretization of Surface Points

The cutting tool envelope is discretized using *axial and radial incremental* parameters. There is a tradeoff between the values of discretization parameters and the time (and space) complexity of the code and the accuracy of the model.

iii. Determination of the Engagement Region

Various checks are done in order to find whether a point lies in the engagement region or not. Logical operations on the tool envelope are used to eliminate the points which do not lie in the cutting zone. Only the points which are present in the cutting zone will contribute in the force calculation. The TCS coordinates are defined keeping the tool tip to be the origin, hence the least z coordinate of the tool profile is zero. As the tool geometry is transformed from TCS to FCN, if the tool has some lead and tilt, the lowermost point of the tool which essentially dictates the depth of cut goes further below x-y plane. This means the lowering of the cutting

tool has to be reduced or the depth of the origin of TCS has to be corrected. Lowest point in the FCN coordinate system is determined. Cutting depth is corrected after locating the lowermost point. Actual cutting depth is expressed as:

$$\text{Actual cutting depth} = \text{cutting depth} + z_{\min}$$

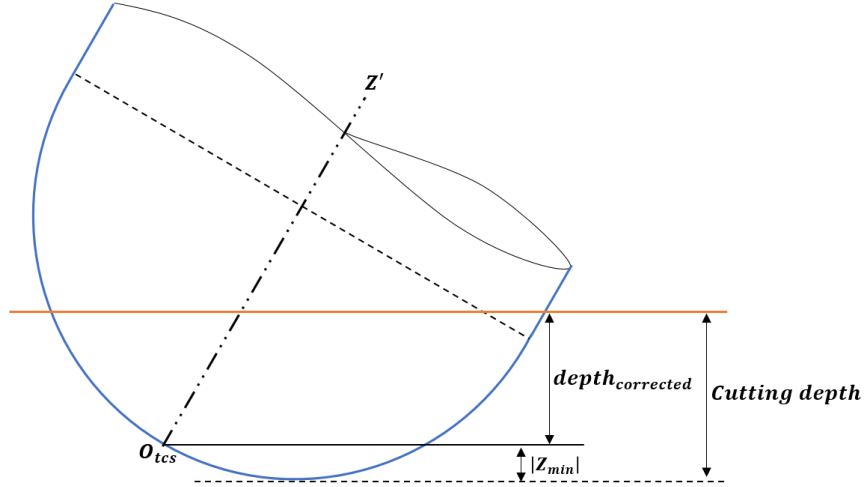


Figure 10: Cutting depth correction

iv. Defining chip dimensions

Separate two-dimensional arrays for chip width, length and thickness are calculated. Points lying outside cutting zone are not involved in the force calculation.

v. Calculation of force

Forces on individual cutting edges are calculated using the values of cutting force and edge force coefficients. Elemental forces in Local Coordinate System (LCS) are calculated for each of the cutting point using the elemental force equations. For the calculation of the final forces in Tool Coordinate System (TCS) corresponding to different values of θ (or i), elemental forces which will contribute for a particular cutting edge are added. For multiple flutes contribution of each flute has been added. Similar calculation has been done for determining the net torque resistance experienced by the tool. Elemental forces are then transformed to Tool Coordinate System using ‘A’ matrix and stored as separate two-dimensional arrays dF_x_{tcs} , dF_y_{tcs} and dF_z_{tcs} . Elemental torque is calculated for each point using elemental torque equation. These elemental forces and torques are added to give the net force and net torque experienced by the tool after transformation into Tool Coordinate System

(TCS). Calculated forces in Tool Coordinate System are then transformed into FCN coordinate system using transformation matrix T which is calculated using given Lead and Tilt angles.

vi. Determination of Optimal Value of Lead and Tilt Angles

This is an extra step and extension of the previous step. The precision of the machined workpiece is determined by maximum deflection of the workpiece from the required geometry, which depends on the maximum shear force experienced by the tool. Net force in x-y directions is calculated for various angular positions of cutting edge, hence maximum force experienced by the tool is calculated. The entire set of operations to find the maximum force experienced by the tool is done for different values of lead and tilt angles. Optimal values of lead and tilt angles are calculated which minimizes the maximum force experienced by the tool under a given set of tool, operations and workpiece conditions. Usually, values of lead and tilt angle for the minimum value of maximum force are found to be ranging between -20^0 to 20^0 . These values of tilt and lead angles are implemented to reduce the tool deflection which will essentially results in precision machining. The model will also help to predict the other machining and tool parameters for which the forces and torque can be further reduced.

Note that all the calculations are done considering general milling tool with helical cutting edges. Also, the results are valid only for workpiece material (Ti6Al4V). Other materials may have different Orthogonal Cutting Database which provides empirical relationships between given set of manufacturing parameters and the material shearing parameters. Other geometries and different material may have different orthogonal cutting database.

3.2 Different Types of Models

Three different models were developed in this project. The first model deals with ball-end mill tool cutting a planar surface and having only horizontal feed. The second model is an extension of the first model where vertical component of the tool feed is also taken into account. In the second model, the engagement zone and the chip dimensions change relative to the first model. The third model is developed for general milling tool. Various kinds of workpiece geometries are also added in the last model. The third model is also extended for the following cut having some step over.

3.2.1 Model 1: Ball-End Mill Cutting Planar Surface having only Horizontal Feed

Ball end tool has hemispherical shaped end attached to a cylinder (see section 2.2.1). Since the feed is only in horizontal direction, the depth of the tool remains constant. This results in static engagement zone. The forces on each element present in the engagement zone are calculated using force coefficients (section 2.4) in Local Coordinate System (LCS) then and transformed into Tool Coordinate System (section 2.5). The procedure of discretization of tool geometry and the determination of the engagement region is discussed in this section.

3.2.1.1 Discretization of tool geometry

To develop the force model on tool, discretization of the surface points is done using the parameters mentioned in the above section. Discretization of the entire surface envelope is done using dividing the surface in constant intervals in radial and axial space. The density of the discretized points is controlled by selecting constant angular incremental ($d\vartheta$) and axial incremental values (dz). K_p divisions are in radial space whereas L_p divisions are there in axial direction (along z-axis in TCS) [3].

$$K_p = \frac{2\pi}{d\vartheta}$$

$$L_p = \frac{R_0}{dz}$$

Coordinates of different infinitesimal cutting points in TCS are expressed as:

$$xx_{tcs}(i,j) = r(z) \sin \Phi(z)$$

$$yy_{tcs}(i,j) = r(z) \cos \Phi(z)$$

$$zz_{tcs}(i,j) = z$$

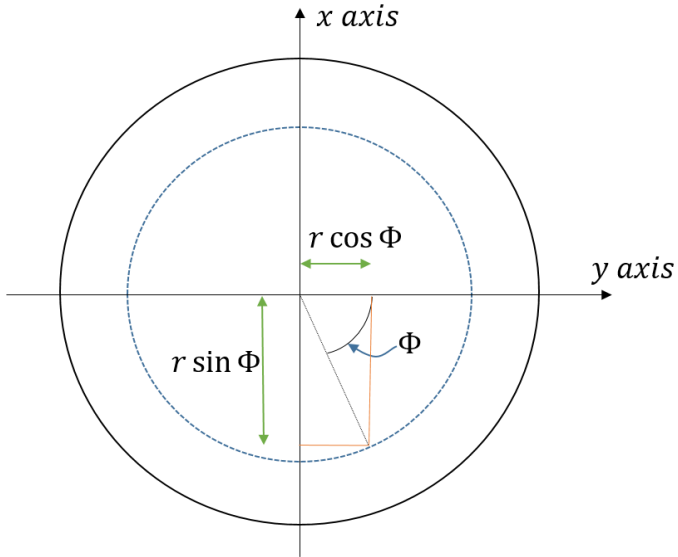


Figure 11: *x* and *y* coordinates in TCS

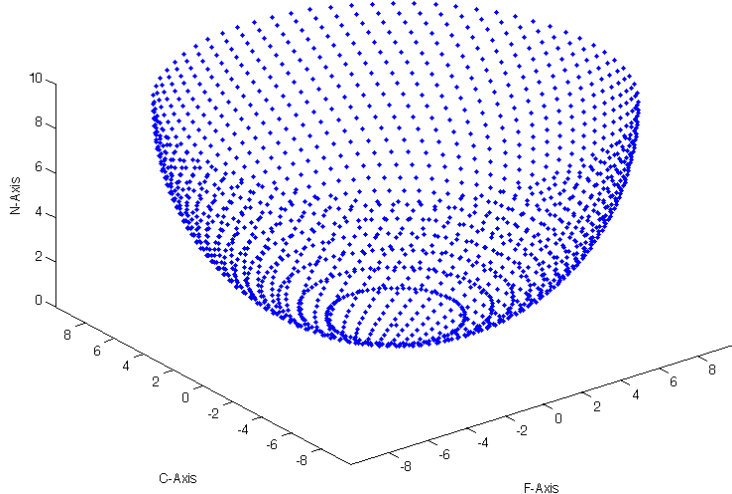


Figure 12: Discretized points in FCN coordinate system

3.2.1.2 Determination of the Engagement Region

Cutting zone/engagement zone is defined as the portion of the tool which is in contact with the workpiece. The infinitesimal cutting elements lying in the cutting zone only can experience the force which the tool is in contact with the workpiece. Hence, determination of cutting zone is important in the modelling of force and torque.

Cutting zone can be identified by removing two set of points from the entire set of cutting points. Firstly, remove the points which are above the cutting depth since they are not in contact with the workpiece. Secondly, remove the points which are lying opposite to the direction of

the feed in FCN coordinate system. i.e. keep the points in cutting zone whose position vector with feed direction leads a non-negative number [2].

$$P(i,j) == (\text{z}(i,j) > \text{cutting depth}) \&\& (\overrightarrow{\text{feed}} \cdot \overrightarrow{OX}(j,i))$$

AND logical operator to be used for the above two conditions to satisfy the cutting zone condition. $\overrightarrow{\text{feed}}$ is the feed vector, and \overrightarrow{OX} is position vector of the point with respect to the new origin in FCN coordinate system.

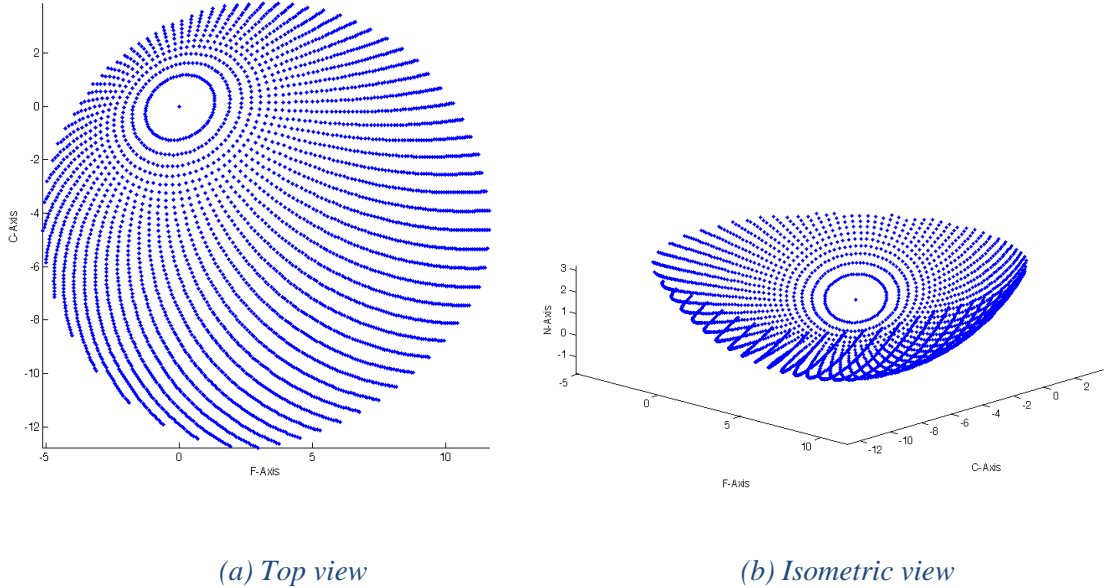


Figure 13: Discretized points below the cutting depth for 20° lead 30° tilt

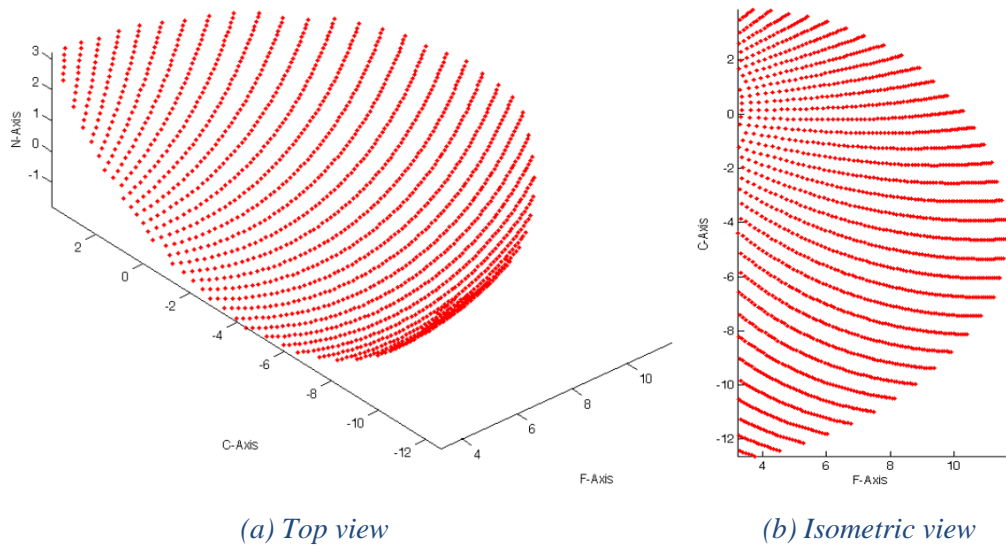


Figure 14: Discretized points in the cutting zone for 20° lead 30° tilt

Logical Matrix (LG) consists of 1s and 0s and used to define the cutting zone. The value to a corresponding point is 1 in logical matrix if the point lies in the cutting zone, else it is 0. LG is used for its multiplication with chip parameters. This implies that the force is only generated due to a cutting edge when the cutting edge is inside the cutting zone.

3.2.1.3 Model Assumptions and Limitations

The assumptions and limitations of the model are:

- 1) Tool profile is ball end mill
- 2) Workpiece Surface is planar
- 3) Feed direction of the tool is only horizontal
- 4) Depth of tool is constant
- 5) Chip thickness does not change with lead and tilt
- 6) No sense of step over and surface roughness

The model developed at later stage of the project has

1. General milling tool having helical profile of the cutting edge
2. Work piece surface need not to be planar
3. Feed direction of the tool can also have a vertical component
4. Depth of the tool can be variable
5. The effect and lead and tilt are considered while calculating chip thickness
6. Step over and surface roughness are also dealt with

3.2.2 Model 2: Ball-End Mill Cutting Planar Surface

In the previous model, since the feed was only horizontal, the depth of the tool does not change with time and the entire model was developed considering the depth to be constant. The engagement region does not change with time. It was determined once and then used for the forces calculation for one revolution (360 degrees) of the tool. In the current model since the tool also has a vertical component of feed, the depth of tool also changes as the tool rotates according to the vertical feed component of the tool. In this model, the engagement region is updated at every angular movement of the tool. The forces are calculated for dynamic depth of the tool.

Declaration of the tool envelope and discretization of the surface points remain same as the previous model. But the determination of engagement region and chip dimensions change. The force calculation part remains same as model 1.

3.2.2.1 Determination of Engagement region

To know whether a point on the surface of tool envelope lies in the engagement zone or not, two checks are done:

- 1) Check for point to be inside the geometry of the workpiece
- 2) Check for normal vector to the surface of the point

3.2.2.1.1 Check for point to be inside the geometry of the workpiece

Let \overrightarrow{feed} be the feed vector, t be the time at which the forces are calculated. The tool center is considered to be the reference point to keep track of the tool position in Global Coordinate System. Let us assume that the tool center at $time = 0$ is at origin of Global Coordinate System. At $time = t$, the tool center vector is $\overrightarrow{feed} \times t$. The coordinates of tool center in TCS are [0,0,R], transforming into FCN coordinate system coordinates of tool center are:

$$\overrightarrow{center} = \begin{Bmatrix} C_x \\ C_y \\ C_z \end{Bmatrix}_{FCN} = [T] \begin{Bmatrix} 0 \\ 0 \\ R \end{Bmatrix}_{TCS}$$

Let the coordinate of any point in FCN be $[xx_{fcn}(i,j), yy_{fcn}(i,j), zz_{fcn}(i,j)] = \overrightarrow{P_{FCN}}(i,j)$, then, the coordinate of any point in Global Coordinate System can be written as:

$$\overrightarrow{P_{GCS}}(i,j) = \overrightarrow{P_{FCN}}(i,j) + \overrightarrow{feed} \times t - \overrightarrow{center}$$

Now the $\overrightarrow{P_{GCS}}(i,j)$ can be checked whether it lies within the workpiece geometry or not as:

If $\overrightarrow{P_{GCS}}(i,j) \cdot \hat{k} > -(R - cutting\ depth)$, then the point does not lie in the cutting region (engagement region).

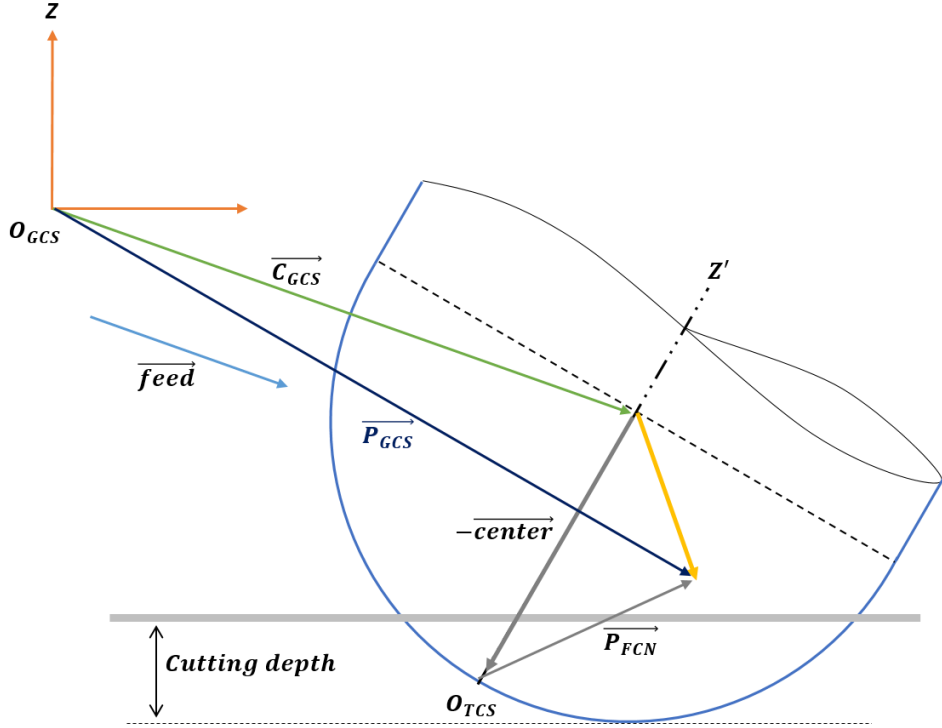


Figure 15: Engagement Zone

3.2.2.1.2 Check for normal vector to the surface of the point

Normal vector to the surface of the point should make an acute angle in FCN coordinate system in order to be in cutting region. An appropriate analogy would be only those points would be in cutting zone who will be visible when the tool is seen from the direction of the feed vector.

This can be checked as:

If $(\overrightarrow{P_{FCN}(i,j)} - \overrightarrow{\text{center}}) \cdot \overrightarrow{\text{feed}} \leq 0$ then point does not lie in the cutting region or engagement region.

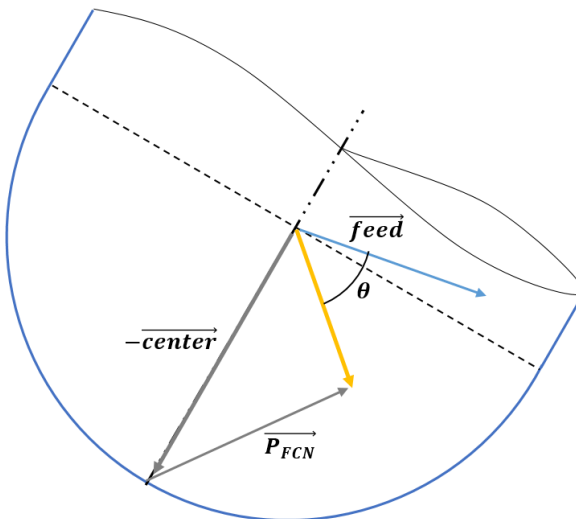


Figure 16: Check for normal vector for Engagement Region

3.2.2.2 Defining Chip Dimensions

Chip length and chip width are a function of discretization parameters of the tool and do not depend on the direction or magnitude of the feed vector. On the other hand, chip thickness also depends on the feed vector. Chip thickness in the previous model was:

$$t_n(S_t, \Phi, \mathcal{K}) = S_t \sin \Phi \sin \mathcal{K}$$

Since, chip thickness is calculated along the direction of the feed vector, the point which makes a surface normal vector which is along the feed direction will be cutting the maximum. In this case, it can be seen that t_n will be maximum when $\mathcal{K} = \Phi = 90^\circ$, it will be point which be cutting maximum amount of workpiece material. From figure 17 it can be seen that the chip thickness for a surface point is nothing but the component of \vec{S}_t along the surface normal vector at the point.

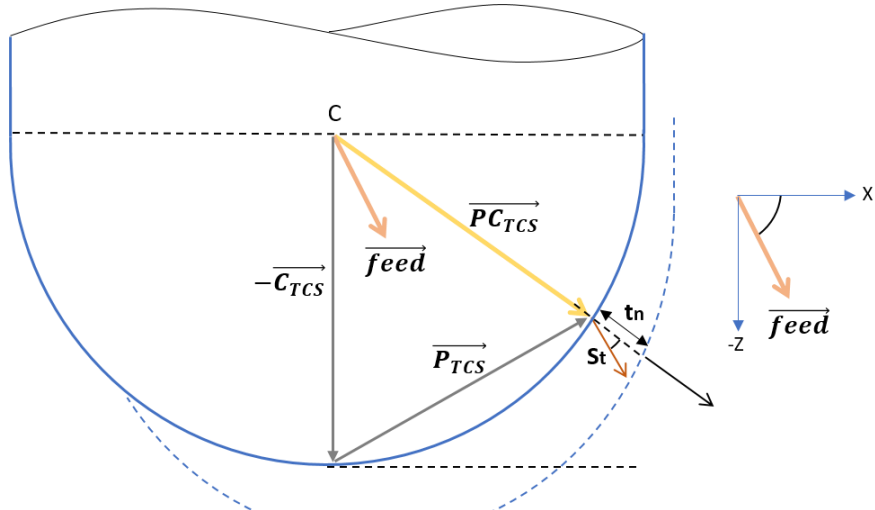


Figure 17: Chip thickness representation

Let $\overrightarrow{\text{feed}}$ makes θ below the x-axis.

Then, $\overrightarrow{\text{feed}} = [F \cos \theta, 0, -F \sin \theta]$

Point $\overrightarrow{P_{TCS}}$ can be written as $[R \sin \mathcal{K} \sin \Phi, R \sin \mathcal{K} \cos \Phi, R - R \cos \mathcal{K}]$

Surface normal vector of a point in case of ball end milling tool is along the line joining the center of the tool and the $\overrightarrow{P_{TCS}}$ i.e. relative vector \overrightarrow{PC} :

$$\overrightarrow{PC_{TCS}} = \overrightarrow{P_{TCS}} - [0, 0, R]$$

$$\overrightarrow{PC_{TCS}} = [R \sin \kappa \sin \Phi, R \sin \kappa \cos \Phi, -R \cos \kappa]$$

Chip thickness of point P can be written as:

$$t_n(S_t, \Phi, \kappa) = S_t \times \frac{\overrightarrow{PC_{TCS}} \cdot \overrightarrow{feed}}{|\overrightarrow{PC_{TCS}}| |\overrightarrow{feed}|}$$

$$t_n(S_t, \Phi, \kappa) = S_t (\sin \kappa \sin \Phi \cos \theta + \cos \kappa \sin \theta)$$

3.2.2.2.1 Correction of chip thickness

In the above section, the effect of lead and tilt has not been considered while calculating the chip thickness and chip thickness is independent of lead and tilt which is not correct.

The $\overrightarrow{PC_{TCS}} = [R \sin \kappa \sin \Phi, R \sin \kappa \cos \Phi, -R \cos \kappa]$ is defined in TCS, it can be transformed into FCN coordinate system as:

$$\begin{Bmatrix} P_x \\ P_y \\ P_z \end{Bmatrix}_{FCN} = [T] \begin{Bmatrix} R \sin \kappa \sin \Phi \\ R \sin \kappa \cos \Phi \\ -R \cos \kappa \end{Bmatrix}_{TCS}$$

Chip thickness of point P can be written as:

$$t_n(S_t, \Phi, \kappa) = S_t \times \frac{\overrightarrow{PC_{FCN}} \cdot \overrightarrow{feed}}{|\overrightarrow{PC_{FCN}}| |\overrightarrow{feed}|}$$

3.2.3 Model 3: General Milling Tool Cutting Planar Surface

The tool envelope is redefined completely according the tool type (section 2.2.2), the determination of the engagement region and chip dimensions change in this model but the force calculation part remain the same as the previous models.

3.2.3.1 Constraints of surface parameters

There are seven geometric parameters which dictate the geometry of the tool. Though these parameters are independent, there are some constraints in selection of these seven parameters:

- 1) $R_z > R_r \tan \alpha$ i.e. center of Arc zone should lie above the line OM
- 2) $(R^2 - R_r^2) \tan^2 \alpha + 2R_r R_z \tan \alpha - R_z^2 + R^2 > 0$ for M_r to be defined

- 3) $(R^2 - R_z^2) \tan^2 \beta + 2R_z(R_r - u) \tan \beta - (R_r - u)^2 + R^2 > 0$ for N_z to be defined
- 4) $M_z \leq N_z$
- 5) $M_r \leq N_r$
- 6) $h > M_z$

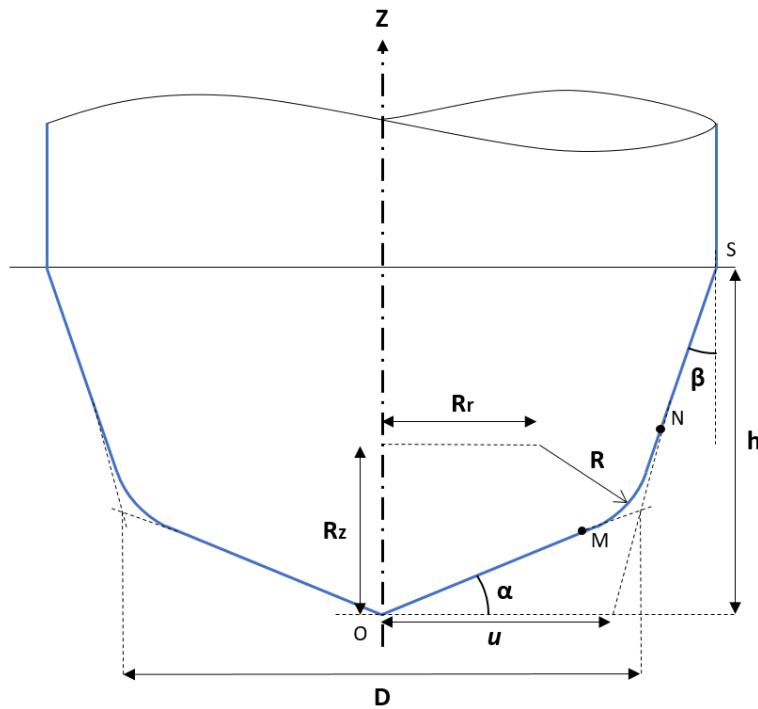


Figure 18: General tool geometric parameters

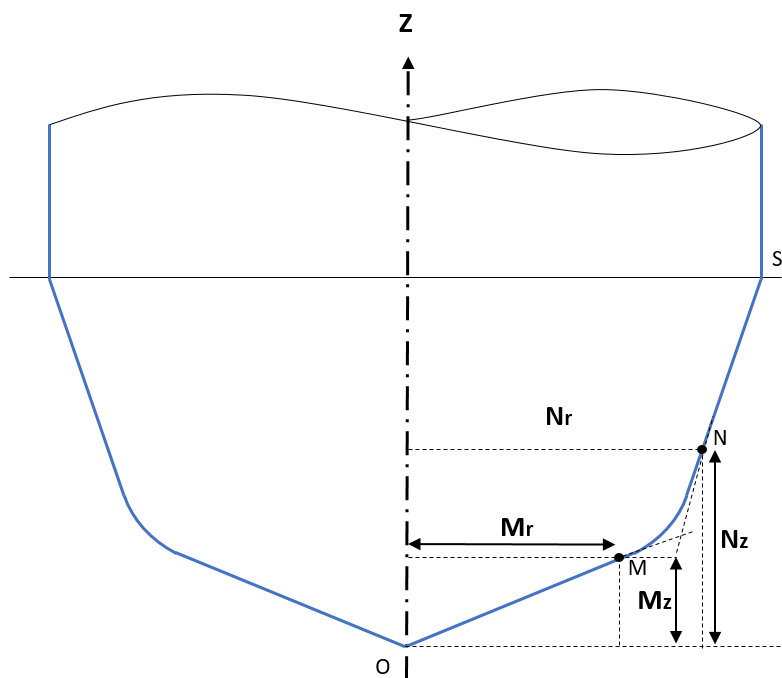


Figure 19: General tool offset parameters

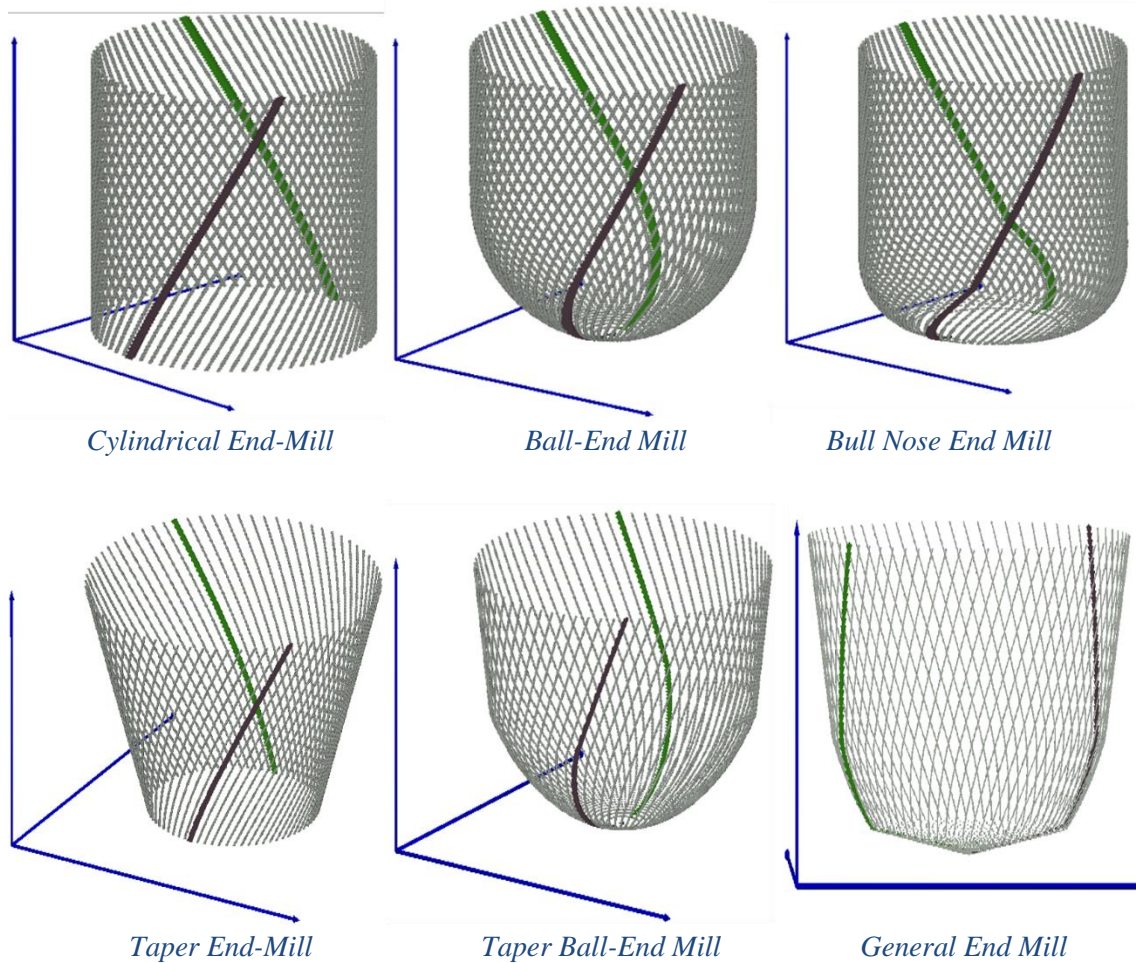
These constraints have to be followed otherwise the tool geometry is no longer physically feasible.

3.2.3.2 Discretization of the Surface Points

The discretization is done as done in the previous case. Coordinates of different infinitesimal cutting points in TCS are expressed as:

$$\begin{cases} xx_{tcs}(i,j) = r(z) \sin \Phi(z) \\ yy_{tcs}(i,j) = r(z) \cos \Phi(z) \\ zz_{tcs}(i,j) = z \end{cases}$$

Where $\Phi(z)$ is the radial immersion angle.



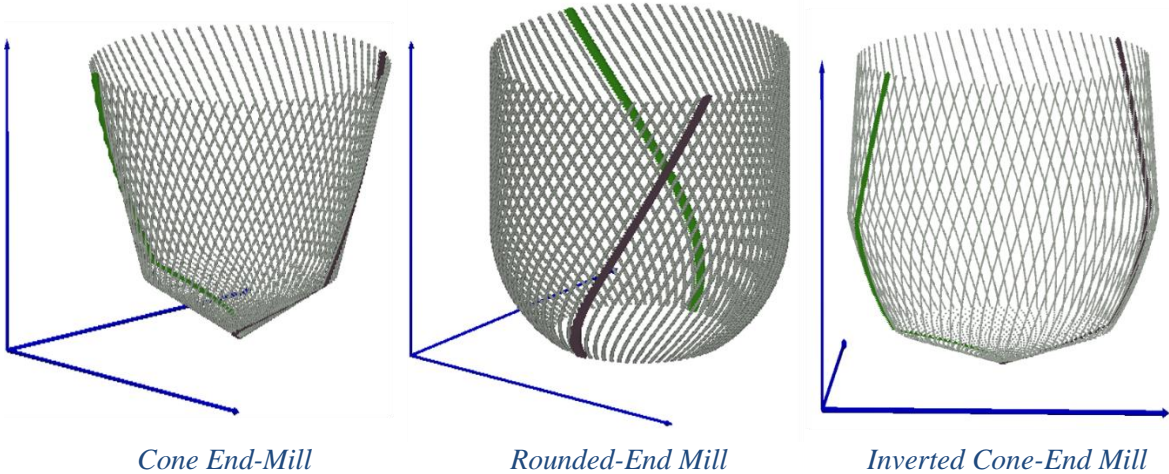


Figure 20: Tool discretization

3.2.3.3 Determination of the engagement region

In this model since tool center is not defined, the tool base point is taken as the reference point to keep track of the tool position in Global Coordinate System. Let us assume that the tool base at $time = 0$ is at $B_0 = [0, 0, -d_{actual}]$ in Global Coordinate System.

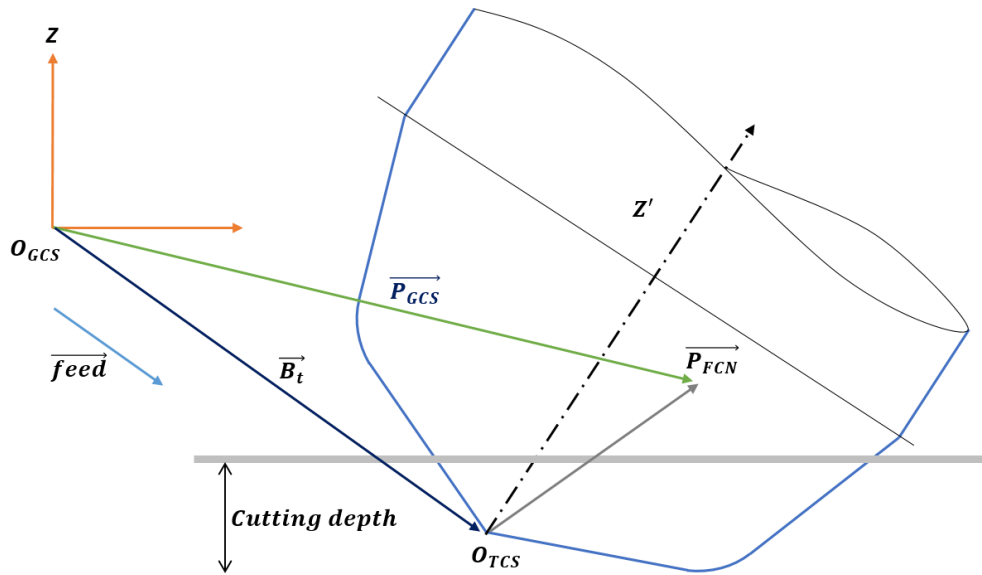


Figure 21: Determination of Engagement Region for general milling tool

Where,

$$d_{actual} = \text{cutting depth} + z_{min} \text{ (see section 3.1.ii)}$$

At $time = t$, the tool base vector is:

$$B_t = B_0 + \overrightarrow{\text{feed}} \times t$$

Let the coordinate of any point in FCN be $[xx_{fcn}(i,j), yy_{fcn}(i,j), zz_{fcn}(i,j)] = \overrightarrow{P_{FCN}}(i,j)$, then, the coordinate of any point in Global Coordinate System can be written as:

$$\overrightarrow{P_{GCS}}(i,j) = \overrightarrow{P_{FCN}}(i,j) + B_t$$

Now the $\overrightarrow{P_{GCS}}(i,j)$ can be checked whether it lies within the workpiece geometry or not as:

If $\overrightarrow{P_{GCS}}(i,j) \cdot \hat{k} > 0$ then point does not lie in the cutting region (engagement region).

3.2.3.4 Defining chip dimensions

Chip length and chip width are a function of discretization parameters of the tool and do not depend on the direction or magnitude of the feed vector. On the other hand, chip thickness also depends on the feed vector. As discussed in section 3.2.2.2 that the chip thickness for a surface point is nothing but the component of \vec{s}_t along the surface normal vector at the point.

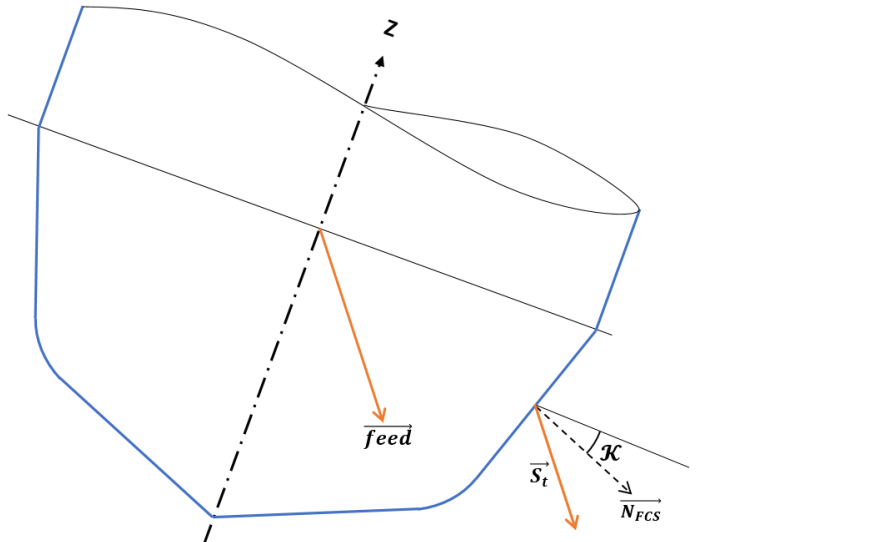


Figure 22: Chip thickness for general milling tool

The normal vector of any point P can be written as (see figure 19):

$$\overrightarrow{N_{TCS}} = [\sin \kappa \sin \Phi, \sin \kappa \cos \Phi, -\cos \kappa]$$

in FCN coordinate system:

$$\begin{Bmatrix} N_x \\ N_y \\ N_z \end{Bmatrix}_{FCN} = [T] \begin{Bmatrix} \sin \kappa \sin \Phi \\ \sin \kappa \cos \Phi \\ -\cos \kappa \end{Bmatrix}_{TCS}$$

Chip thickness of point P can be written as:

$$t_n(S_t, \Phi, \mathcal{K}) = S_t \times \frac{\overrightarrow{N_{FCN}} \cdot \overrightarrow{feed}}{|\overrightarrow{feed}|}$$

3.3 Determination of engagement region for non-planar surfaces

In this model, the engagement region was determined for different kind of surfaces. Apart from the check for surface normal vector of the point, (see section 3.2.2.1.2) additional surface related checks are discussed in this section. The checks are defined for a point P in Global Coordinate System i.e. $\overrightarrow{P_{GCS}}(i, j)$. (see section 3.2.3.3)

Let $\overrightarrow{P_{GCS}}(i, j) = [P_x, P_y, P_z]$

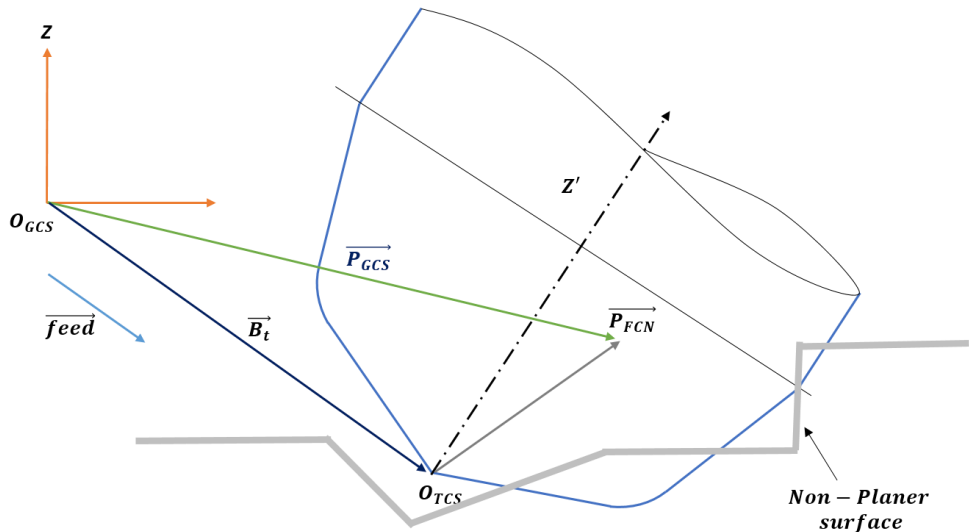


Figure 23: Engagement region for non-planar surfaces

There are many surfaces possible other than planar surface, this model incorporates some surfaces for example slope, edge, step, corner. The engagement zone checks for these surfaces are:

3.3.1 Slope

3.3.1.1 Case 1: Tool is going inside the slope

The point $P(i, j)$ does not lie in the engagement region in the following conditions:

- 1) If $P_x \leq X$ and $P_z > 0$
- 2) If $P_x > X$ and $P_z > (P_x - X) \tan \alpha$

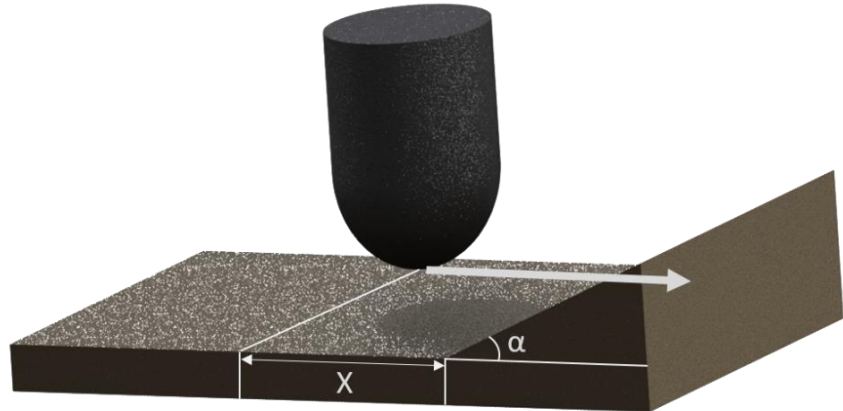


Figure 24: Geometry - slope

3.3.1.2 Case 2: Tool is moving parallel to the slope

The point $P(i, j)$ does not lie in the engagement region in the following conditions:

- 1) If $P_y \leq Y$ and $P_z > 0$
- 2) If $P_y > Y$ and $P_z > (P_y - Y) \tan \beta$

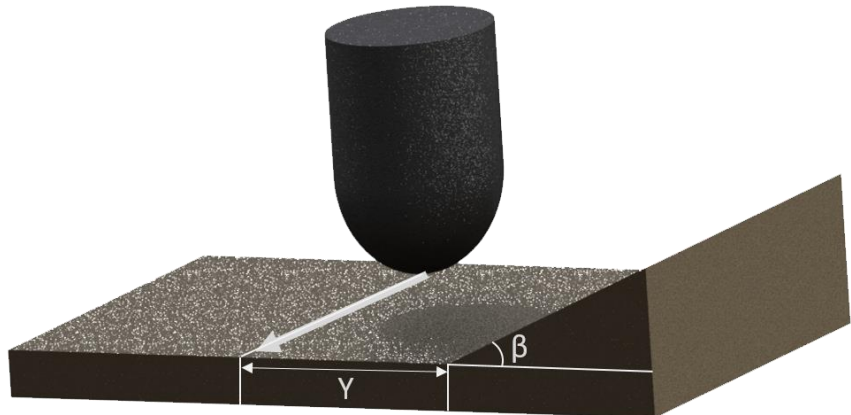


Figure 25: Geometry - slope

3.3.2 Edge

The point $P(i, j)$ does not lie in the engagement region in the following conditions:

- 1) If $P_y \leq Y$
- 2) If $P_y > Y$ and $P_z > (P_y - Y) \tan \beta$

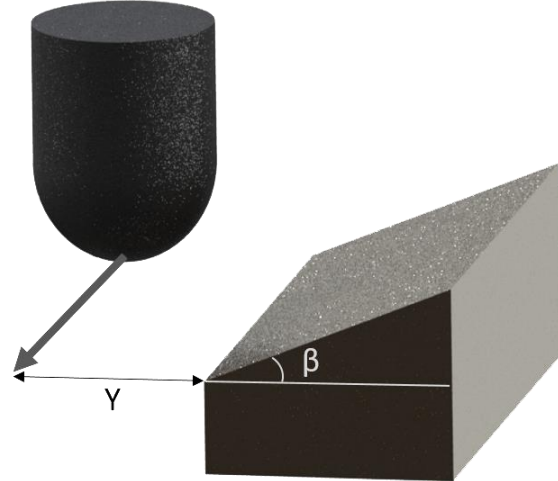


Figure 26: Geometry - edge

3.3.3 Step

The point $P(i,j)$ does not lie in the engagement region in the following conditions:

- 1) If $P_x \leq X$ and $P_z > 0$
- 2) If $P_x > X$ and $P_z > Z$

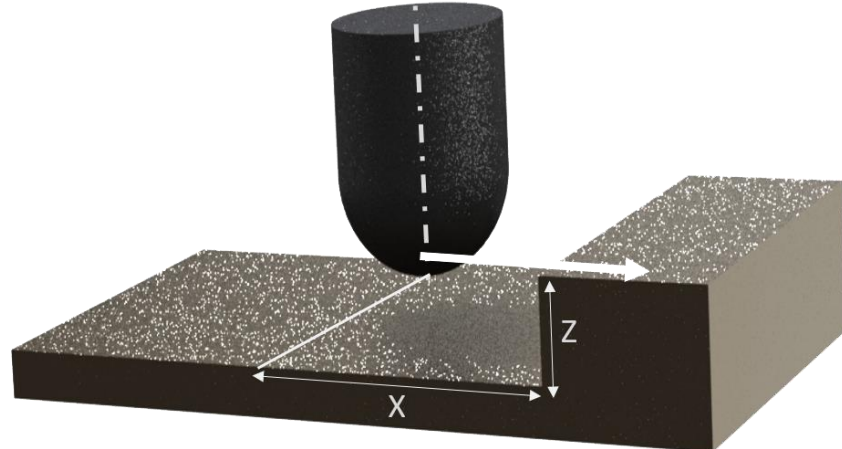


Figure 27: Geometry - step

3.3.4 Corner

The point $P(i,j)$ does not lie in the engagement region in the following conditions:

- 1) If $P_x \leq X$ and $P_z > 0$
- 2) If $P_x > X$ and $P_z > (P_x - X) \tan \alpha$
- 3) If $P_y \leq Y$ and $P_z > 0$
- 4) If $P_y > Y$ and $P_z > (P_y - Y) \tan \beta$

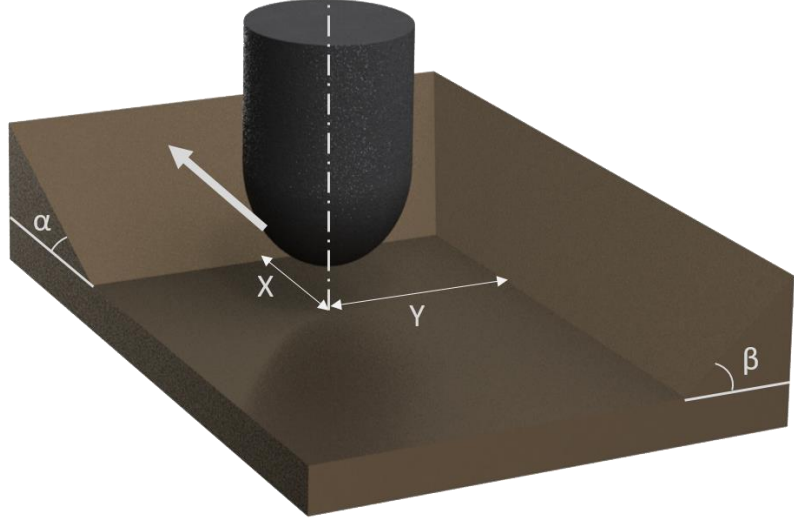


Figure 28: Geometry - corner

3.3.5 User Defined Surface

The model also provides an option to develop user defined surfaces in piecewise linear fashion (fig 26).

The point $P(i, j)$ does not lie in the engagement region in the following conditions:

- 1) If $P_y \leq Y$
- 2) If $P_y > Y$ and $P_z > Z(x)$ (*from user defined surface*)

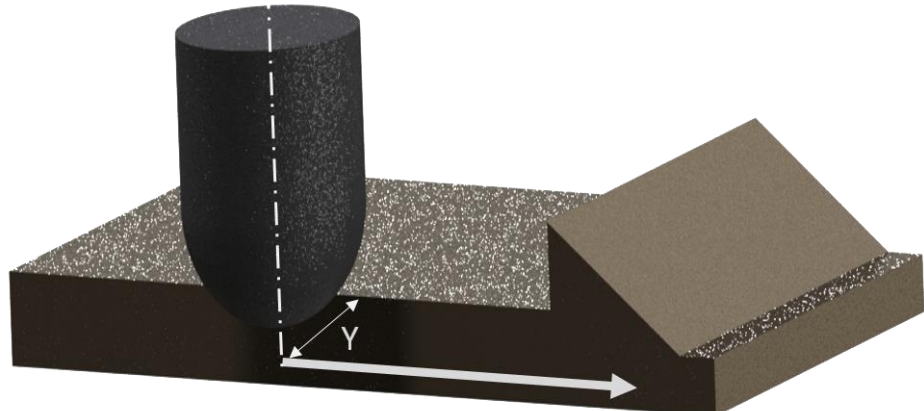


Figure 29: Geometry - custom surface

3.4 Step Over and Surface Roughness

The surface roughness is an important factor for any finished surface. Some applications require very smoother finish whereas some applications do not. For smoother finished surfaces the number of times the tool cuts the workpiece is large. Hence, there is a tradeoff between the

roughness and the time to machine the workpiece. The first cut, following cut, step over and scallop height are defined as:

- i. **First Cut:** the workpiece is being machined for the first time
- ii. **Following Cut:** the workpiece is already being cut
- iii. **Step over:** It is the distance between the adjacent cutting step in the cross-feed axis (C). Step over can take positive as well as negative value depending on the direction of uncut material with the following cut.
- iv. **Scallop height (h_s):** Measure of surface roughness, it is the height of the remaining workpiece material between two consecutive cuts.

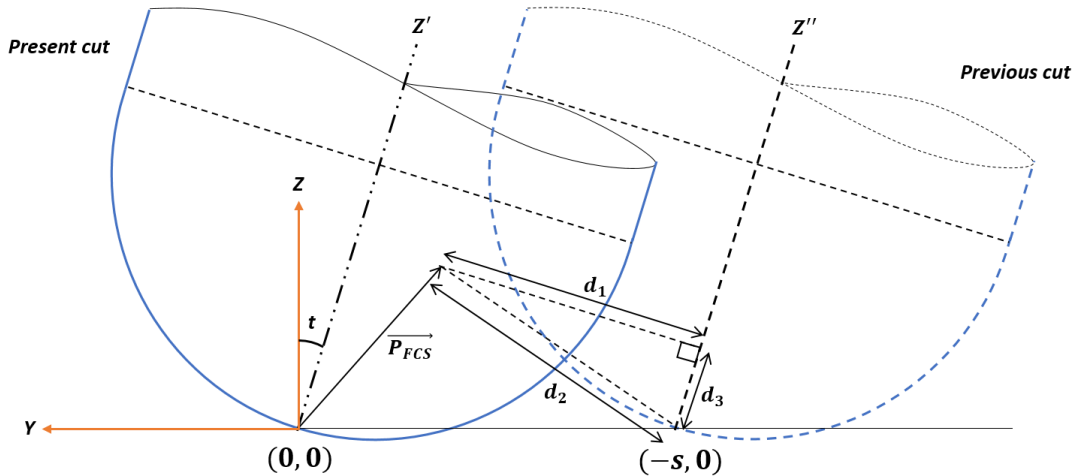


Figure 30: Step over representation

The engagement region differs in first cut and following cut, so as the forces experienced by the tool. The engagement zone in the following cut and the h_s change with tilt angle and step over but lead angle does not have any effect on them. In the following cut, additional checks are done on any point P in Feed Coordinate System (see section 3.2.3.3).

$$\overrightarrow{P_{FCN}}(i,j) = [P_x, P_y, P_z]$$

Consider tool tip to be origin in y-z plane. For step over (s), the previous cut tool tip position is $(-s, 0)$. Let d_1 be the distance of point P from the tool axis of the previous cut, d_2 be the distance of point P from tool tip of the previous cut (figure 27).

Equation of tool axis of the previous cut:

$$z = m(y + s) \text{ Where, } m = \tan(90^\circ + t), t = \text{tilt angle}$$

Then,

$$d_1 = \left| \frac{P_z - m(P_y + s)}{\sqrt{1 + m^2}} \right| \text{ and } d_2 = \sqrt{(P_y + z)^2 + P_z^2}$$

d_1, d_2 and d_3 form a right-angled triangle, d_3 can be calculated as:

$$d_3 = \sqrt{d_2^2 - d_1^2}$$

Since, tool profile is known i.e. radius is known as a function of z.

If $d_1 \leq \text{radius}(d_3)$ then the point is not present and has already been cut in the previous cut and won't be present in the engagement zone.

Scallop height can be determined using geometry of the tool. h_s is a function of step over, radius of tool, and tilt angle:

$$h_s = \begin{cases} R - \sqrt{R^2 - \frac{s^2}{4}} & \text{if } s \leq 2R \cos t \\ R - \sqrt{R^2 - (R - s \cos t)^2} \cos t - (R - s \cos t) \sin|t| & \text{if } s > 2R \cos t \end{cases}$$

In the case when $s \leq 2R \cos t$, h_s only depends on the tool geometry and not on tilt angle.

CHAPTER 4

RESULTS AND VALIDATION

4.1 Results Based on Model 1

In order to verify the model, data generated for forces and torque are compared with data given in published literature [4][10]. The simulation has been done for the given value of input parameter in literature. After the validation of the model, more simulations have been done to understand the results generated in 5-axis milling process. Case 1-3 are taken for the validation of the model. Case 4 is taken as a general case for three cutting edges to explain the results qualitatively.

4.1.1 Case 1: Force Simulation for $N_f = 1$, $lead = tilt = 0$

Input parameters: *Diameter, D = 19.05mm; Helix angle, $i_0 = 30^0$; Rake angle, $\alpha = 0^0$; Number of flukes, $N_f = 1$; Spindle speed, n=269 rpm; Table feed, $S_t = 13.6652 \text{ mm/min}$; Depth of cut = 6.35mm; Lead angle = 0^0 ; Tilt angle = 0^0*

In the simulated results of forces in FCN, since the ball-end tool has only 1 cutting edge, the F force is negative when the tool enters the cutting zone, in this region the chips are applying a force in negative F direction. As the tool rotates further, a part of tool crosses the 90^0 zone, and chips on that side start applying force in opposite F direction, giving a decrement (in magnitude) in the net force. The cutting edge further crosses that region and force from the chips starts getting a net positive value in F direction. For the N direction, force does not change after it reaches to a maximum value which is needed to keep the tool in place while rotation. As the cutting edge starts coming out of the cutting region all the three components start tending to zero.

In the simulated result of torque, the value of torque first increases, reaches to a maximum and then decreases to zero at angle around 200^0 . As the tool comes out of the cutting zone completely.

Figure 31: Published result for case 1 [4]

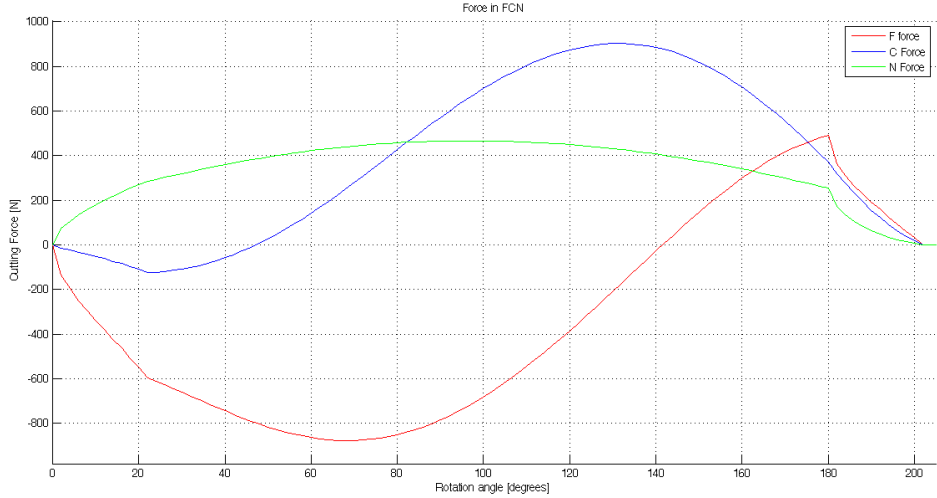


Figure 32: Simulated forces for case 1

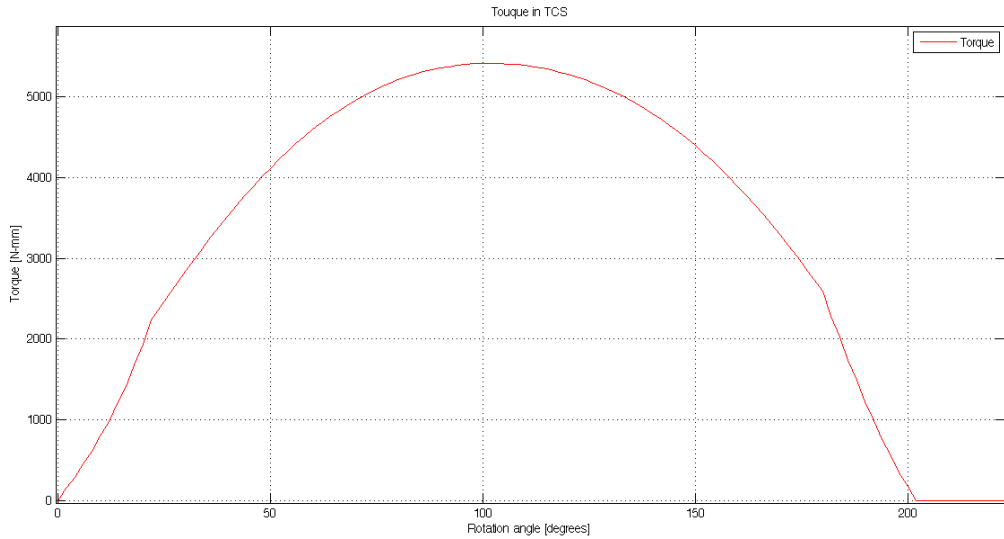


Figure 33: Simulated torque for case 1

4.1.2 Case 2: Force Simulation for $N_f = 2$, $lead = 30^\circ$, $tilt = 30^\circ$

Input parameters: *Diameter, D = 12mm; Helix angle, $i_0 = 30^\circ$; Rake angle, $\alpha = 8^\circ$; Number of flukes, $N_f = 2$; Spindle speed, $n=500 \text{ rpm}$; Table feed, $S_t = 100 \text{ mm/min}$; Depth of cut = 1.5mm; Lead angle = 30° ; Tilt angle = 30°*

In case 2, lead and tilt angles are not zero, i.e. one of the cutting edge is already in the cutting zone and hence forces and torque do not start from zero. The force and torque curves

repeat themselves two times within 360^0 rotation, this is because there are two cutting edges and each gives the same result after a phase lag of 180^0 .

The results obtained from case 1 and case 2 are consistant with the results given in published paper [10]. The error present in the results is primarily due to multiple shortcomings of the model used, which are discussed in section 5.1 in this report.

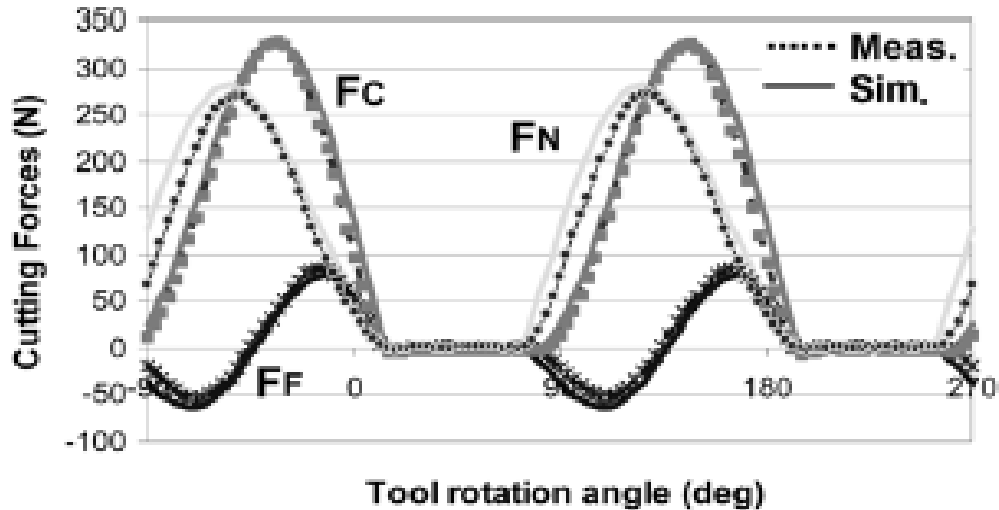


Figure 34: Published result for case 2 [10]

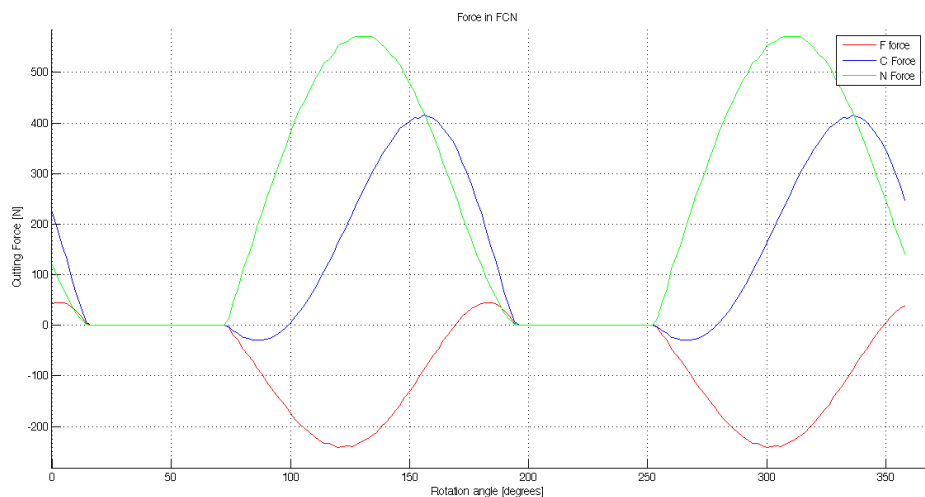


Figure 35: Simulated forces for case 2

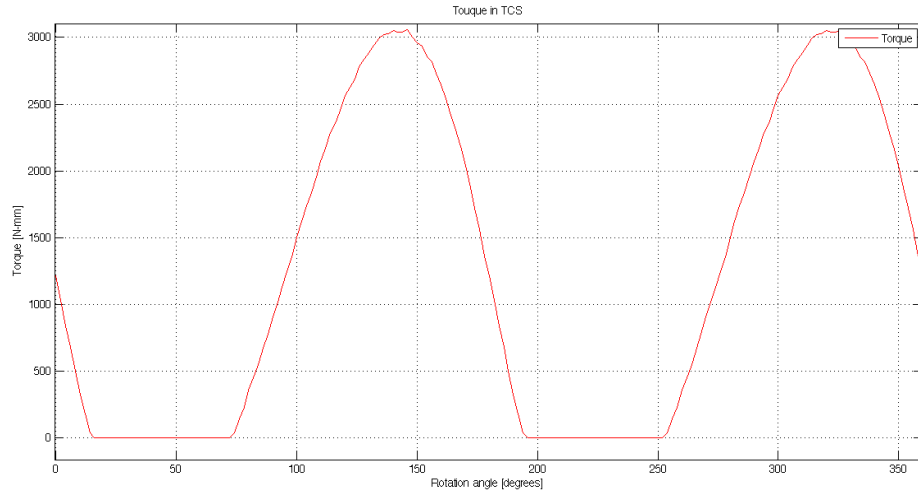


Figure 36: Simulated Torque for case 2

4.1.3 Case 3: Force Simulation for $N_f = 2$, $\text{lead} = 15^0$, $\text{tilt} = 0^0$

Input parameters: *Diameter, D = 12mm; Helix angle, $i_0 = 30^0$; Rake angle, $\alpha = 8^0$; Number of flukes, $N_f = 2$; Spindle speed, $n=500 \text{ rpm}$; Table feed, $S_t = 100 \text{ mm/min}$; Depth of cut = 3mm; Lead angle = 15^0 ; Tilt angle = 0^0*

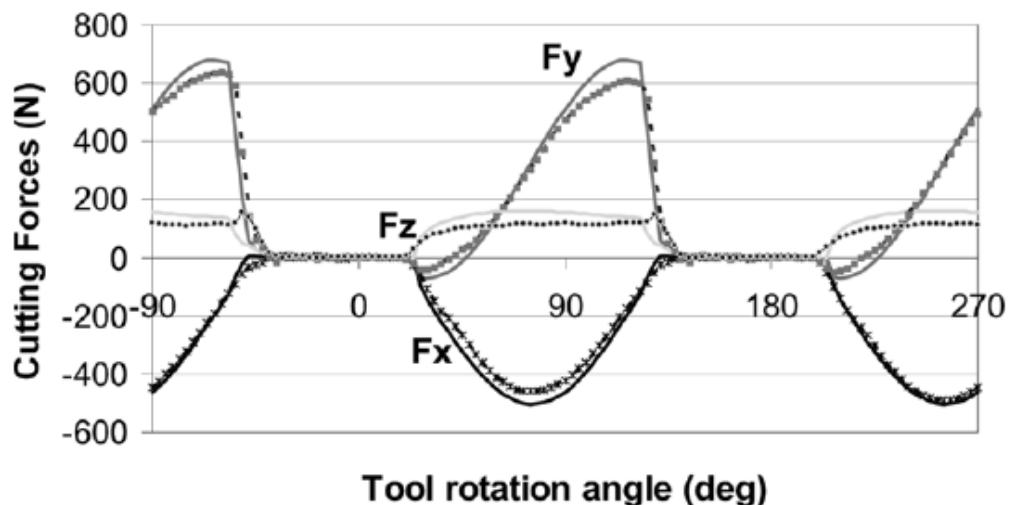


Figure 37: Published result for case 3 [10]

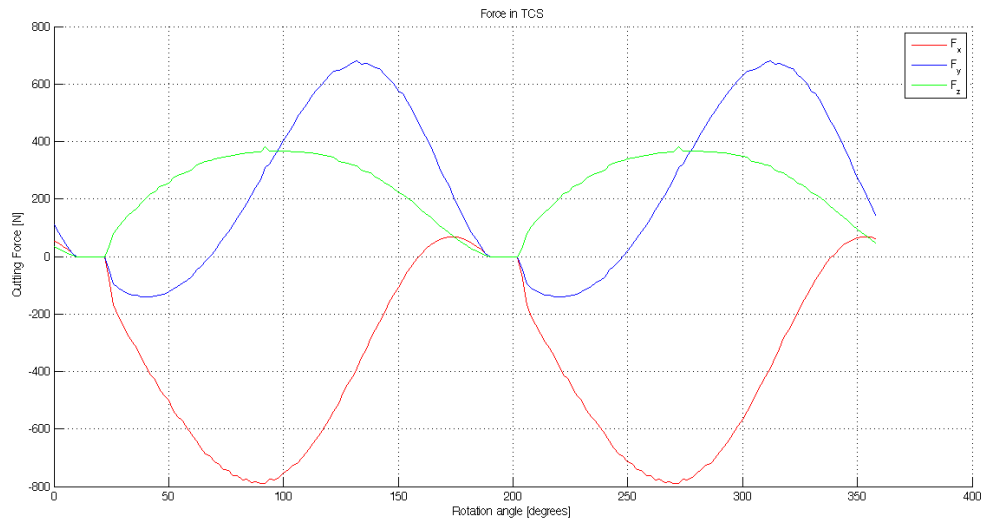


Figure 38: Simulated cutting force for case 3

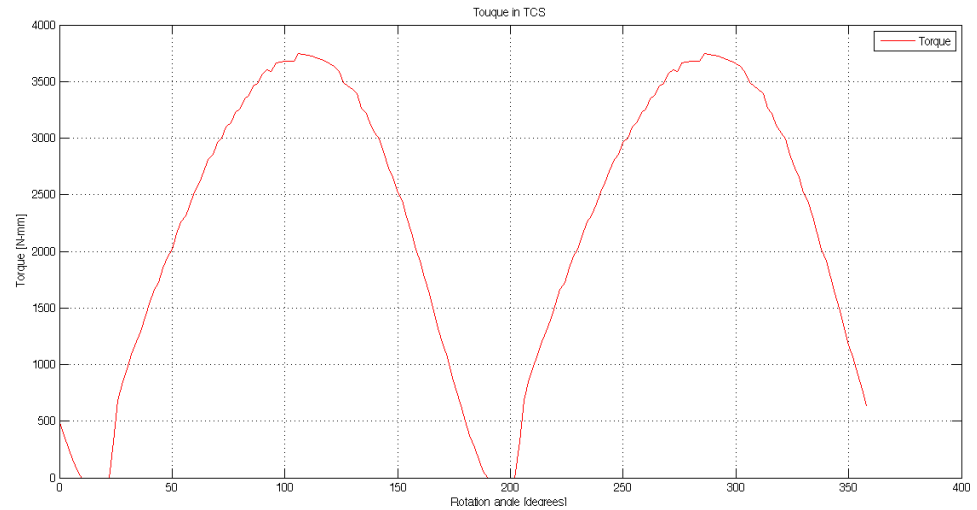


Figure 39: Simulated torque for case 3

4.1.4 Case 4: Force Simulation for $N_f = 3$, $lead = 20^0$, $tilt = 10^0$

Input parameters: *Diameter, D = 20mm; Helix angle, $i_0 = 30^0$; Rake angle, $\alpha = 0^0$; Number of flukes, $N_f = 3$; Spindle speed, $n=500$ rpm; Table feed, $S_t = 100$ mm/min; Depth of cut = 10mm; Lead angle = 20^0 ; Tilt angle = 10^0*

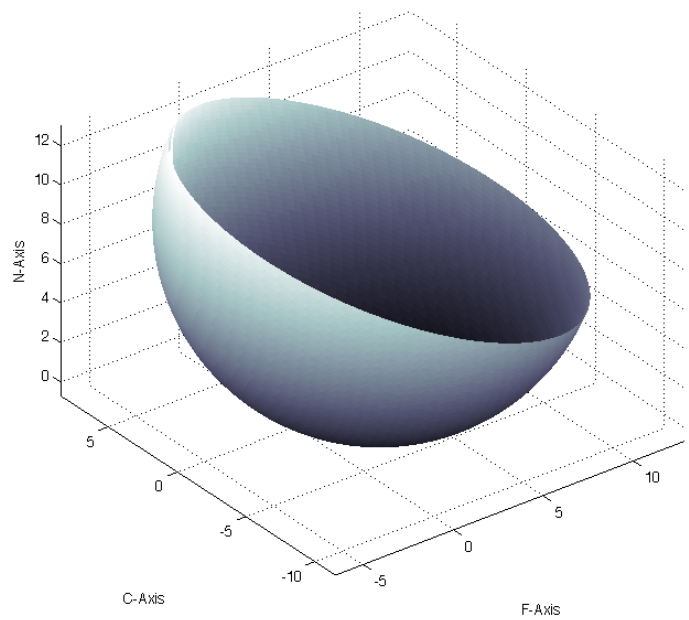


Figure 40: Ball-end cutting tool profile for 20^0 lead, 10^0 Tilt angle

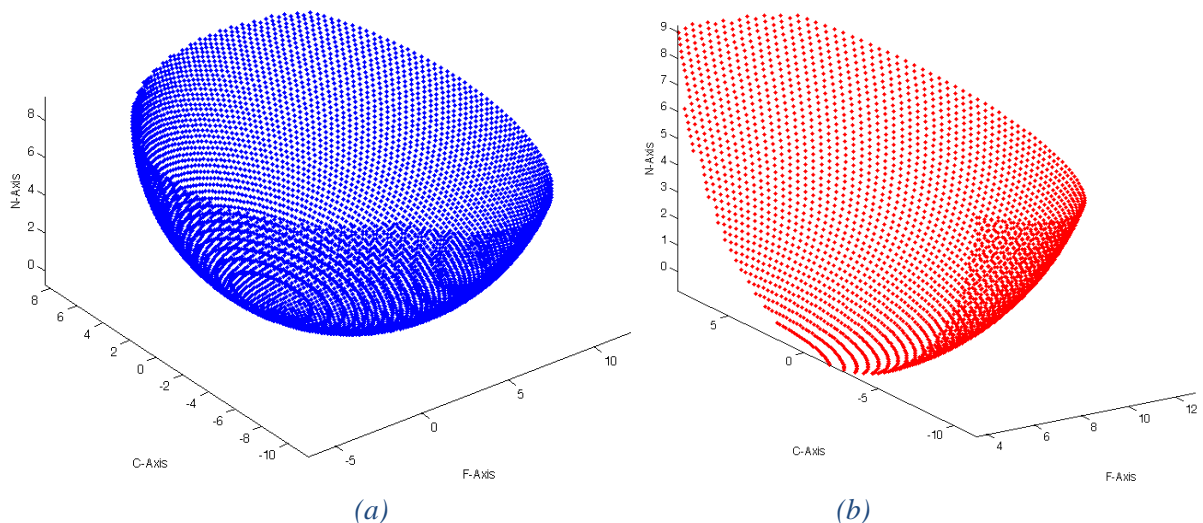


Figure 41: Discretized point profile for cutting tool (a) below depth of cut & (b) cutting zone

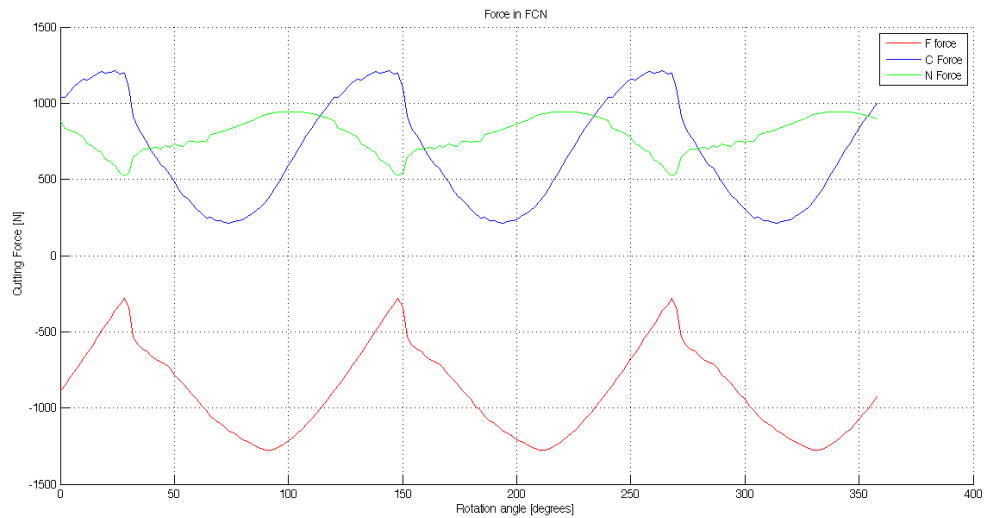


Figure 42: Cutting force in FCN coordinate system

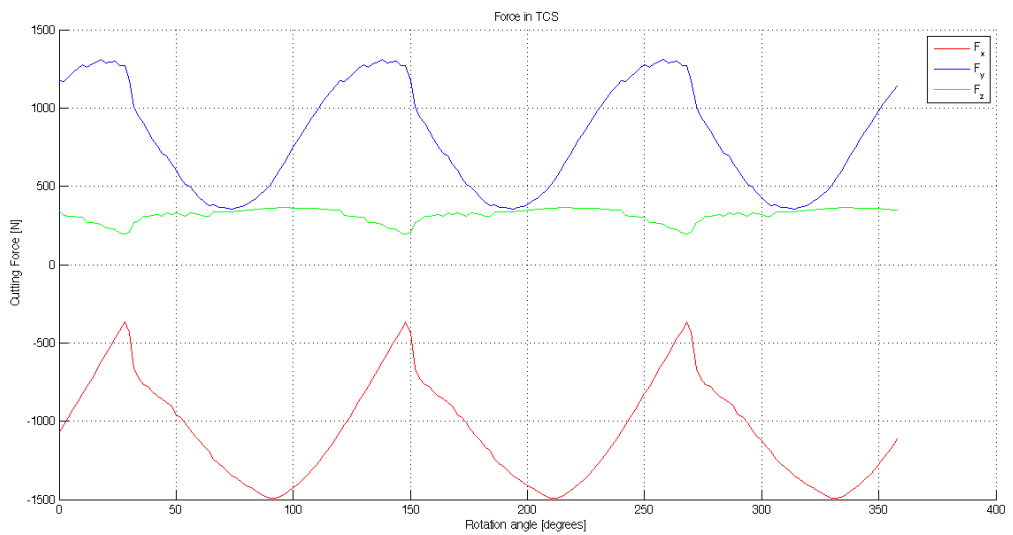


Figure 43: Cutting force in FCN coordinate system

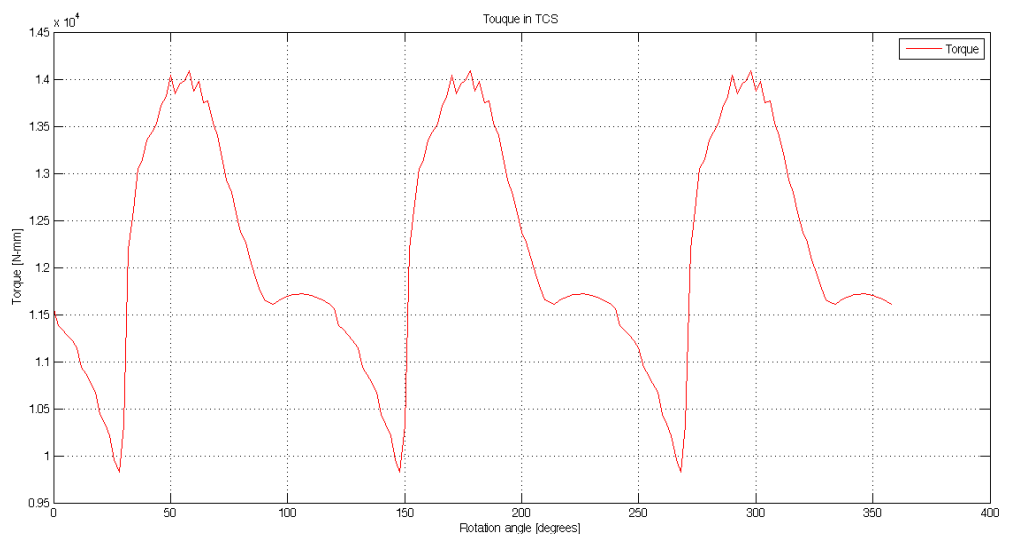


Figure 44: cutting tool discretized point profile lying in cutting zone

Forces and torque in FCN and TCS shows periodicity after a period of 120^0 . In general, the n cutting edge tool has $360/n^0$ axis of symmetry as a result the graph will be having periodicity of the same rotational angle.

4.1.5 Case 5: Lead and Tilt optimization for $N_f = 2$, depth of cut = 2.5mm

The maximum cutting force experienced by the tool is plotted against lead and tilt angles. The range for lead and tilt angle is selected from -50^0 to 50^0 and -20^0 to 20^0 . Values of lead angles are chosen to minimize the net cutting force in x-y direction under the given machining conditions. The graph given below represents the variation of F_{xy_max} with lead and tilt angles.

Input parameters: Diameter, $D = 20\text{mm}$; Helix angle, $i_0 = 30^0$; Rake angle, $\alpha = 5^0$; Number of flukes, $N_f = 2$; Spindle speed, $n = 500 \text{ rpm}$; Table feed, $S_t = 100 \text{ mm/min}$; Depth of cut = 2.5mm.

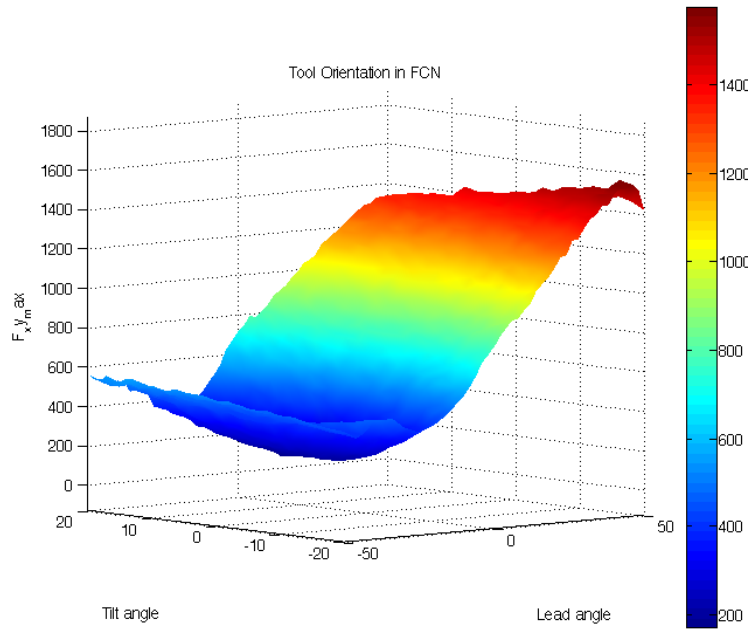


Figure 45: Variation of F_{xy_max} with lead and tilt angles for case 5

Lead and tilt angles for minimum force on the cutting tool are -20^0 and 4^0 respectively.

4.1.6 Case 6: Lead and Tilt optimization for $N_f = 2$, depth of cut = 5mm

Input parameters: Diameter, $D = 20\text{mm}$; Helix angle, $i_0 = 30^0$; Rake angle, $\alpha = 5^0$; Number of flukes, $N_f = 2$; Spindle speed, $n = 500 \text{ rpm}$; Table feed, $S_t = 100 \text{ mm/min}$; Depth of cut = 5mm.

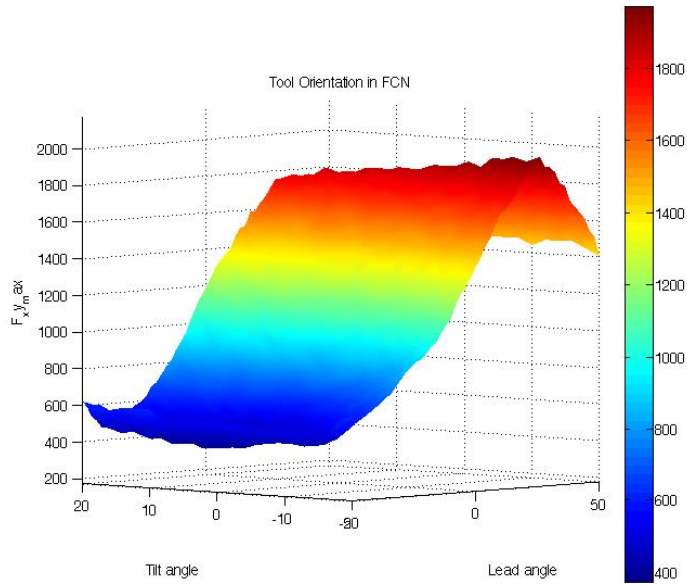


Figure 46: Variation of $F_{xy\max}$ with lead and tilt angles for case 6

Lead and tilt angles for the minimum shear force on the cutting tool are -34^0 and 8^0 respectively.

Comparing case 5 and case 6, it can be seen that as we increase the depth of cut, the lead angle also needs to be increased (magnitude) to get the minimum value of F_{xy_max} .

4.1.7 Reason for Abruptness in Plots

The force and torque plots do not have a smooth transition and have some within abruptness. In this model the curve of the cutting edge is considered as piecewise defined straight lines. This roughness arises due to abrupt entry and exit of discretized set of points into the cutting zone.

This abruptness of the plots can be minimized by reducing the axial incremental value (dz). Taking smaller values of dz will increase the computational cost. Hence, there is a tradeoff between result accuracy and computational time.

Prediction of lead and tilt angles for the minimization of maximum shear force is also dependent on the axial and radial incremental values, but, in this case maximum value of shear force is required which is not much affected by the lowering of dz . It is represented in figure 26 and figure 27. Lowering the value of dz reduces the abruptness of the curve but does not affect the maximum values of cutting force.

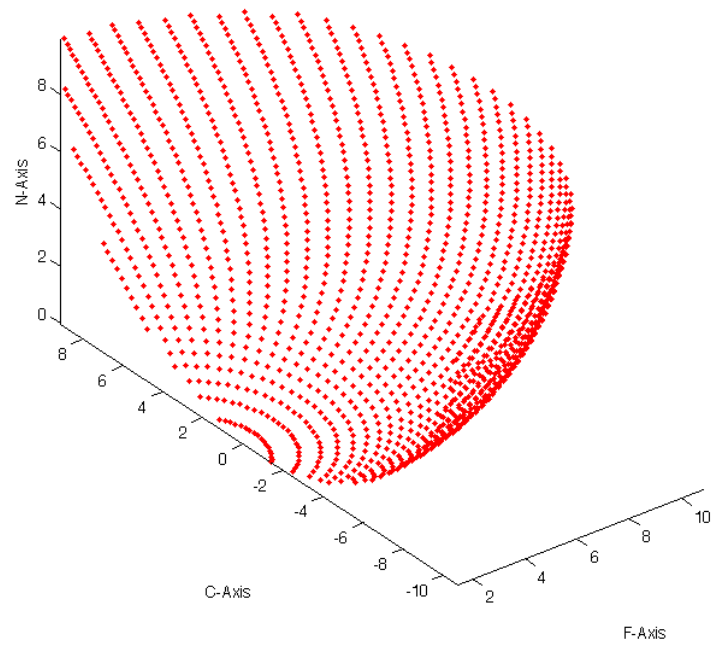


Figure 47: Representation of abrupt entry and exit into the cutting zone



Figure 48: Cutting forces for 20 axial divisions



Figure 49: Cutting forces for 50 axial divisions

4.2 Results Based on Model 2

Model 2 deals with only ball-end toll but the table feed can also take a vertical component. Simulation for three cases are done varying initial depth of cut (depth is changing as feed has a vertical component) and feed.

4.2.1 Case 1: $\text{depth of cut} = 10\text{mm}$, $\overrightarrow{\text{feed}} = -100\hat{k} \text{ mm/min}$

Input parameters: *Diameter, D = 20mm; Helix angle, $i_0 = 30^\circ$; Rake angle, $\alpha = 0^\circ$; Number of flukes, $N_f = 2$; Spindle speed, $n=500 \text{ rpm}$; Table feed, $S_t = -100\hat{k} \text{ mm/min}$; Depth of cut = 10 mm; Lead angle = 0° ; Tilt angle = 0°*

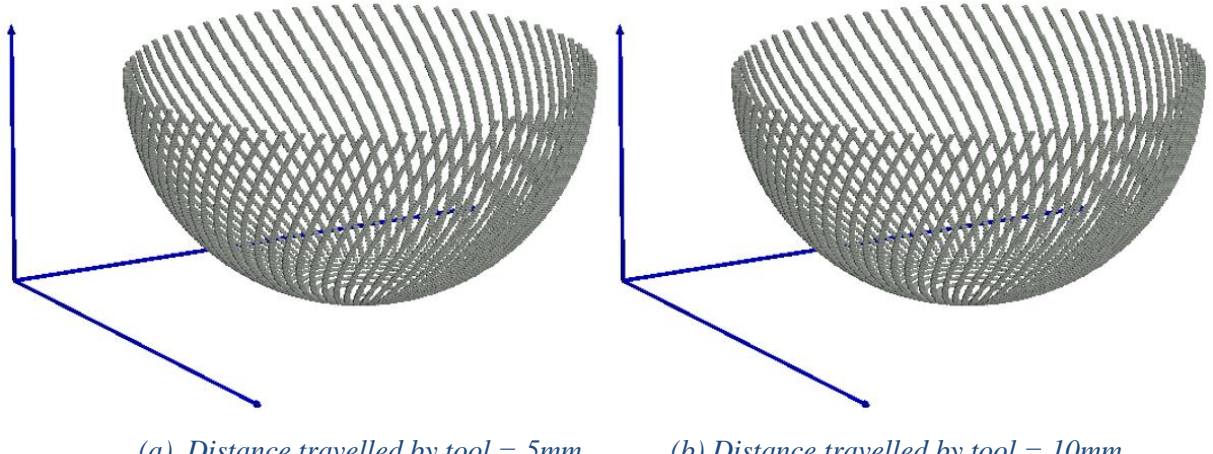


Figure 50: Engagement zone at different instances for case 1

In this case the initial depth of cut is same as R, since the lead and tilt angles are zero, cylindrical part of tool is not in the engagement zone. This results in static engagement region with time.

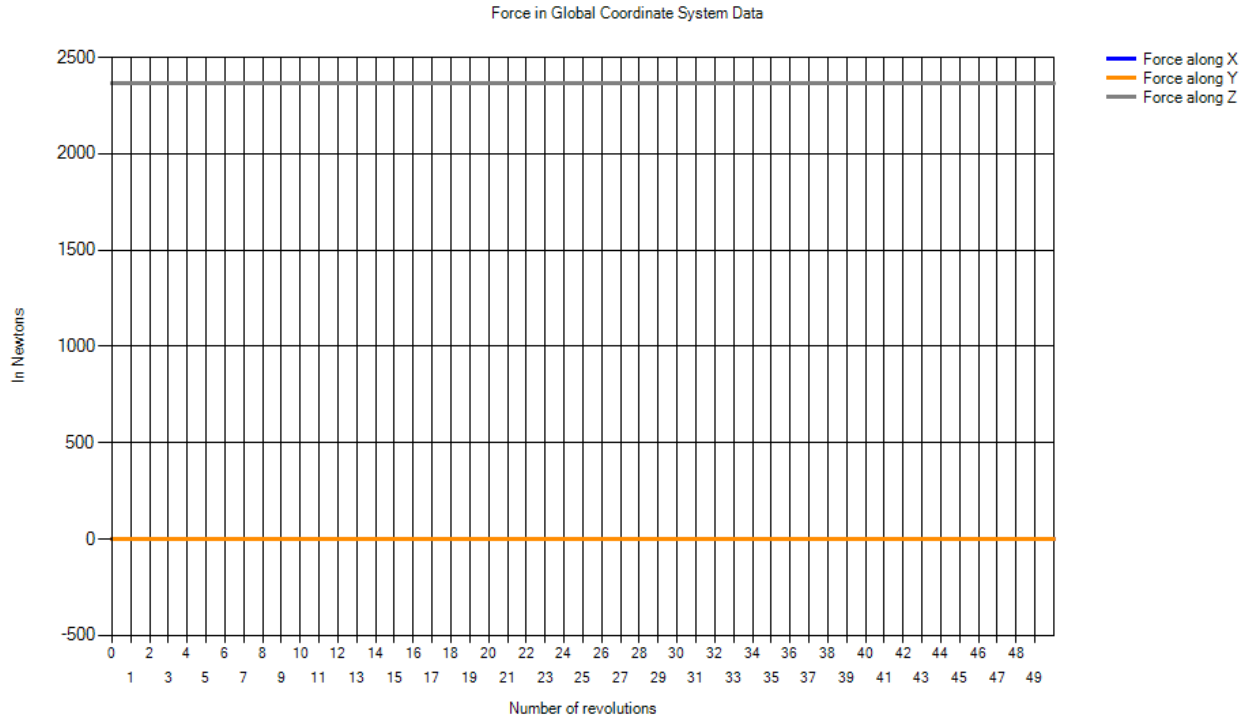


Figure 51: Forces in GCS for case 1

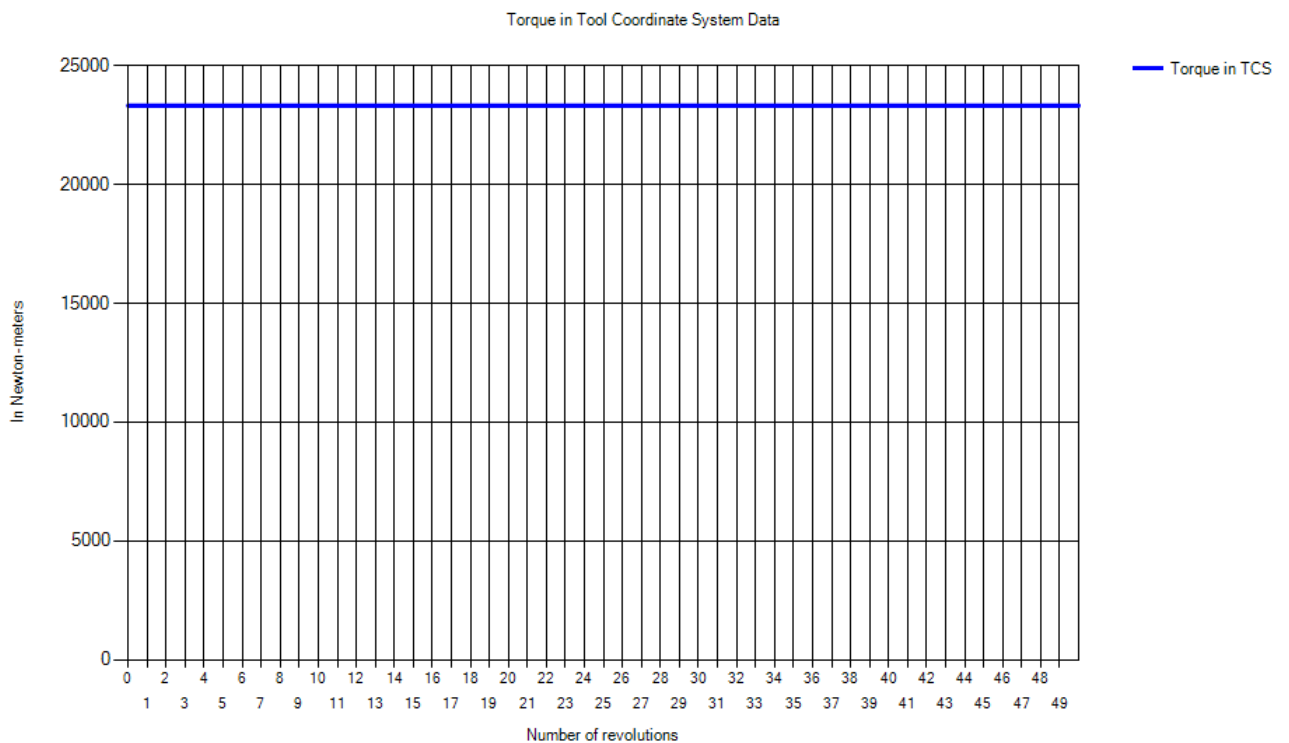


Figure 52: Torque in TCS for case 1

It can be seen from the figures that forces along X and Y direction are always zero and force along Z direction is always constant. This can be explained due to symmetry of the tool, since lead and tilt angles are zero the forces originated on both the edges are equal and opposite and cancel out to give zero resultant. Force along Z direction and the torque are constant since the engagement zone is static with respect to time.

4.2.2 Case 2: $\text{depth of cut} = 0\text{mm}$, $\overrightarrow{\text{feed}} = -100\hat{k} \text{ mm/min}$

Input parameters: *Diameter, $D = 20\text{mm}$; Helix angle, $i_0 = 30^\circ$; Rake angle, $\alpha = 0^\circ$; Number of flukes, $N_f = 2$; Spindle speed, $n=500 \text{ rpm}$; Table feed, $S_t = -100\hat{k} \text{ mm/min}$; Depth of cut = 0 mm; Lead angle = 0° ; Tilt angle = 0°*

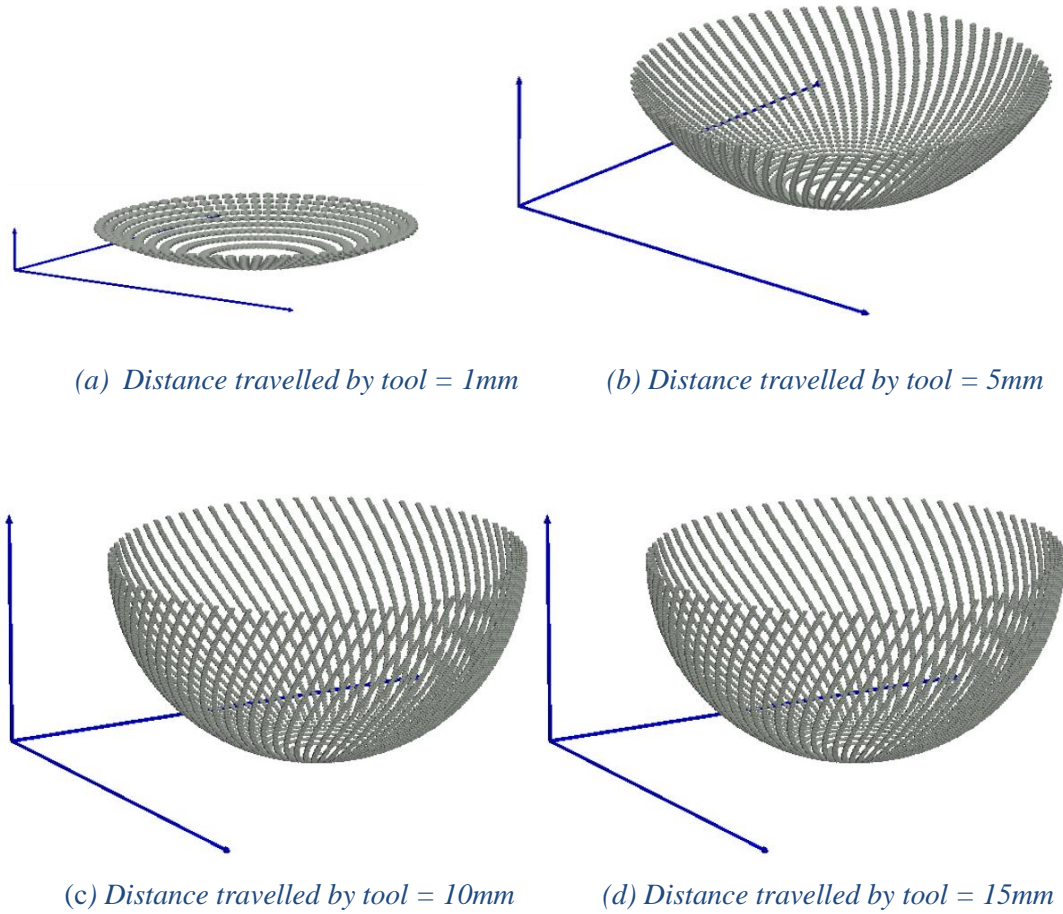


Figure 53: Engagement zone at different instances for case 2

In this case the initial depth of cut is zero and increasing with time due to vertical feed. The engagement region is increasing as the tool moves inside the workpiece.

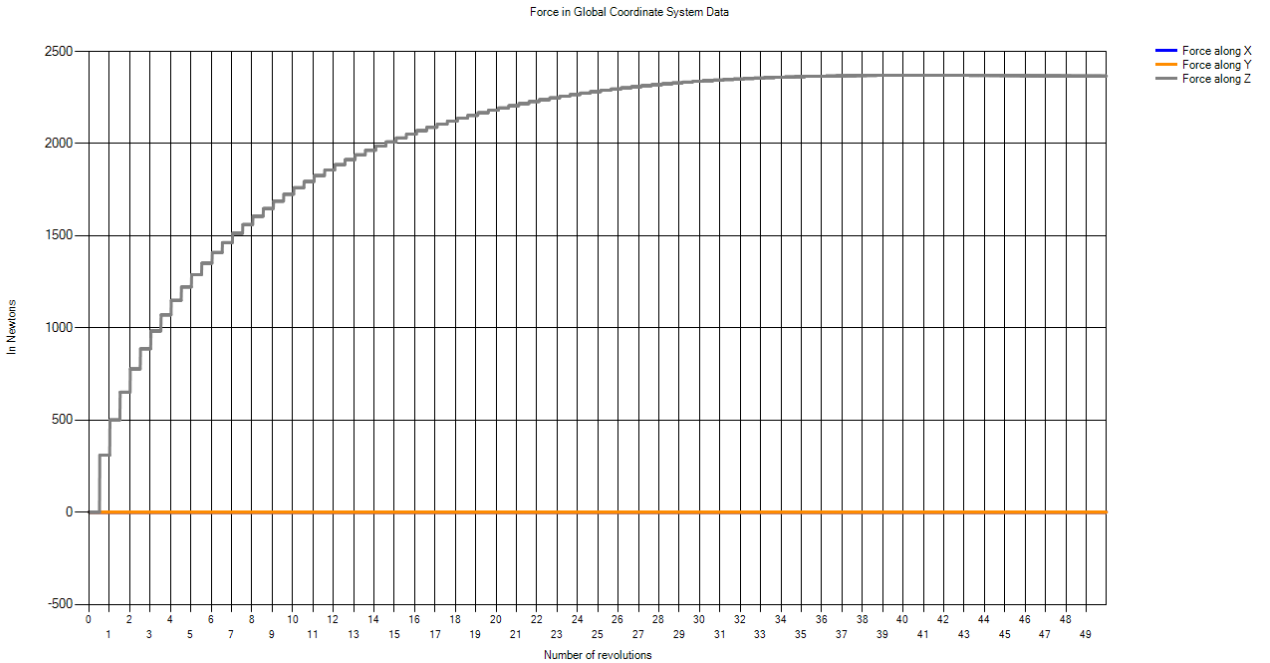


Figure 54: Forces in GCS for case 2

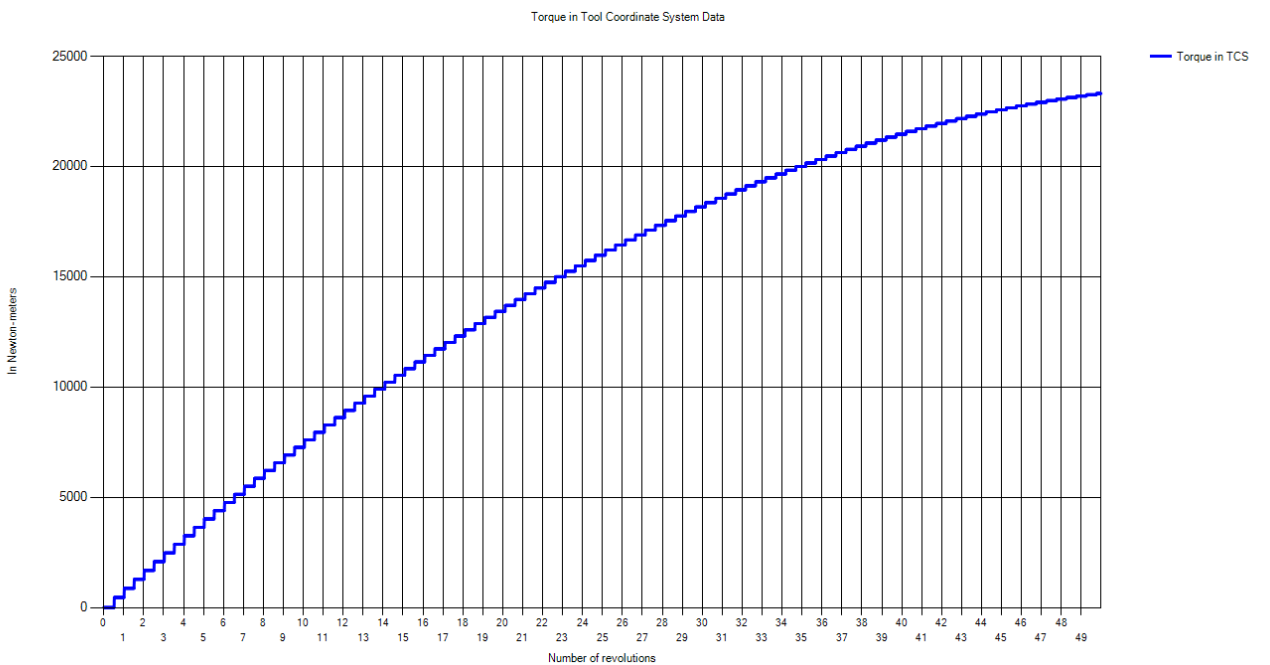


Figure 55: Torque in TCS for case 2

It can be seen from the figures that forces along X and Y direction are always zero and force along Z direction is increasing in a parabolic fashion and then becoming constant. This can be explained due to symmetry of the tool, since lead and tilt angles are zero the forces originated on both the edges are equal and opposite and cancel out to give zero resultant. Force along Z direction and the torque are increasing since the engagement zone is increasing due to feed along z axis.

4.2.3 Case 3: $\text{depth of cut} = 0\text{mm}$, $\overrightarrow{\text{feed}} = 100\hat{i} - 100\hat{k} \text{ mm/min}$

Input parameters: *Diameter, D = 20mm; Helix angle, $i_0 = 30^0$; Rake angle, $\alpha = 0^0$; Number of flukes, $N_f = 2$; Spindle speed, $n=500 \text{ rpm}$; Table feed, $S_t = 100\hat{i} - 100\hat{k} \text{ mm/min}$; Depth of cut = 0 mm; Lead angle = 0^0 ; Tilt angle = 0^0*

In this case the initial depth of cut is zero and increasing with time due to vertical component of the feed. The engagement region is increasing as the tool moves inside the workpiece.

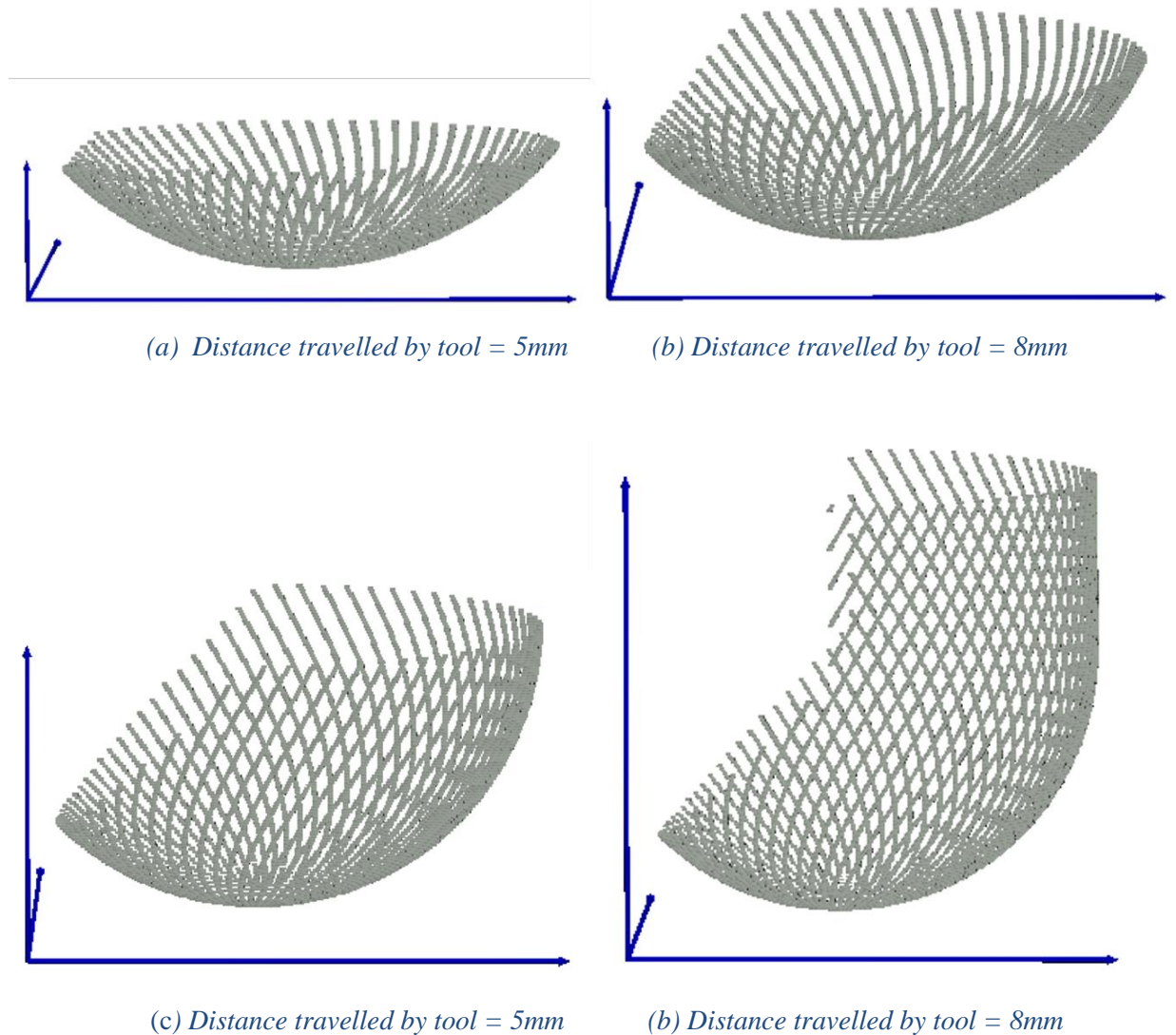


Figure 56: Engagement zone at different instances for case 3

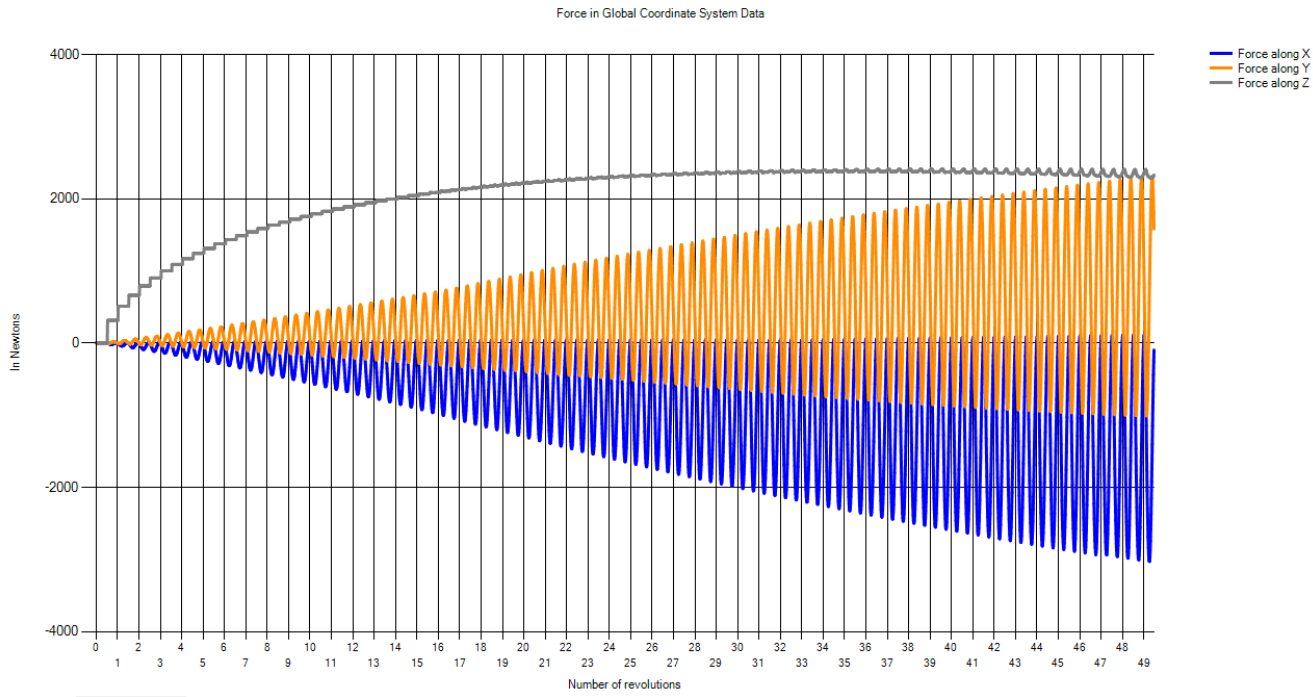


Figure 57: Forces in GCS for case 3

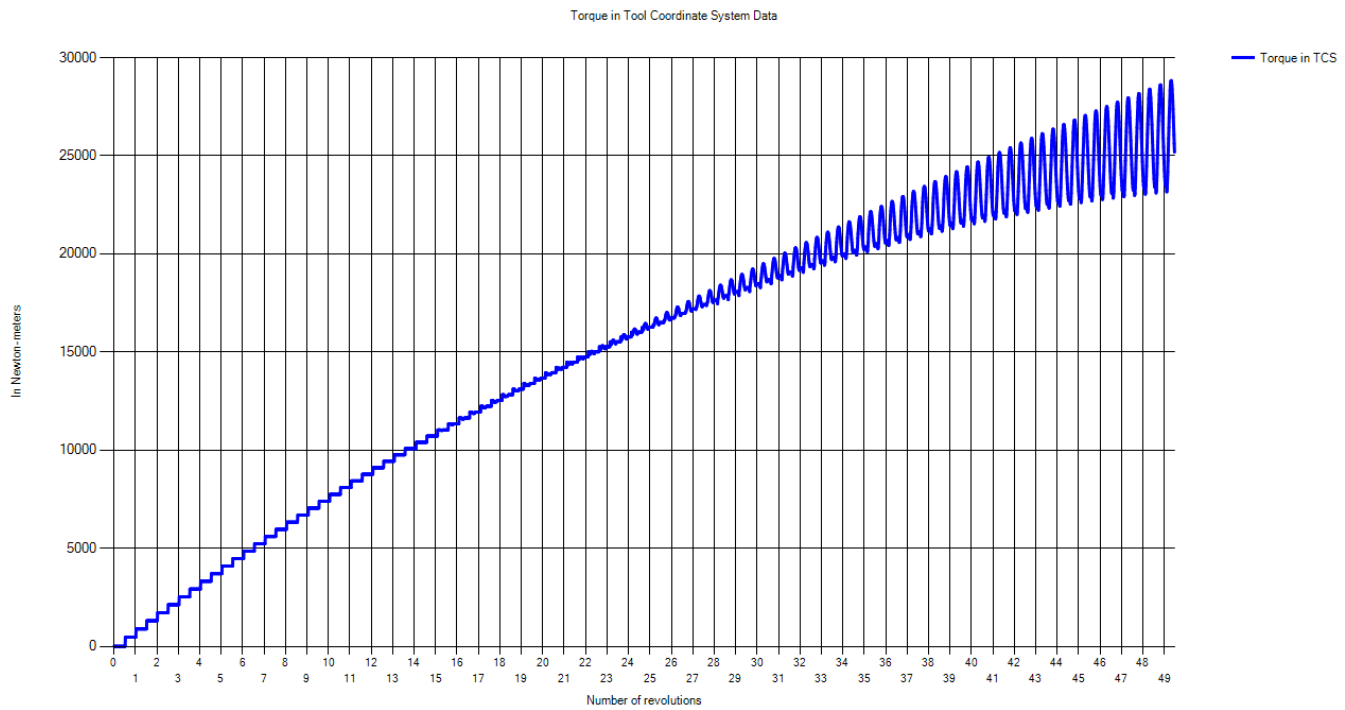


Figure 58: Torque in TCS for case

It can be seen from the figures that forces along X and Y direction are oscillating and force along Z direction is increasing in a parabolic fashion and then becoming constant. Force along Z direction and the torque is increasing since the engagement zone is increasing due to feed along z axis.

4.3 Results Based on Model 3

Model 3 is the most generic one. The model involves integration of general milling cutters and multiple non-planar surfaces. The model can do calculation for slotting as well as following cut.

Force and torque simulations were done for different kinds of tools for one complete revolution of the tool i.e. 360^0 in case 1 to case 8. The simulations were done for only planer surfaces in these cases and the tool having only horizontal feed. Force and torque simulations were done for different kinds of surfaces in case 9 to case 14 for only ball-end mill to compare the results. All cases from case 1 to case 14 are performed for first cut/slotting and not for following cut and having lead and tilt angles to be zero.

In case 15 and 16 simulations were done for the following cut keeping the tool to be ball-end mill on planer surfaces to compare the effects of tilt and step over on surface roughness.

Common input parameters: *Helix angle, $i_0 = 30^0$; Rake angle, $\alpha = 0^0$; Number of flukes, $N_f = 2$; Spindle speed, $n=500 \text{ rpm}$; Depth of cut = 10 mm; Lead angle = 0^0 ; Tilt angle = 0^0*

4.3.1 Case 1: Tool → Cylindrical End Mill

Input parameters: *Depth of cut = 10 mm; Table feed = 100mm/sec; D=20 mm; h=20mm*

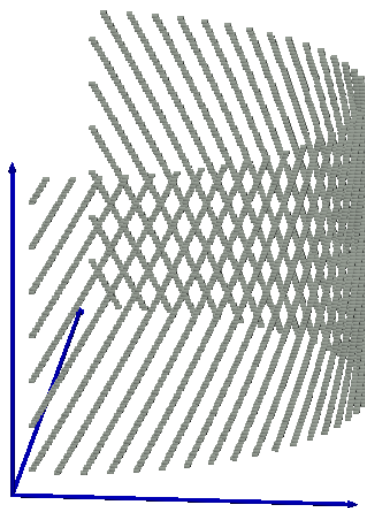


Figure 59: Engagement region for case 1

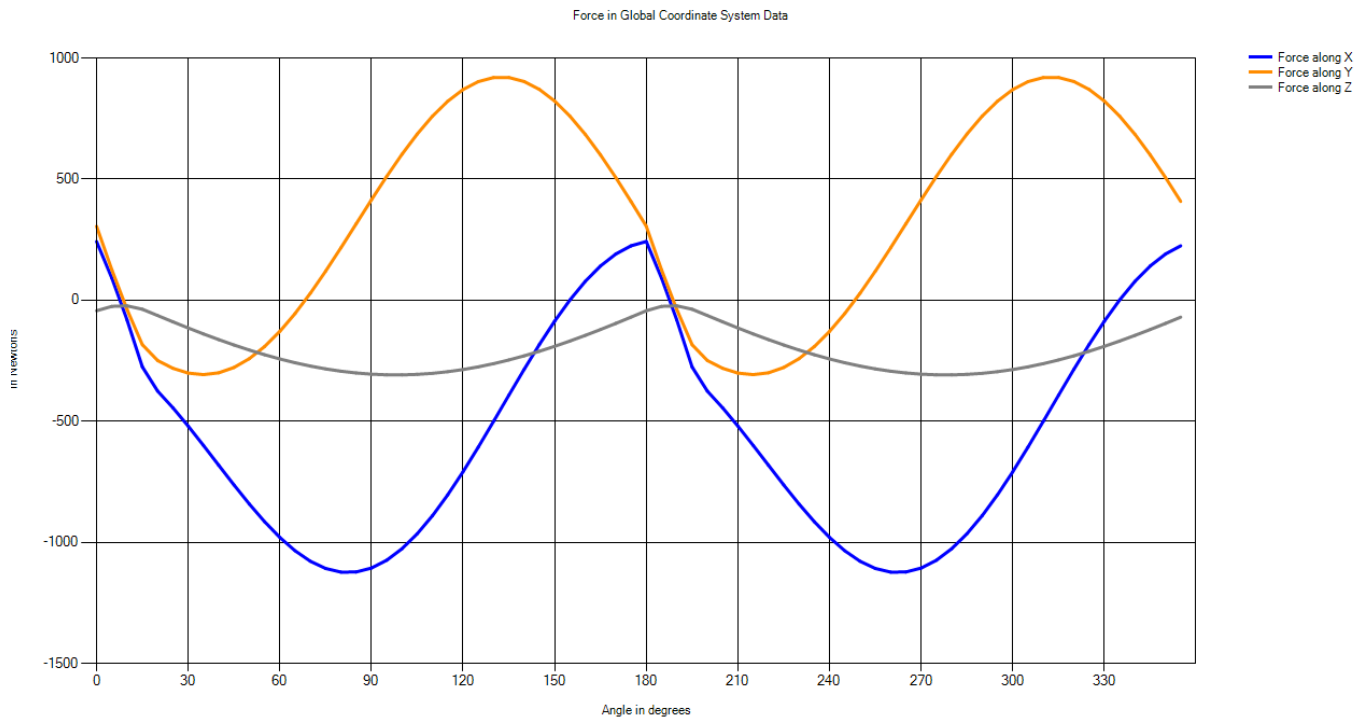


Figure 60: Forces in GCS for case 1

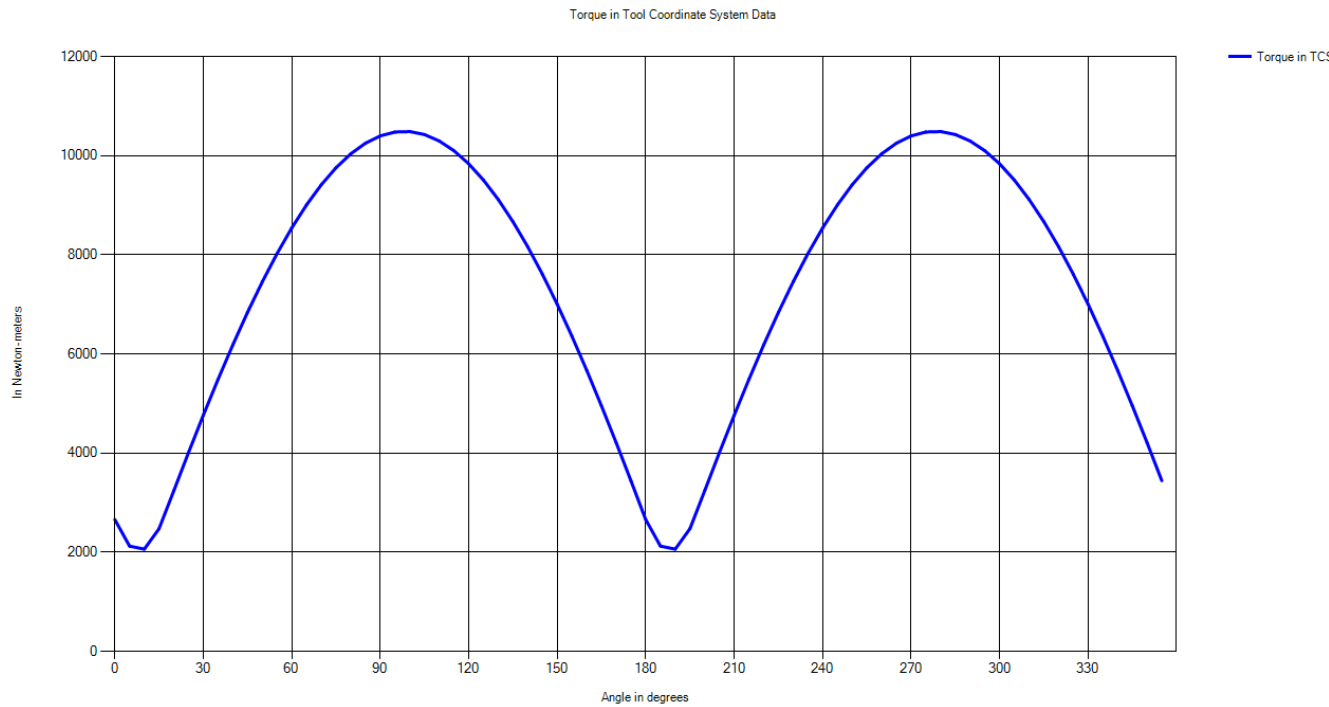


Figure 61: Torque in TCS for case 1

4.3.2 Case 2: Tool → Bull Nose End Mill

Input parameters: *Depth of cut = 10 mm; Table feed = 100mm/sec; D = 20 mm; h = 20mm*

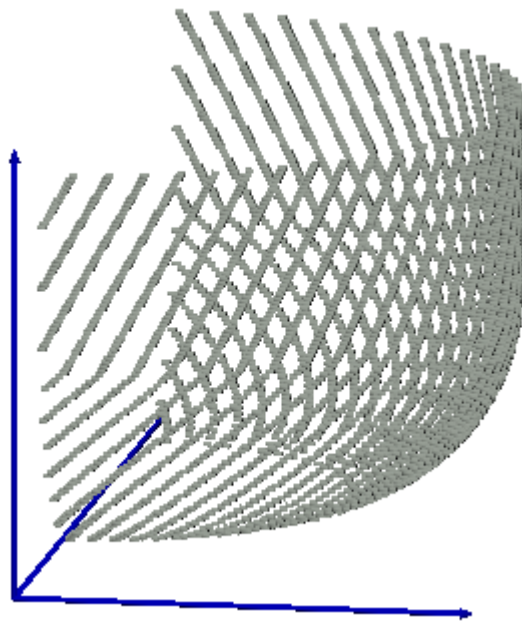


Figure 62: Engagement region for case 2

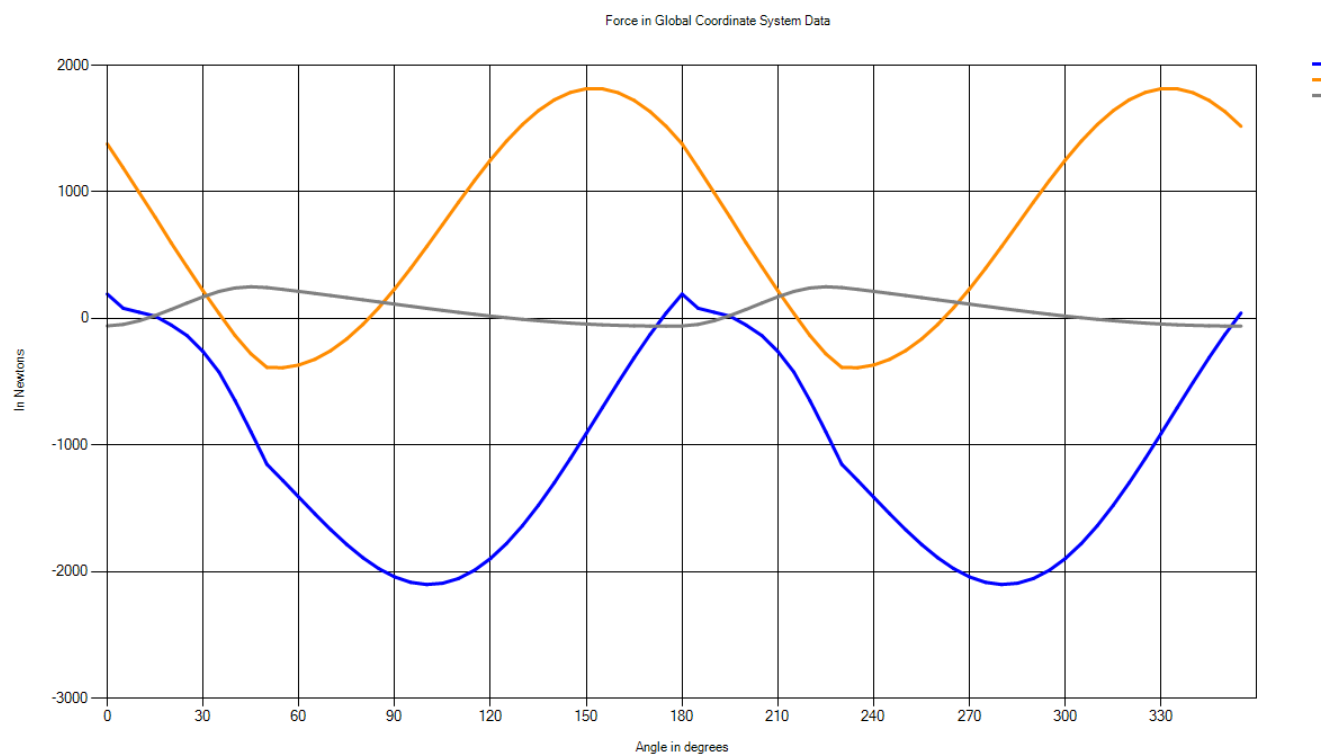


Figure 63: Forces in GCS for case 2

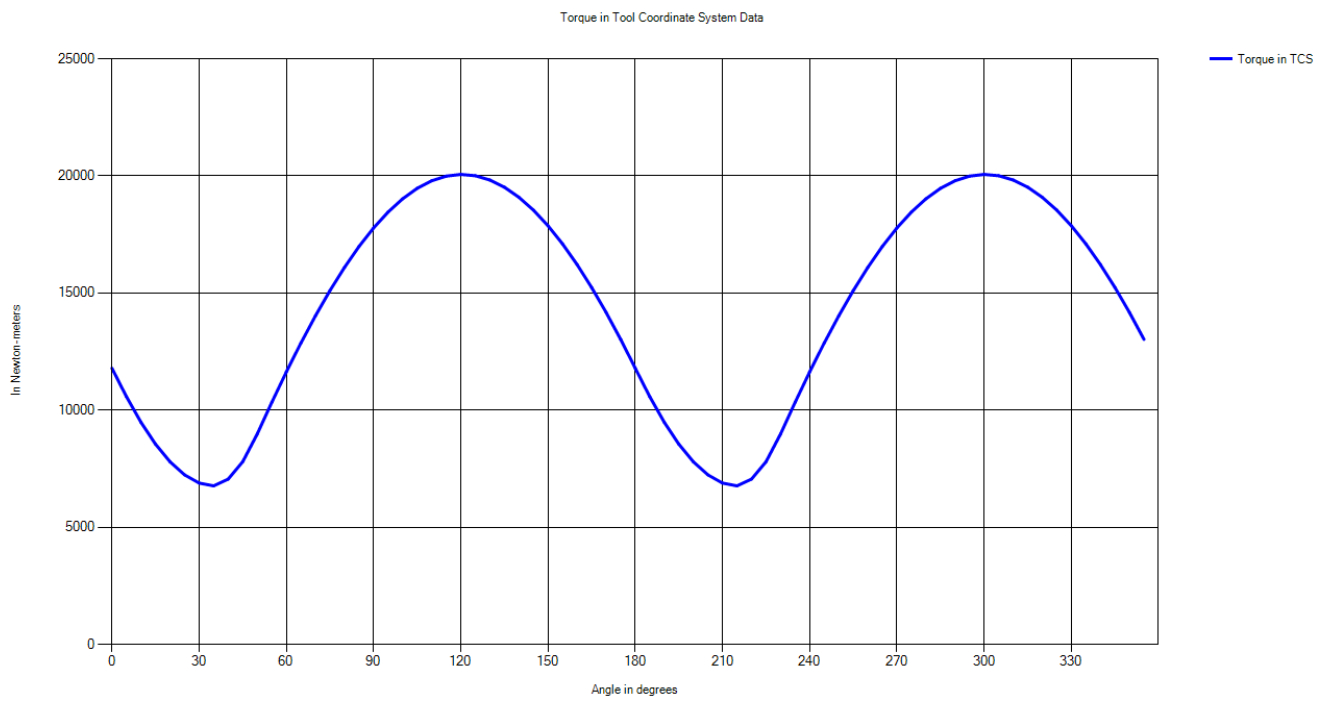


Figure 64: Torque in TCS for case 2

4.3.3 Case 3: Tool → Taper End Mill

Input parameters: *Depth of cut = 10 mm; Table feed = 100mm/sec; D=20 mm; $\beta = 20^\circ$; h = 20 mm*

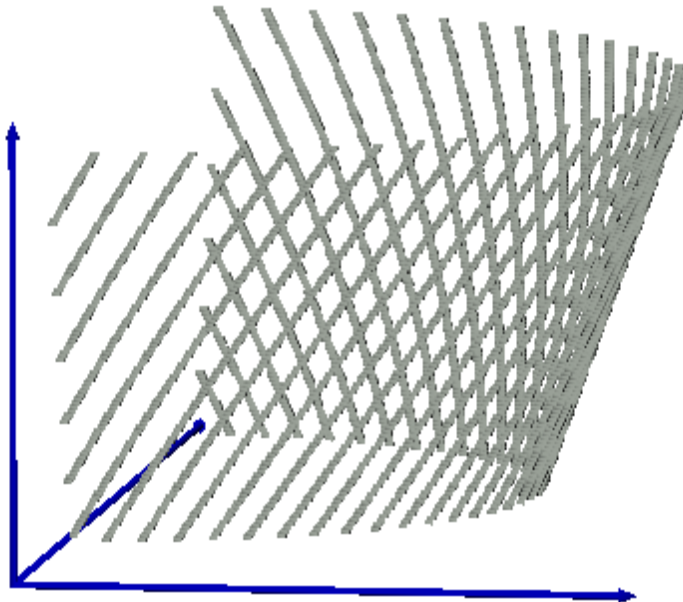


Figure 65: Engagement region for case 3

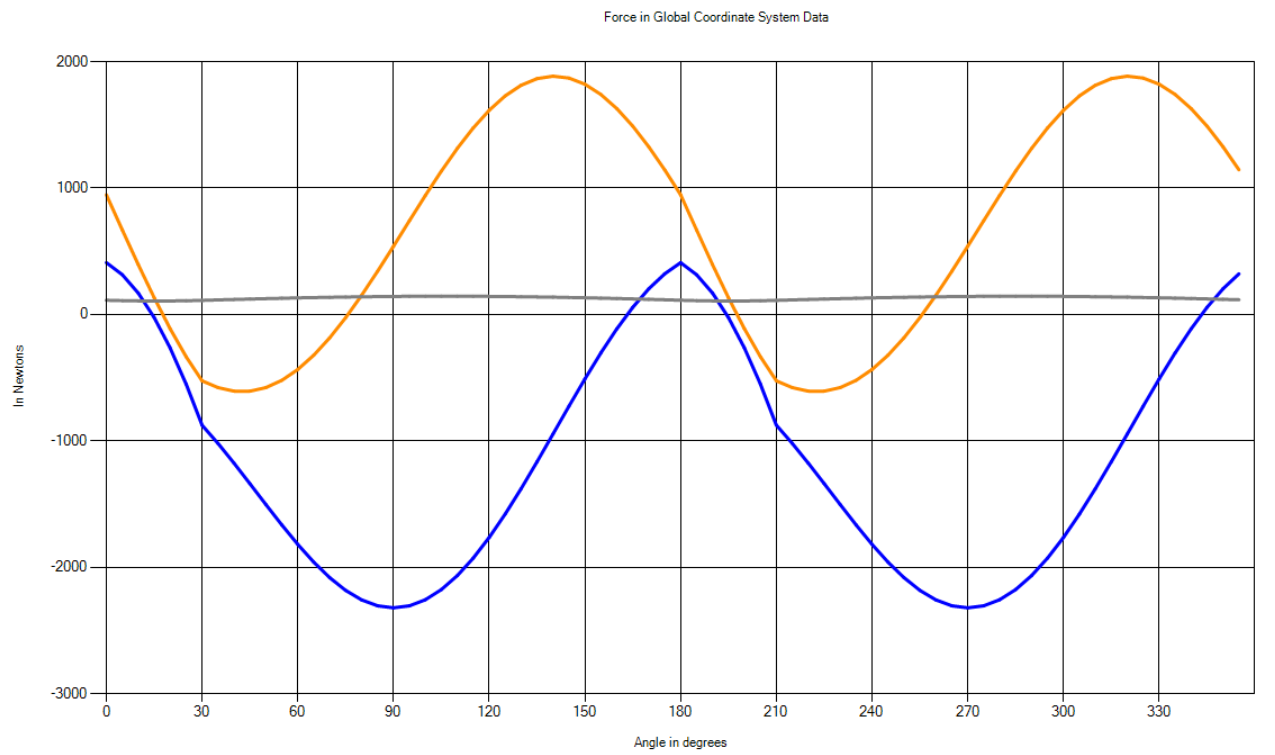


Figure 66 : Forces in GCS for case 3

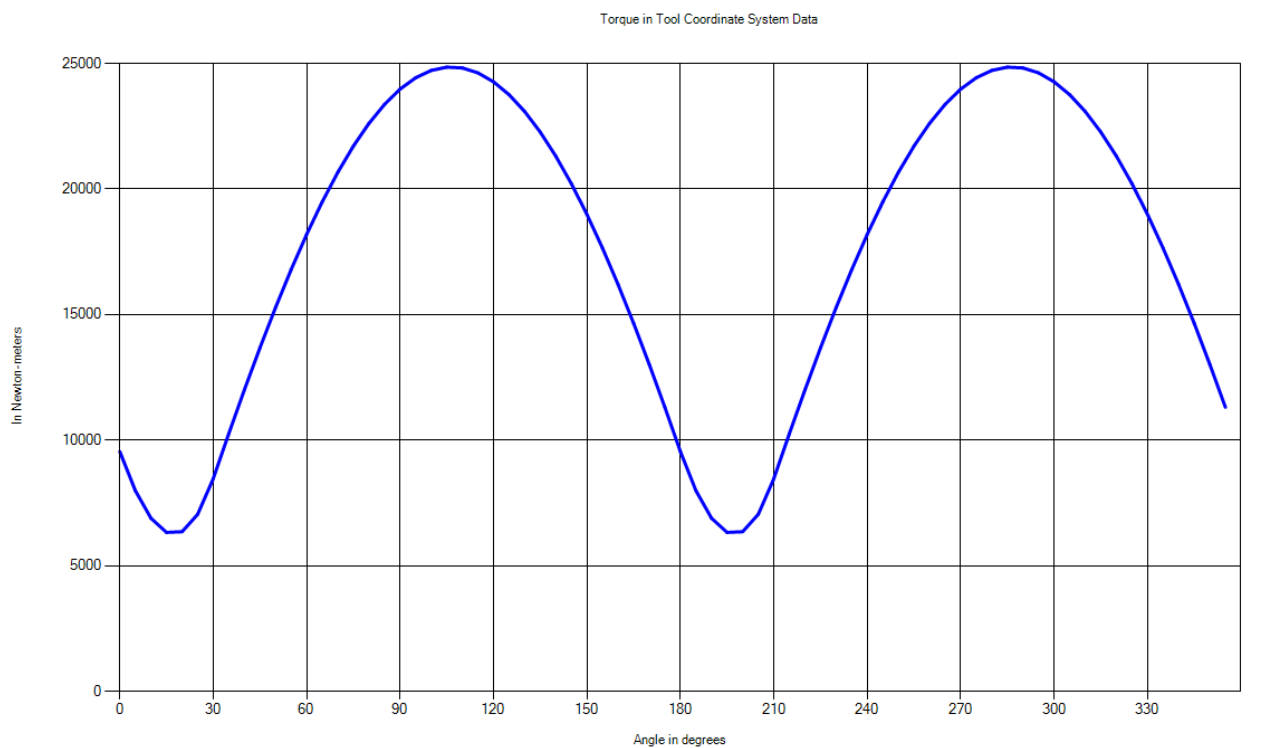


Figure 67 : Torque in TCS for case 3

4.3.4 Case 4: Tool → Taper Ball End Mill

Input parameters: *Depth of cut = 10 mm; Table feed = 100mm/sec; D=20 mm; R = 20mm; β = 10°; h = 20 mm*

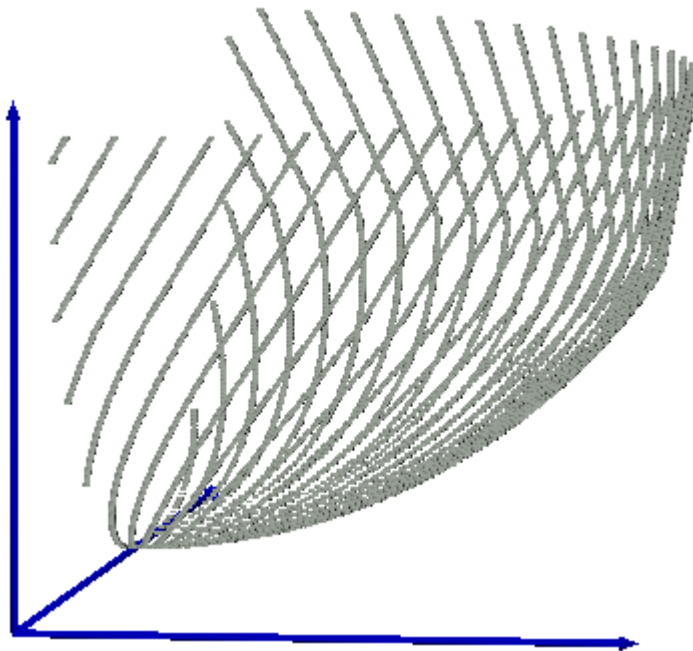


Figure 68: Engagement region for case 4

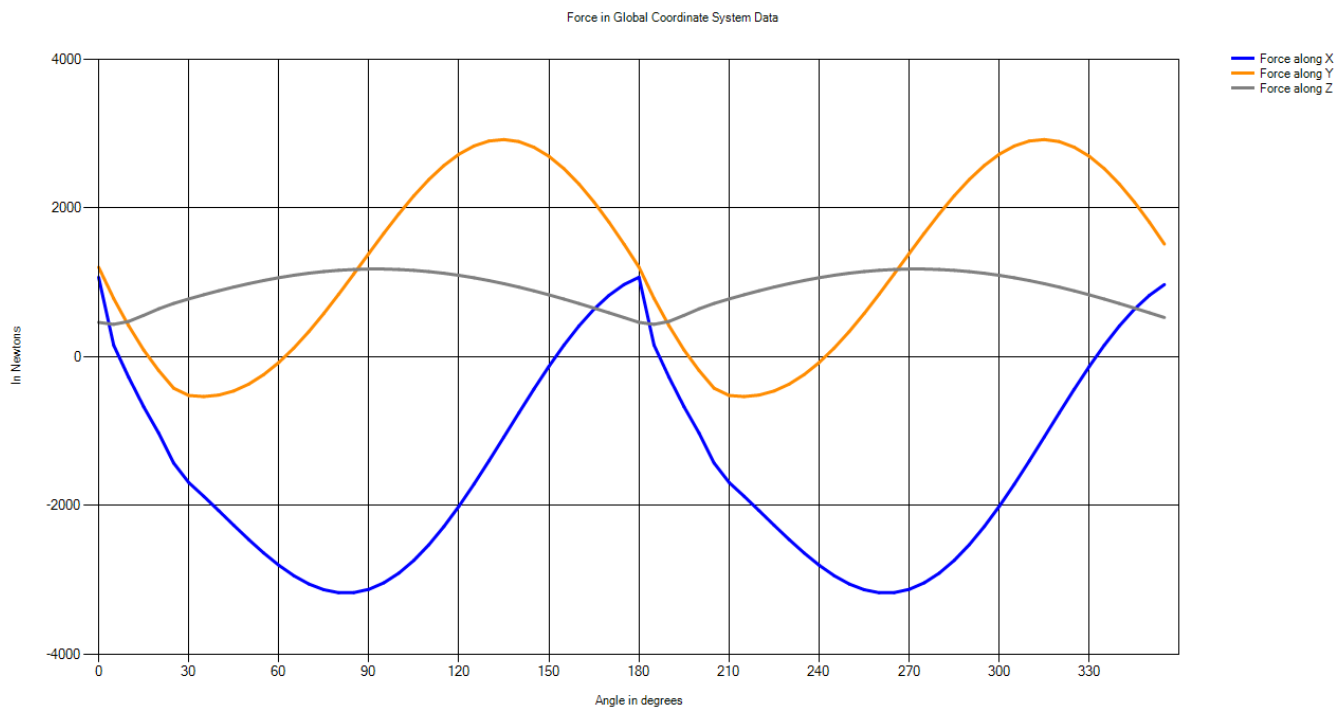


Figure 69: Forces in GCS for case 4

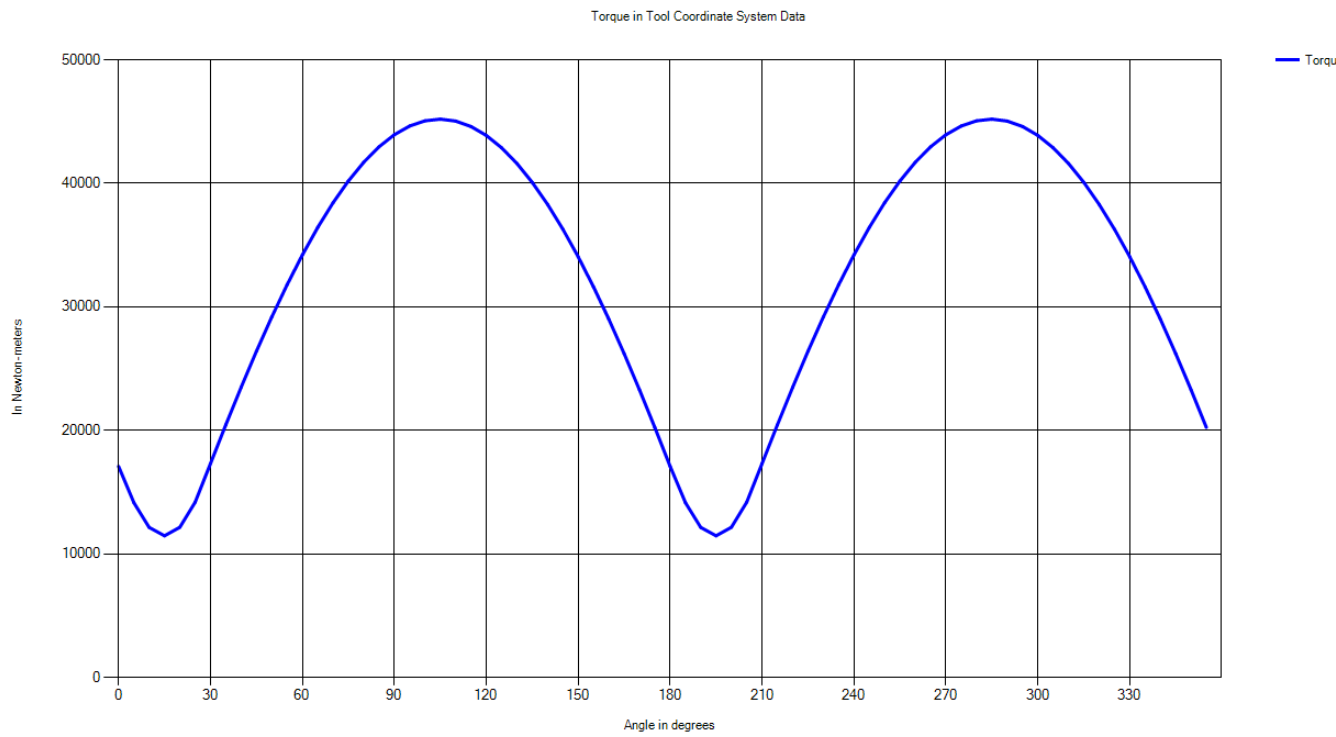


Figure 70: Torque in TCS for case 4

4.3.5 Case 5: Tool → General End Mill

Input parameters: *Depth of cut = 10 mm; Table feed = 100mm/sec; D=30 mm; R = 20mm; R_r = 2 mm; R_z = 18 mm; α = 7°; β = 10°; h = 20 mm*

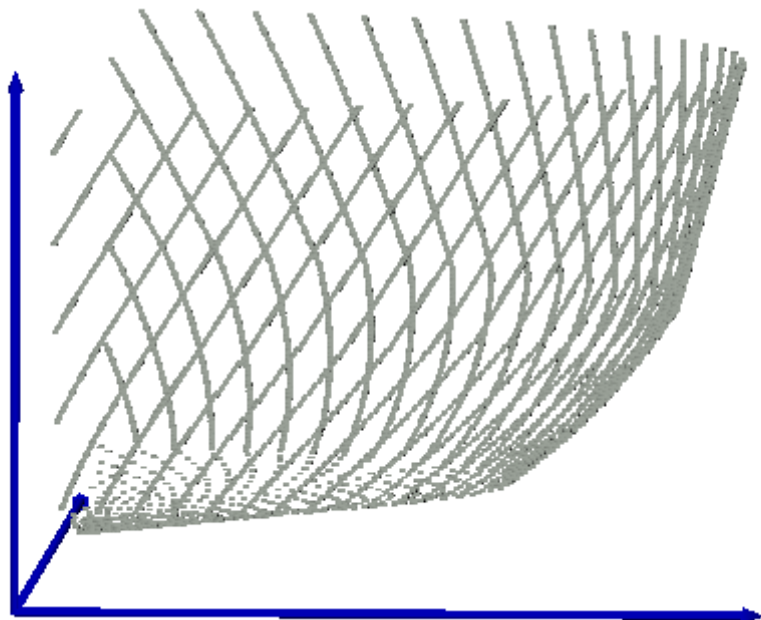


Figure 71: Engagement region for case 5

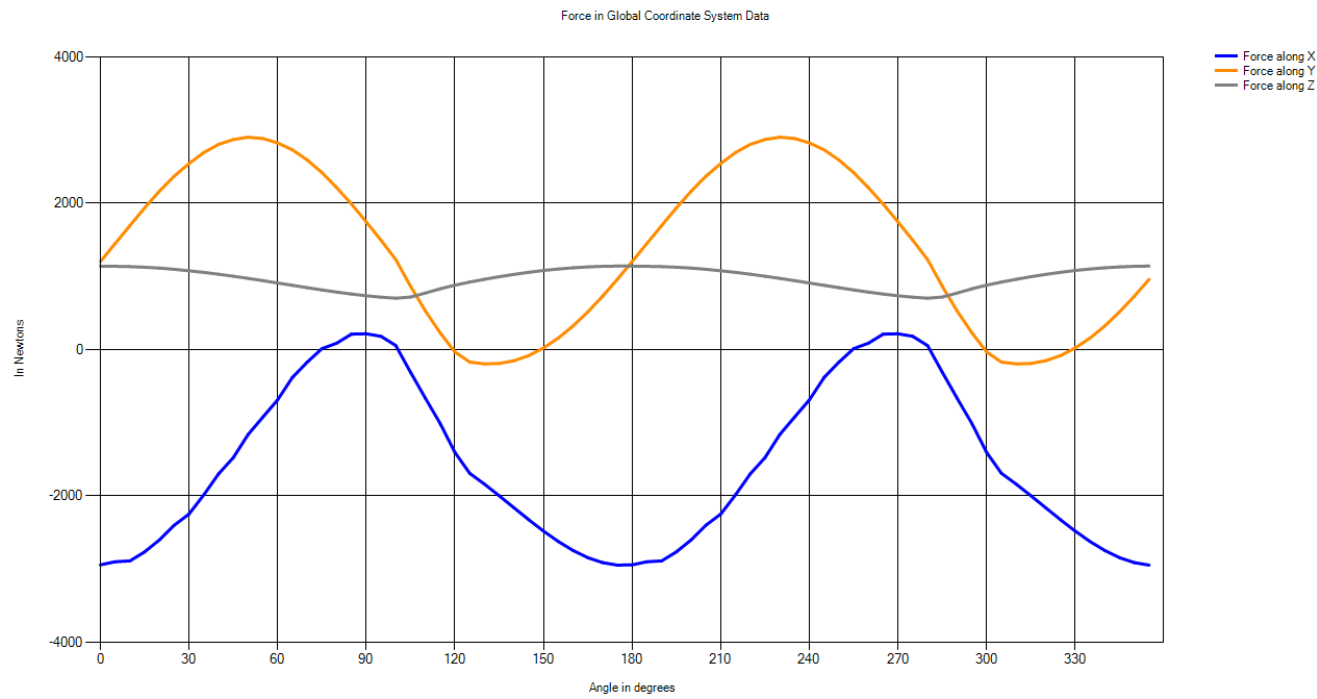


Figure 72: Forces in GCS for case 5

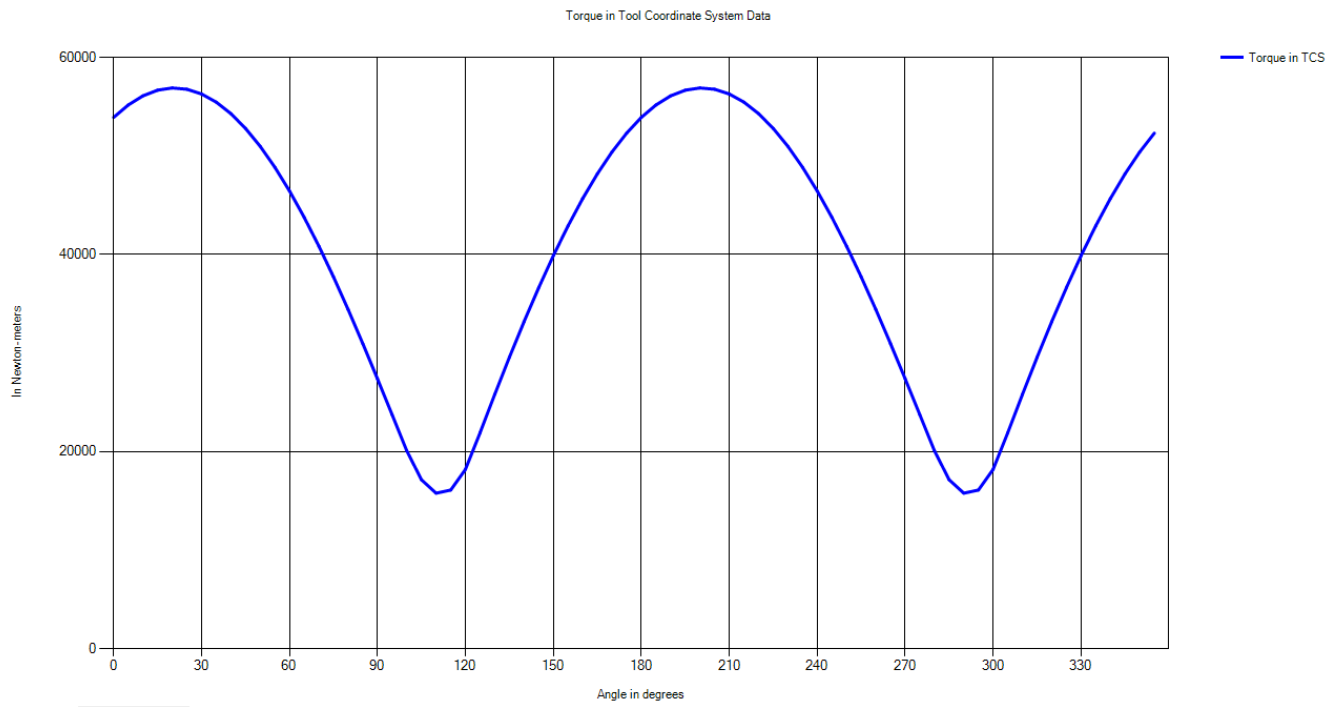


Figure 73: Torque in TCS for case 5

4.3.6 Case 6: Tool → Cone End Mill

Input parameters: *Depth of cut = 10 mm; Table feed = 100mm/sec; D=20 mm; R_z= 4.66 mm; α = 25°; β = 20°; h = 20 mm*

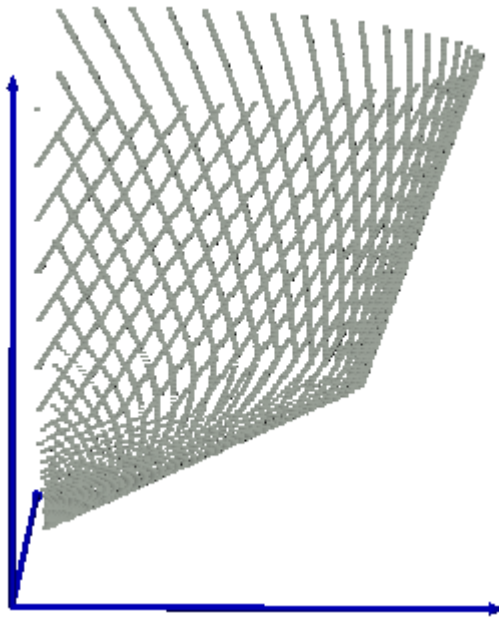


Figure 74 : Engagement region for case 6

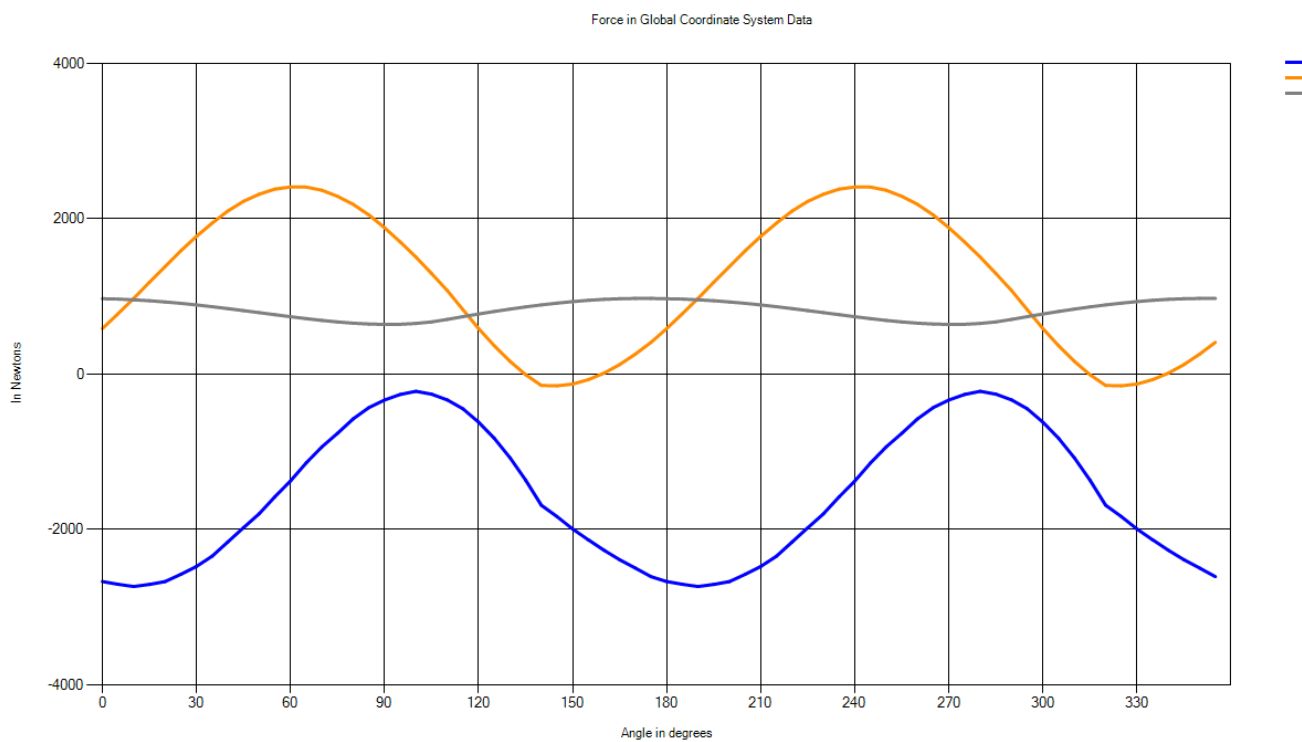


Figure 75 : Forces in GCS for case 6

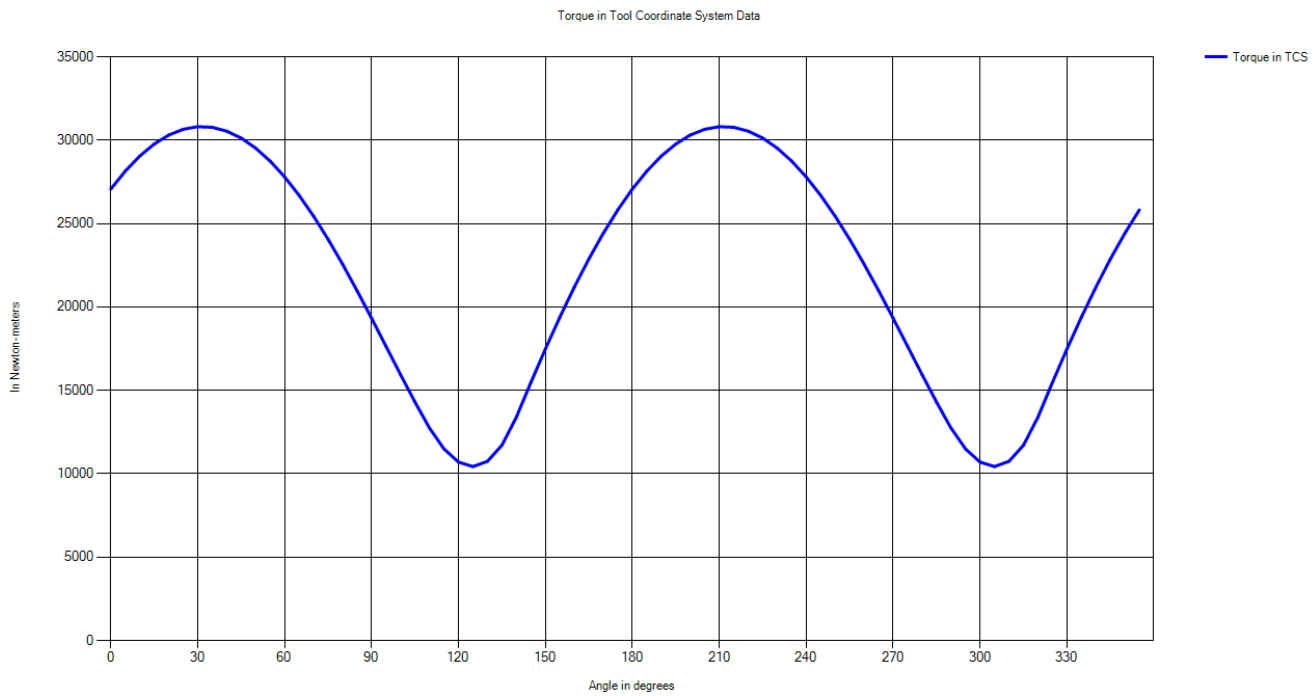


Figure 76 : Torque in TCS for case 6

4.3.7 Case 7: Tool → Rounded End Mill

Input parameters: *Depth of cut = 10 mm; Table feed = 100mm/sec; D=20 mm; R = 10 mm; R_z = 8 mm; h = 20 mm*

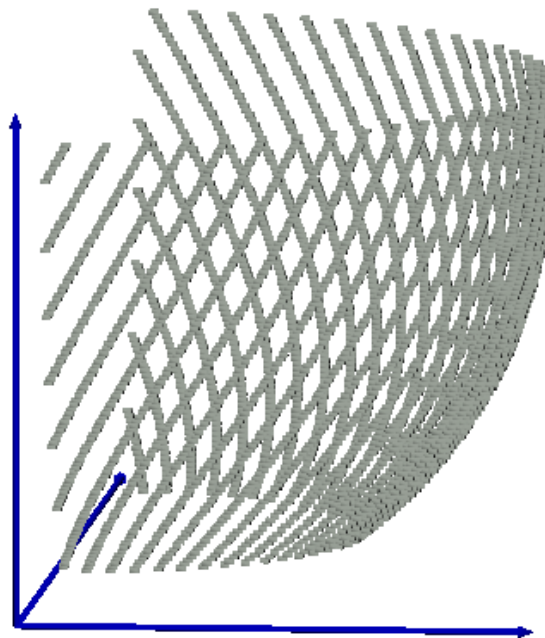


Figure 77: Engagement region for case 7

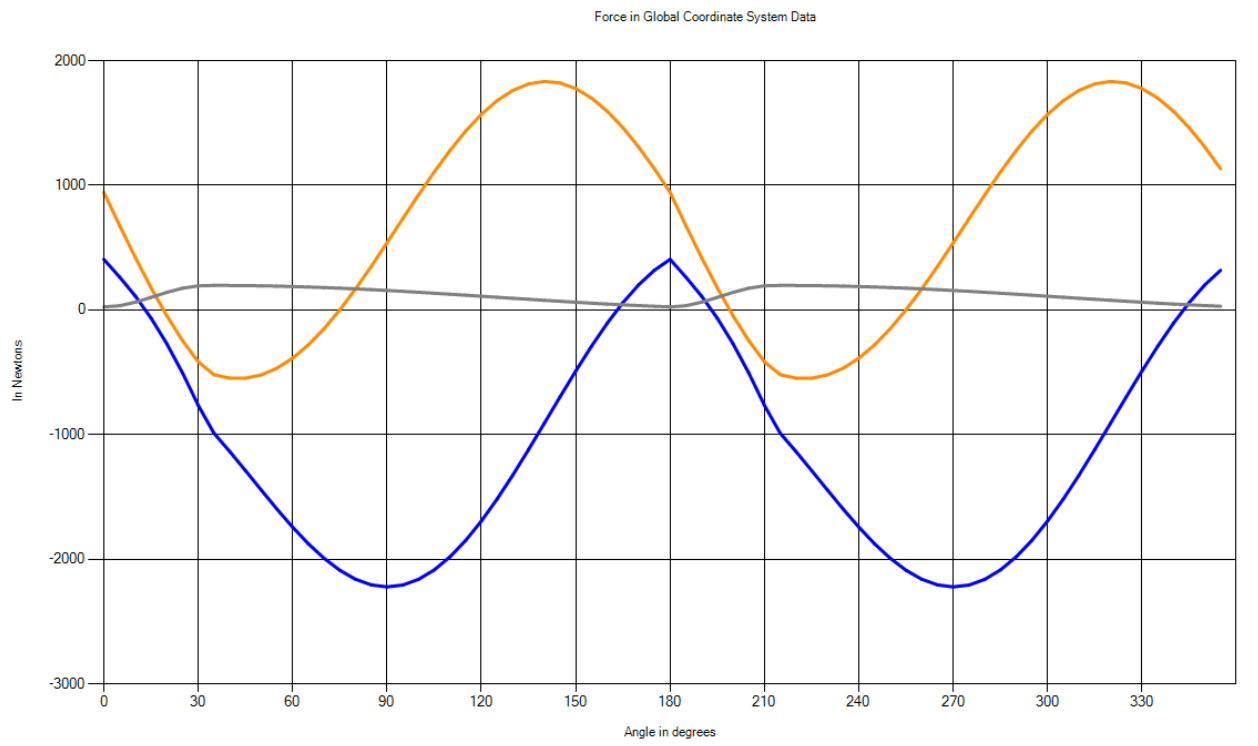


Figure 78: Forces in GCS for case 7

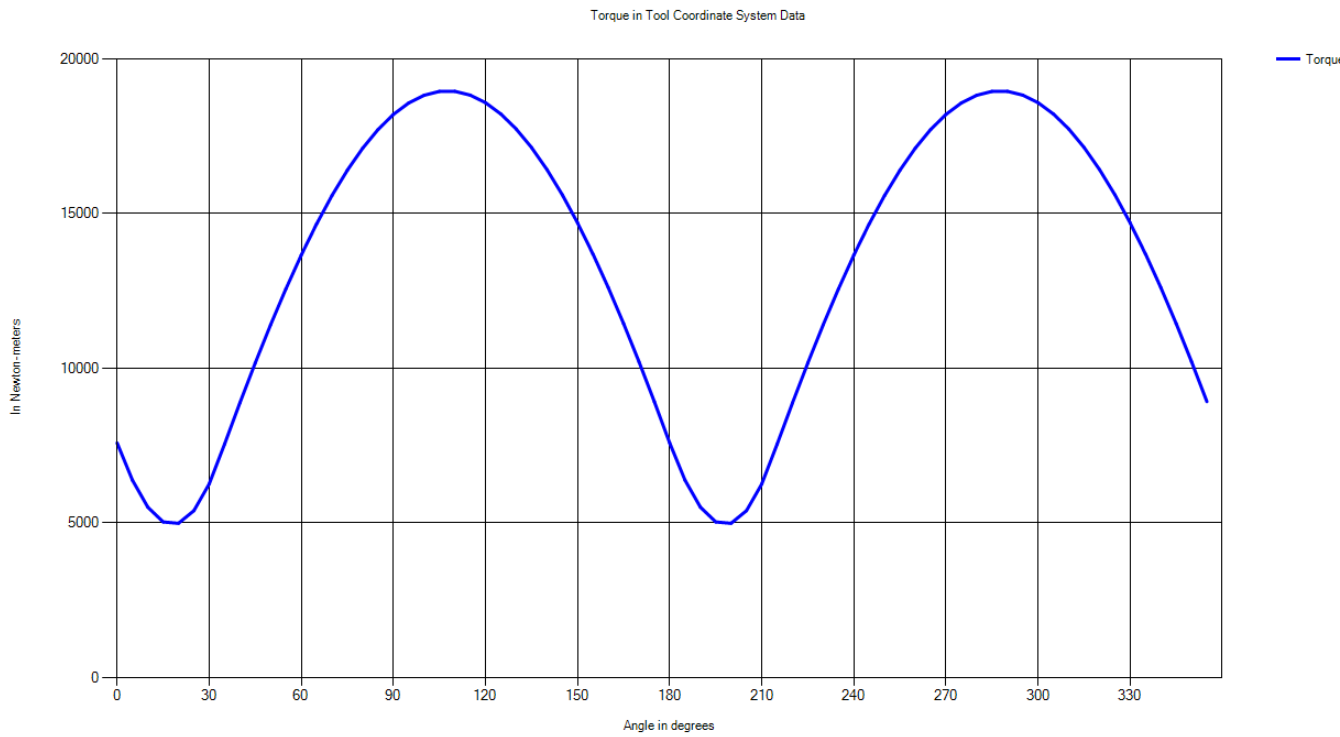


Figure 79: Torque in TCS for case 7

4.3.8 Case 8: Tool → Inverted Cone End Mill

Input parameters: *Depth of cut = 10 mm; Table feed = 100mm/sec; D=40 mm; R = 20 mm; R_r= 1 mm; R_z= 18 mm; α = 10°; β = -7°; h = 20 mm,*

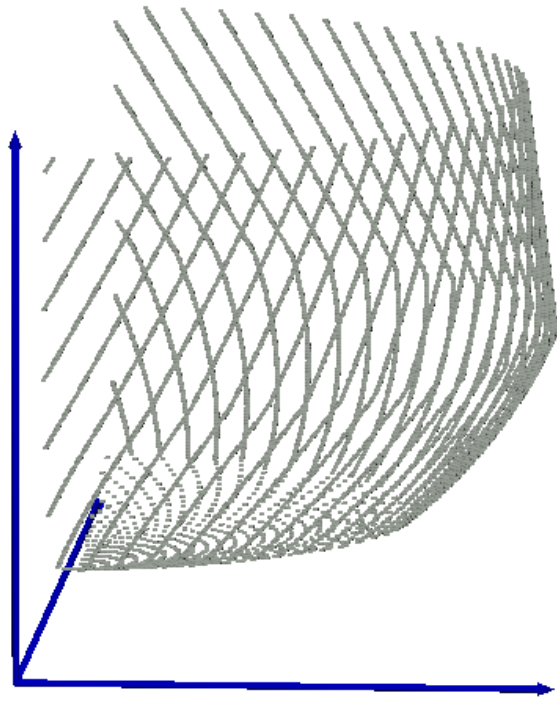


Figure 80: Engagement region for case 8

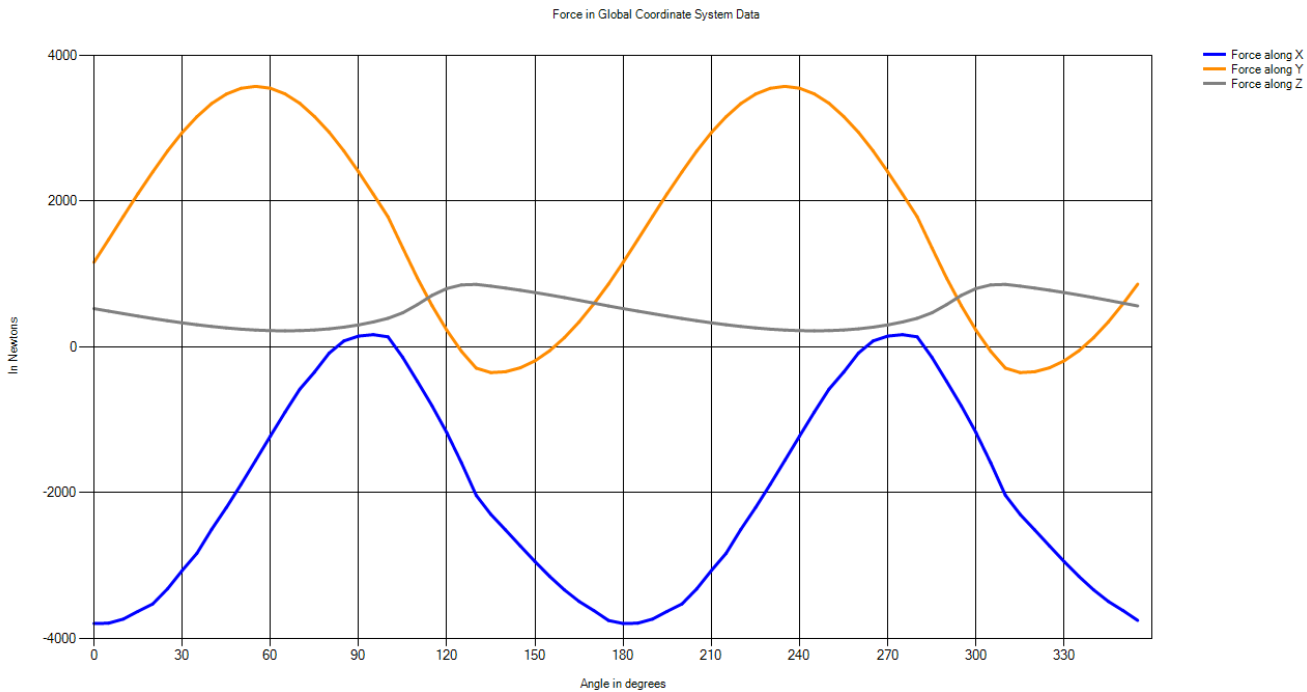


Figure 81 : Forces in GCS for case 8

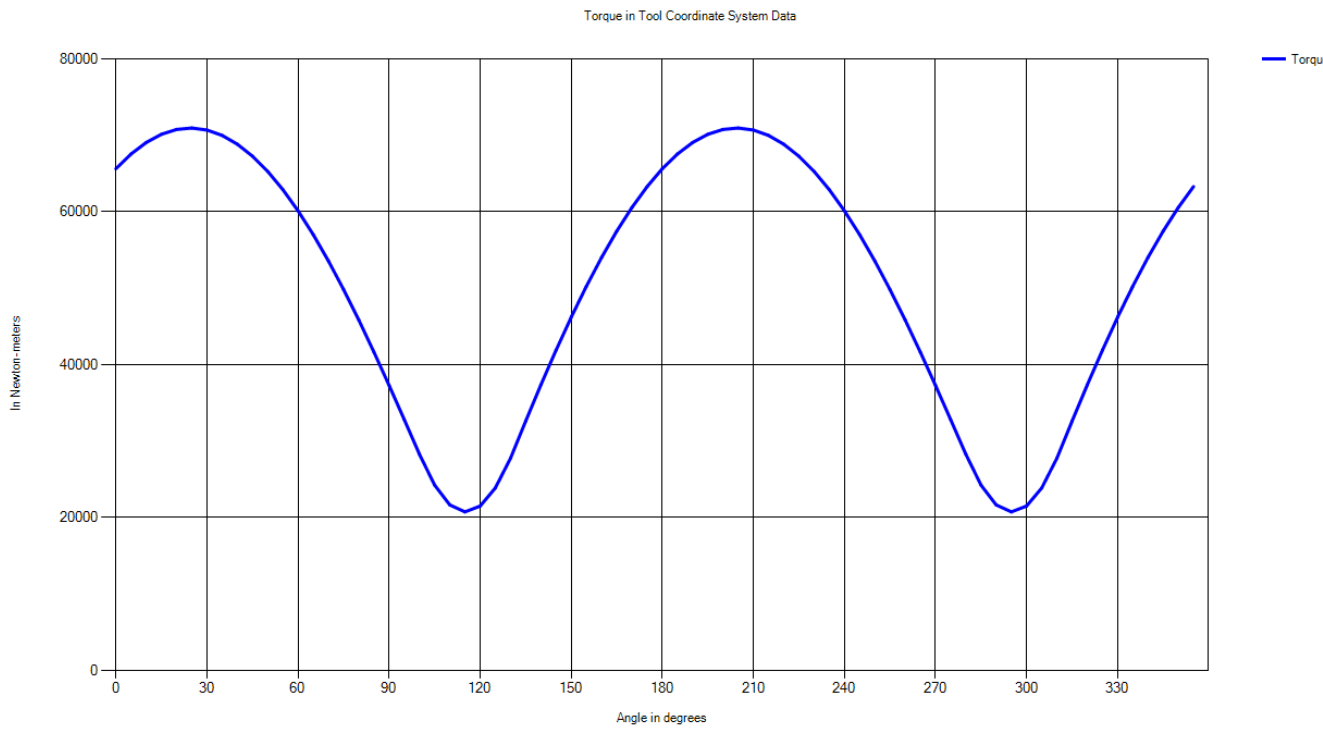
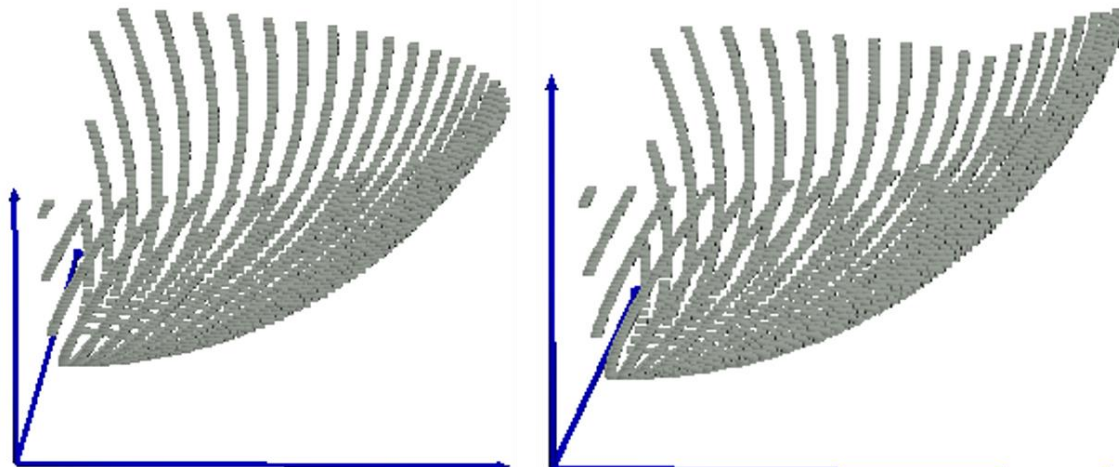


Figure 82: Torque in TCS for case 8

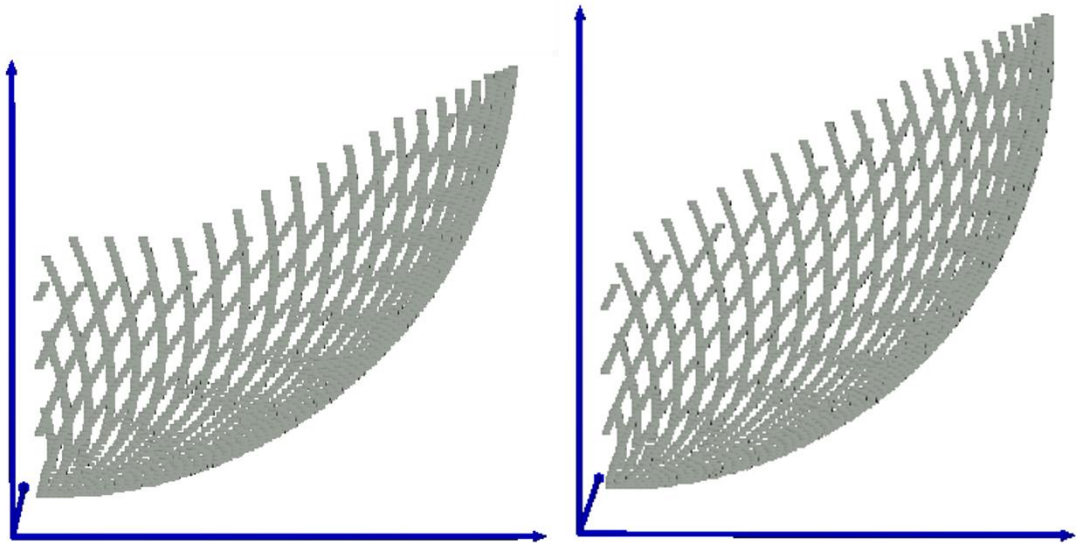
4.3.9 Case 9: Surface → Slope, Tool is Moving Inside the Slope

Input parameters: *Depth of cut = 5 mm; Table feed = 100 mm/sec; D=20 mm; h = 20 mm, $\alpha_{surface} = 30^\circ$, $X_{surface} = 10 \text{ mm}$; distance traveled by tool (simulation) = 10 mm*



(a) Distance travelled by tool = 0 mm

(b) Distance travelled by tool = 3.5 mm



(c) Distance travelled by tool = 7 mm (d) Distance travelled by tool = 10 mm

Figure 83: Engagement zone at different instances for case 9

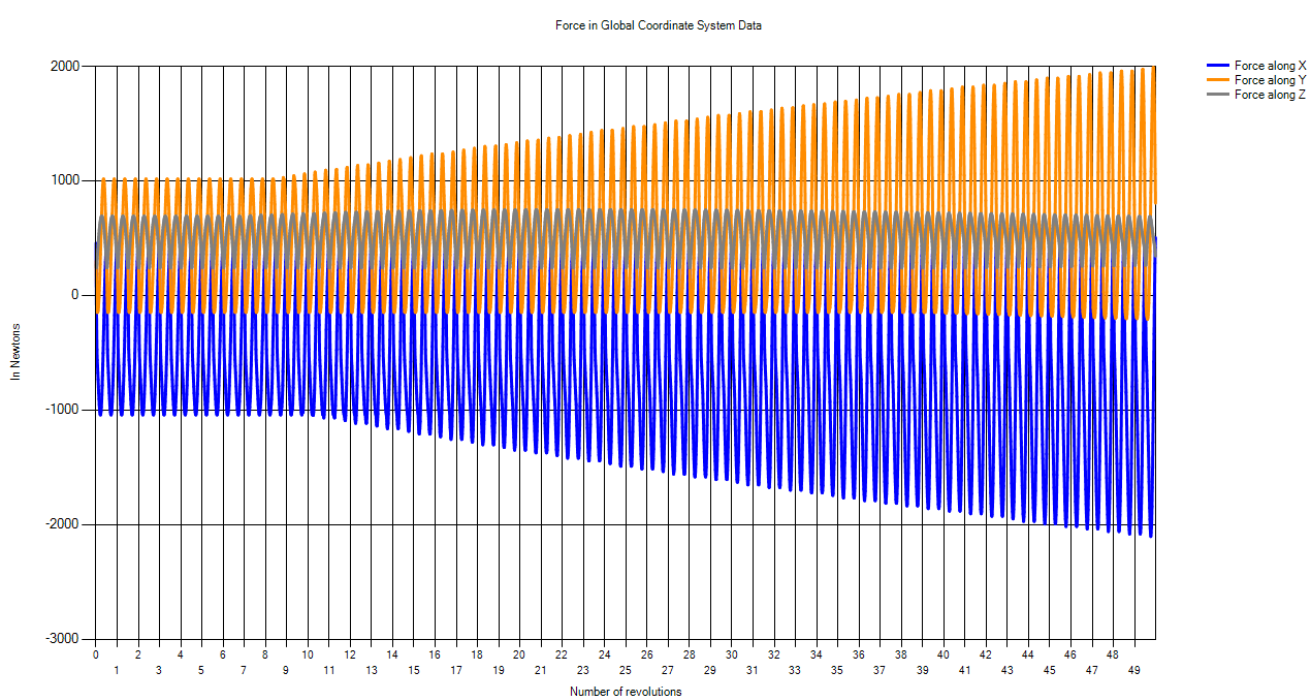


Figure 84: Forces in GCS for case 9

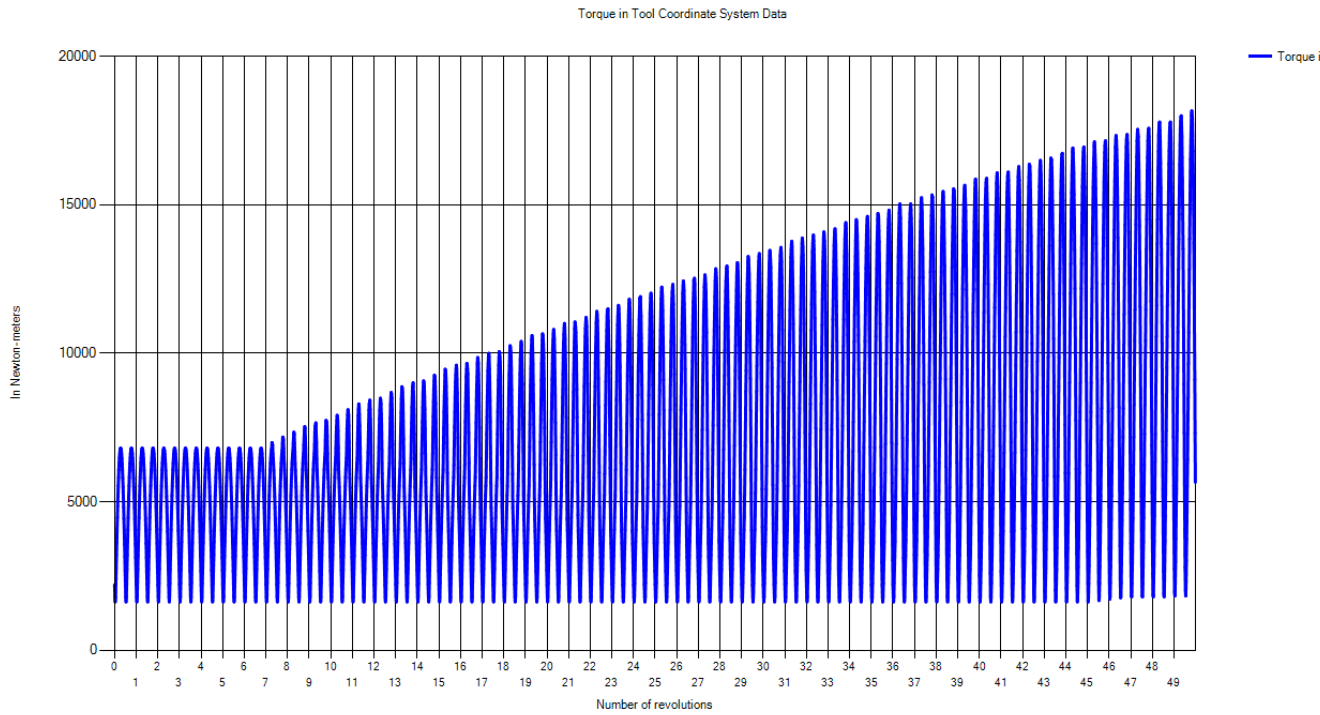


Figure 85: Torque in TCS for case 9

4.3.10 Case 10: Surface → Slope, Tool is Moving Parallel the Slope

Input parameters: *Depth of cut = 5 mm; Table feed = 100 mm/sec; D=20 mm; h = 20 mm, $\beta_{surface} = 45^0$, $Y_{surface} = 5 \text{ mm}$; distance traveled by tool (simulation)= 10 mm*

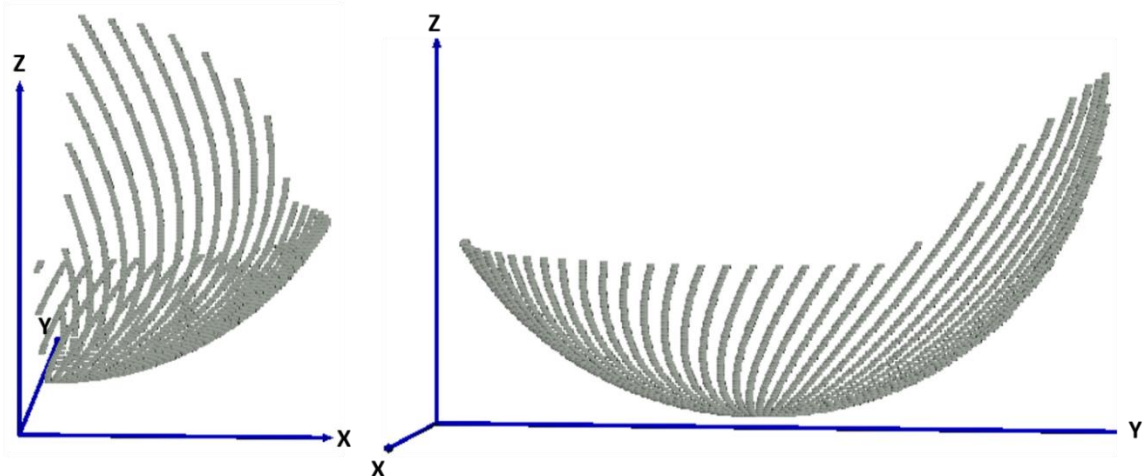


Figure 86: Engagement region for case 10

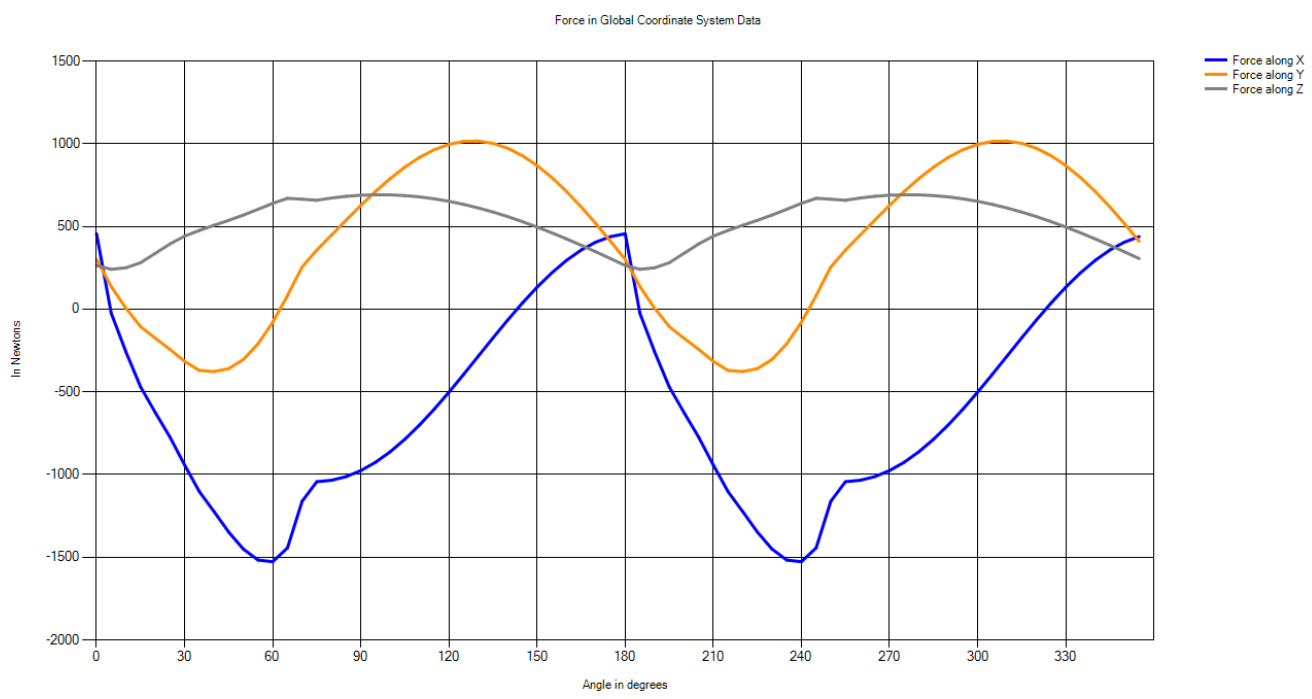


Figure 87: Forces in GCS for case 10

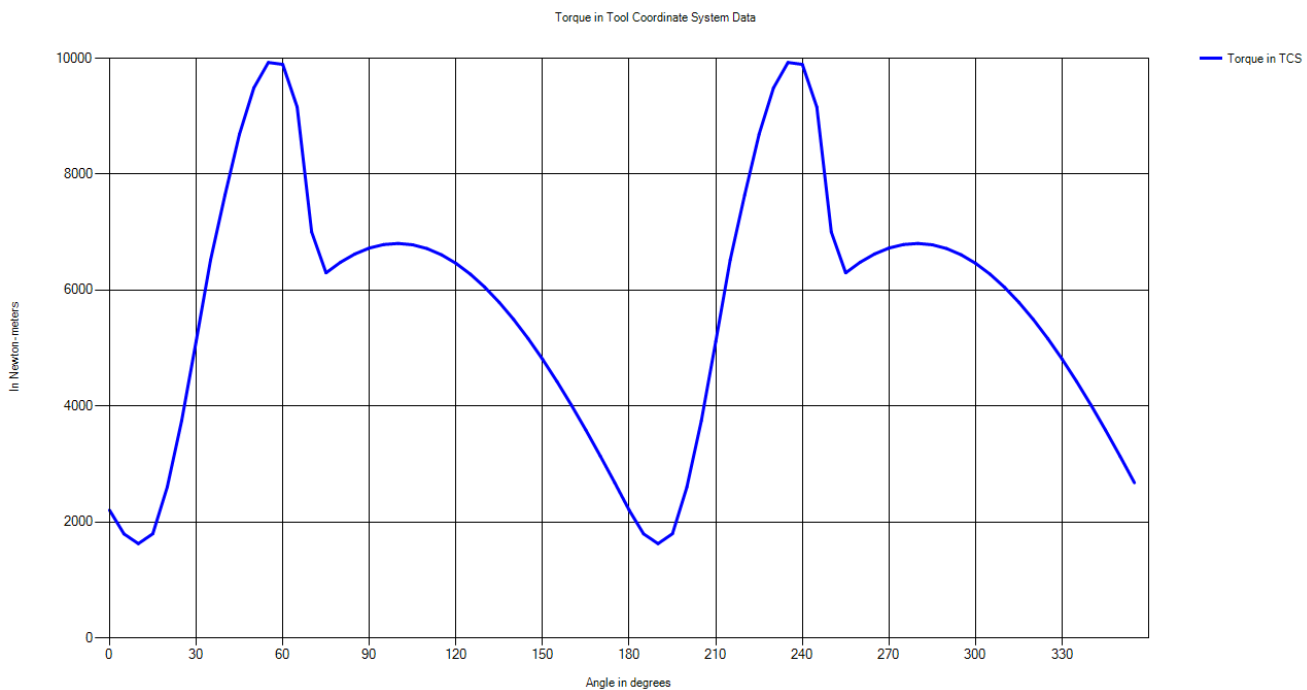


Figure 88: Torque in TCS for case 10

4.3.11 Case 11: Surface → Edge

Input parameters: *Depth of cut = 5 mm; Table feed = 100 mm/sec; D=20 mm; h = 20 mm, $\beta_{surface} = 45^\circ$, $Y_{surface} = 0 \text{ mm}$; simulation is done for 1 revolution of tool*

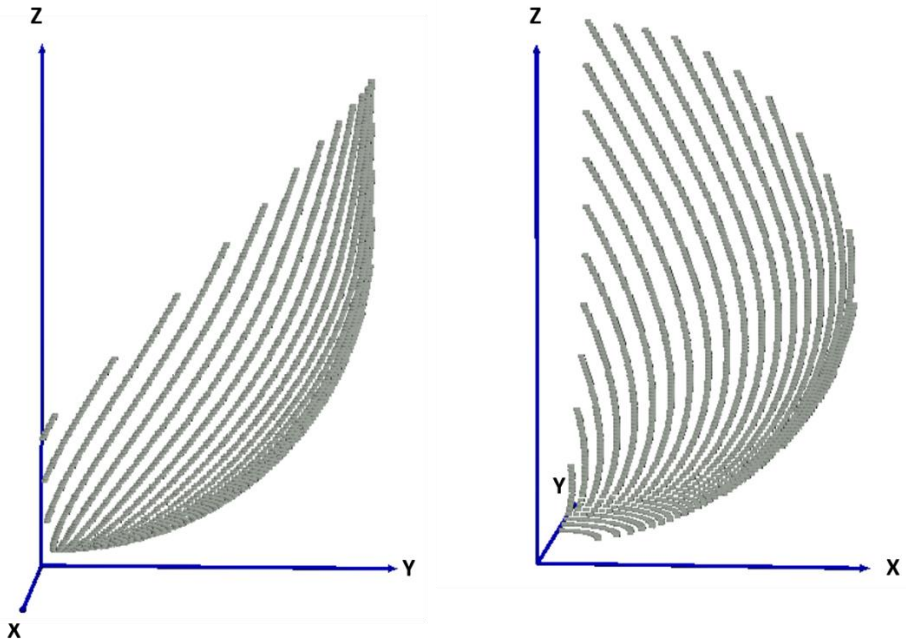


Figure 89: Engagement region for case 11

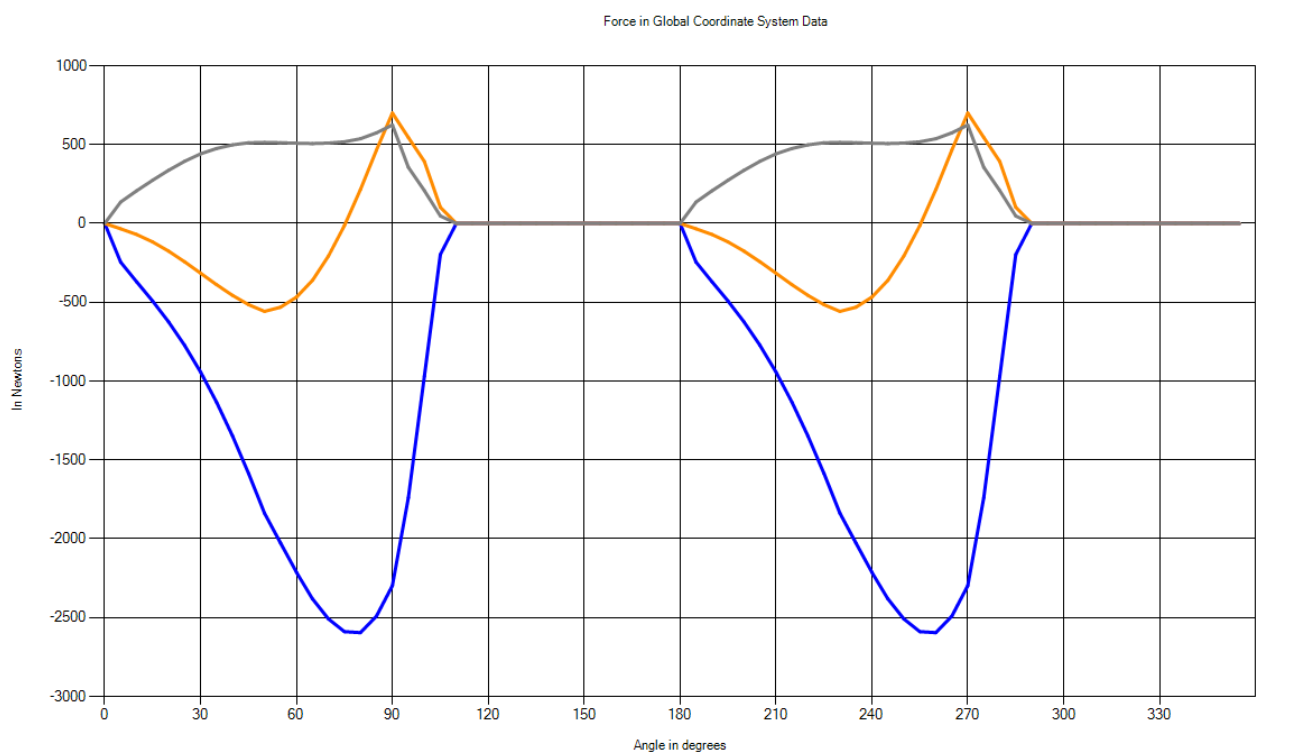


Figure 90: Forces in GCS for case 11

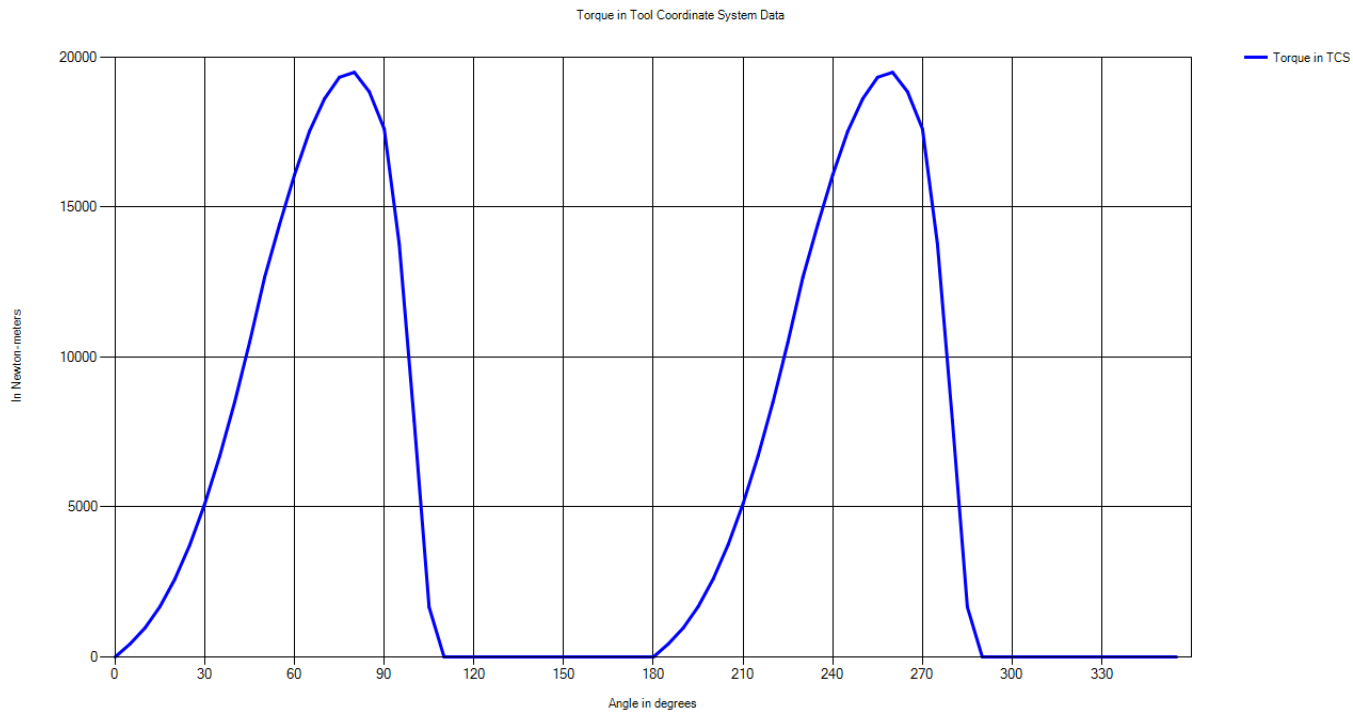
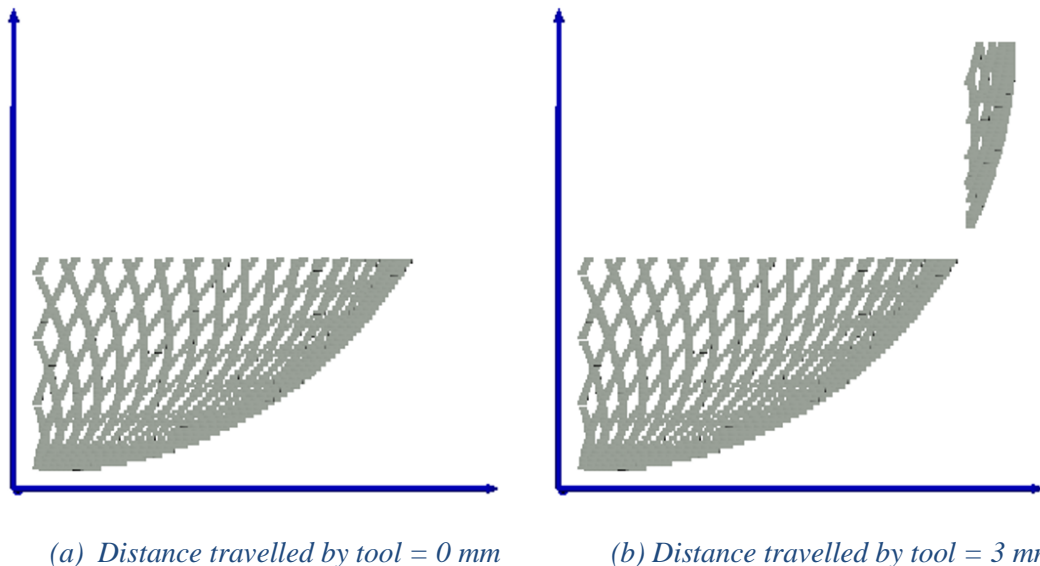
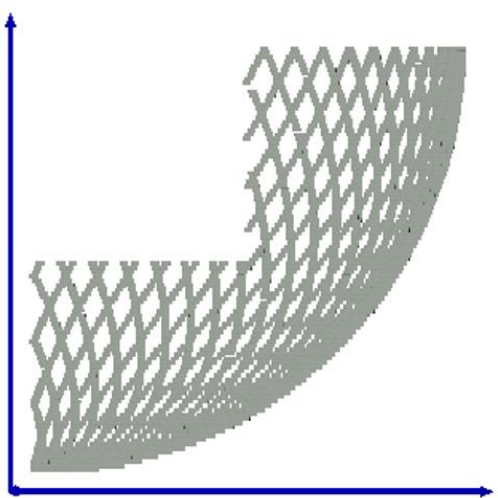


Figure 91: Torque in TCS for case 11

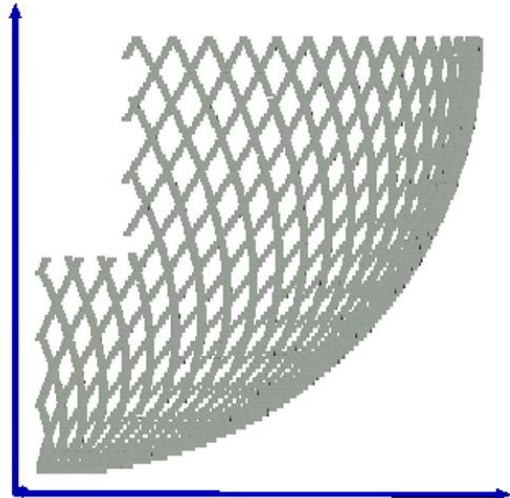
4.3.12 Case 12: Surface → Step

Input parameters: *Depth of cut = 5 mm; Table feed = 100 mm/sec; D=20 mm; h = 20 mm, Z_{surface}= 5 mm, X_{surface}= 12 mm; distance traveled by tool (simulation)= 10 mm*





(c) Distance travelled by tool = 7 mm



(d) Distance travelled by tool = 10 mm

Figure 92: Engagement zone at different instances for case 12

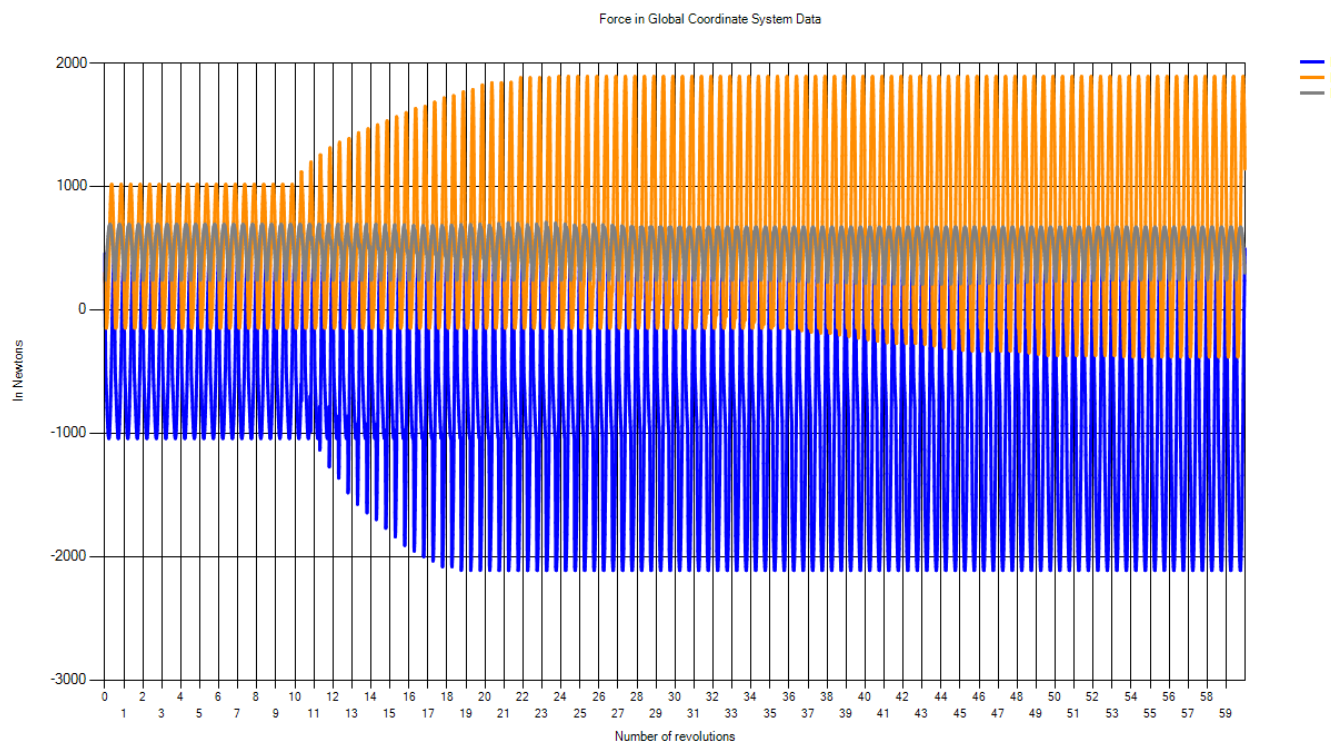


Figure 93: Forces in GCS for case 12

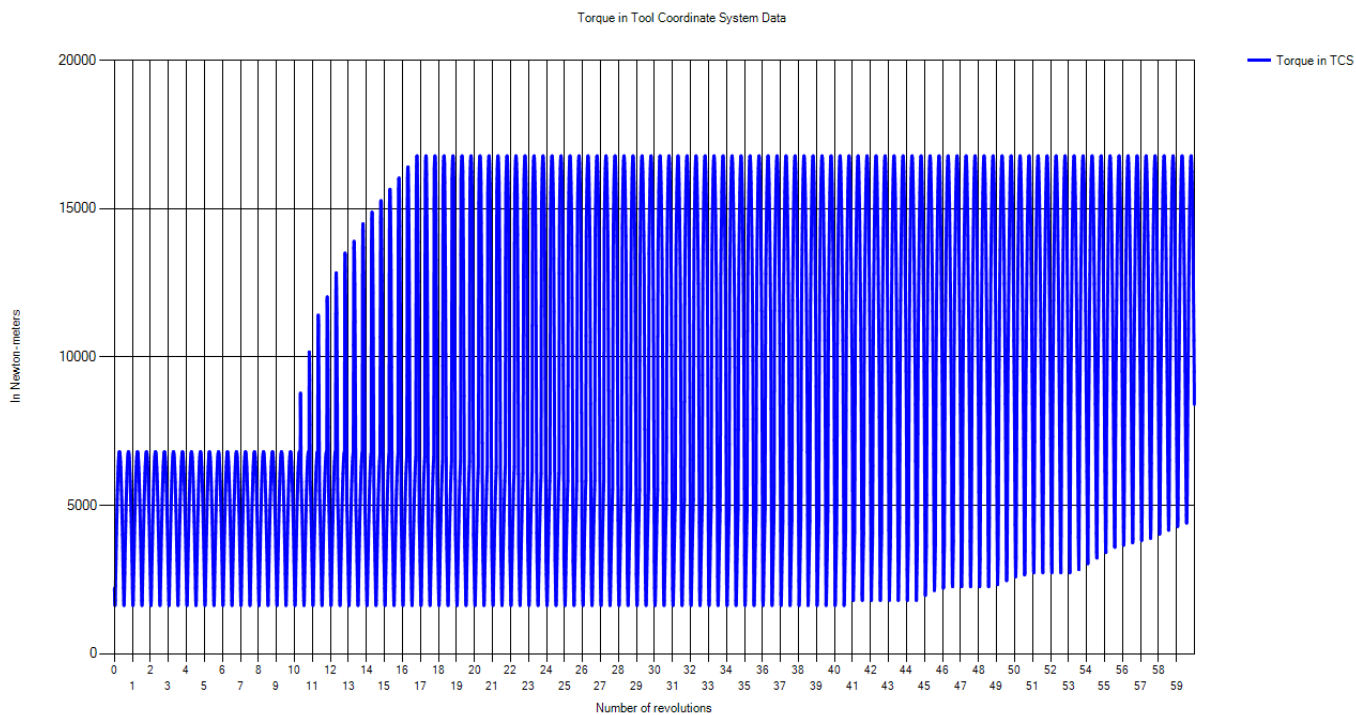
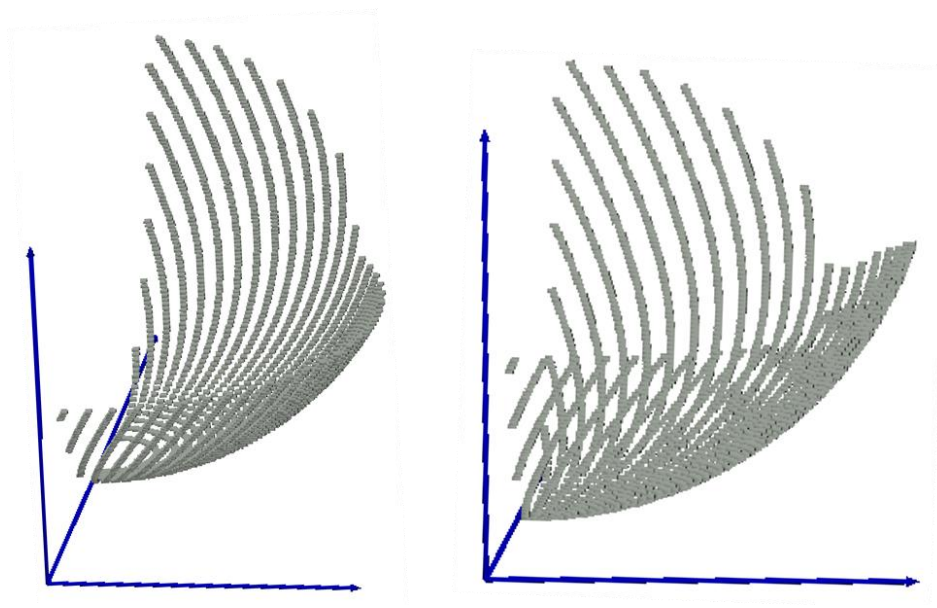


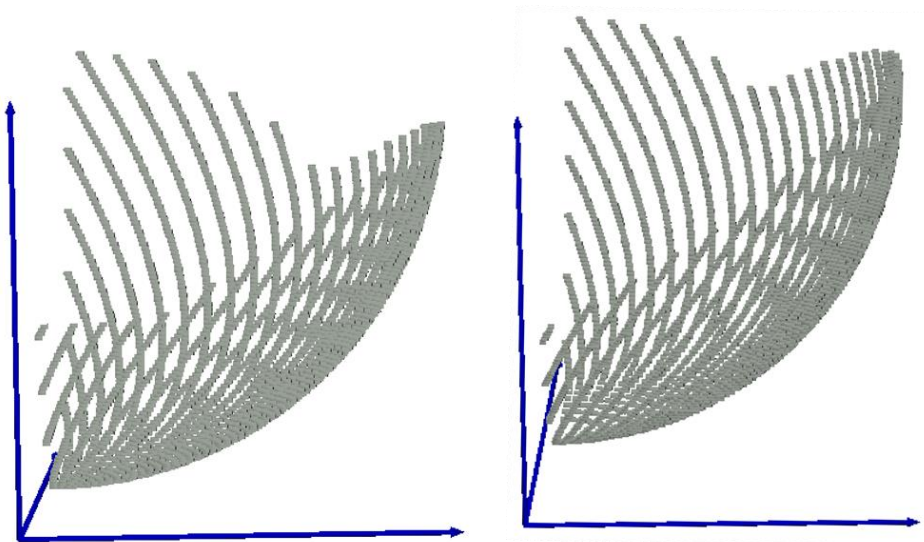
Figure 94: Torque in TCS for case 12

4.3.13 Case 13: Surface → Corner

Input parameters: $Depth\ of\ cut = 5\ mm$; $Table\ feed = 100\ mm/sec$; $D = 20\ mm$; $h = 20\ mm$, $X_{surface} = 5\ mm$, $Y_{surface} = 5\ mm$; $\alpha = 30^\circ$; $\beta = 45^\circ$; $distance\ traveled\ by\ tool\ (simulation) = 10\ mm$



(a) Distance travelled by tool = 0 mm (b) Distance travelled by tool = 3.5 mm



(c) Distance travelled by tool = 7 mm (d) Distance travelled by tool = 10 mm

Figure 95; Engagement zone at different instances for case 13

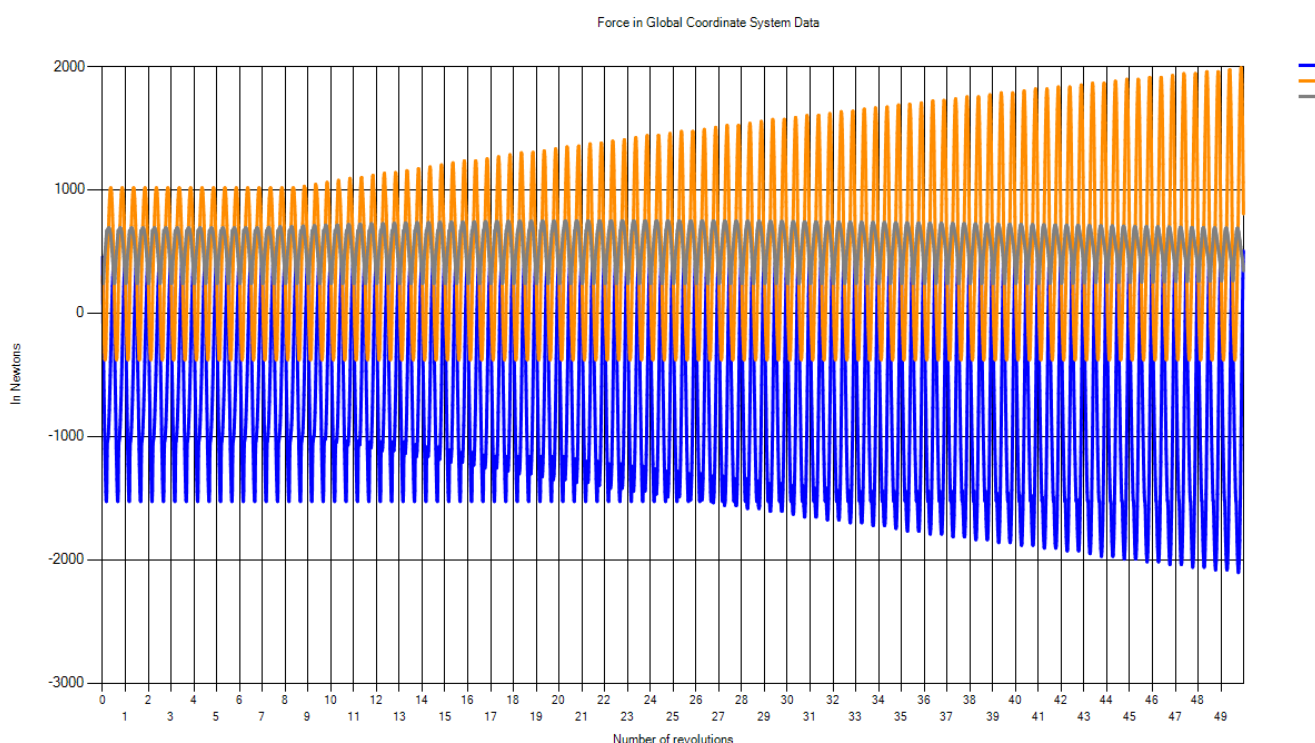


Figure 96: Forces in GCS for case 13

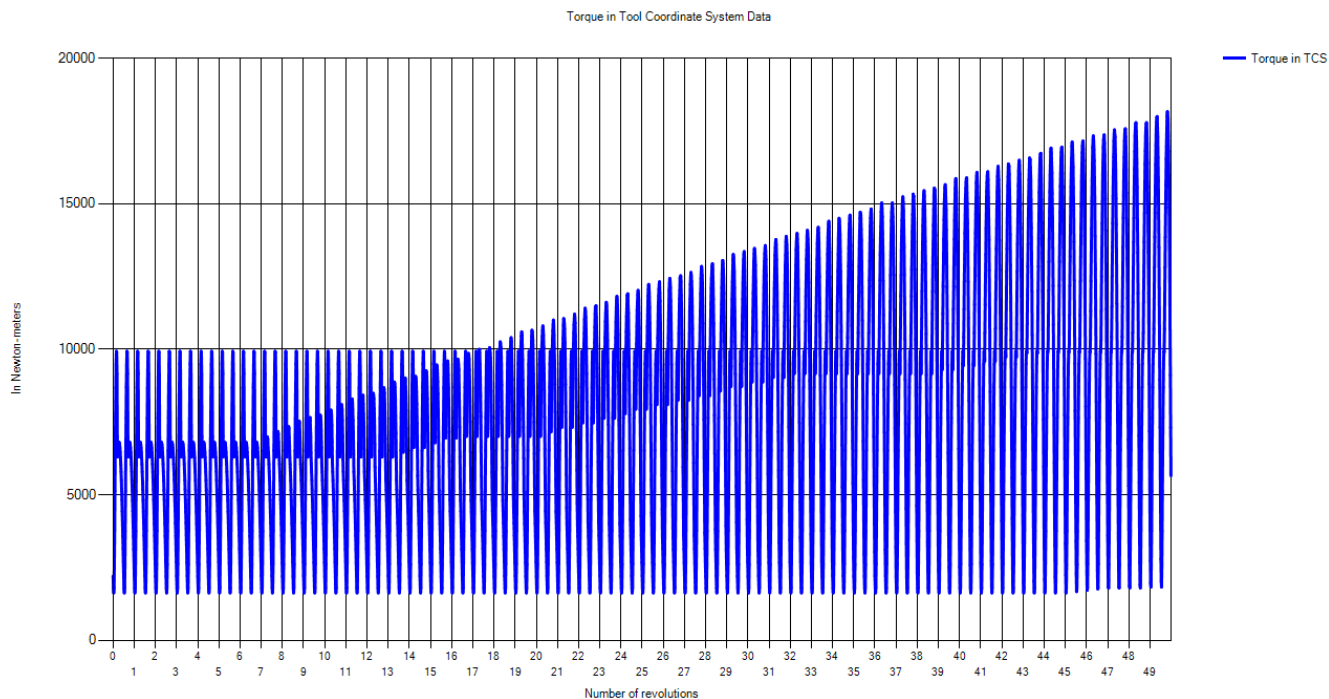


Figure 97: Torque in TCS for case 13

4.3.14 Case 14: Surface → Custom Surface

Input parameters: *Depth of cut = 5 mm; Table feed = 100 mm/sec; D = 20 mm; h = 20 mm, X_{surface} = 5 mm, Y_{surface} = -5 mm; simulation is done for 1 revolution of tool*

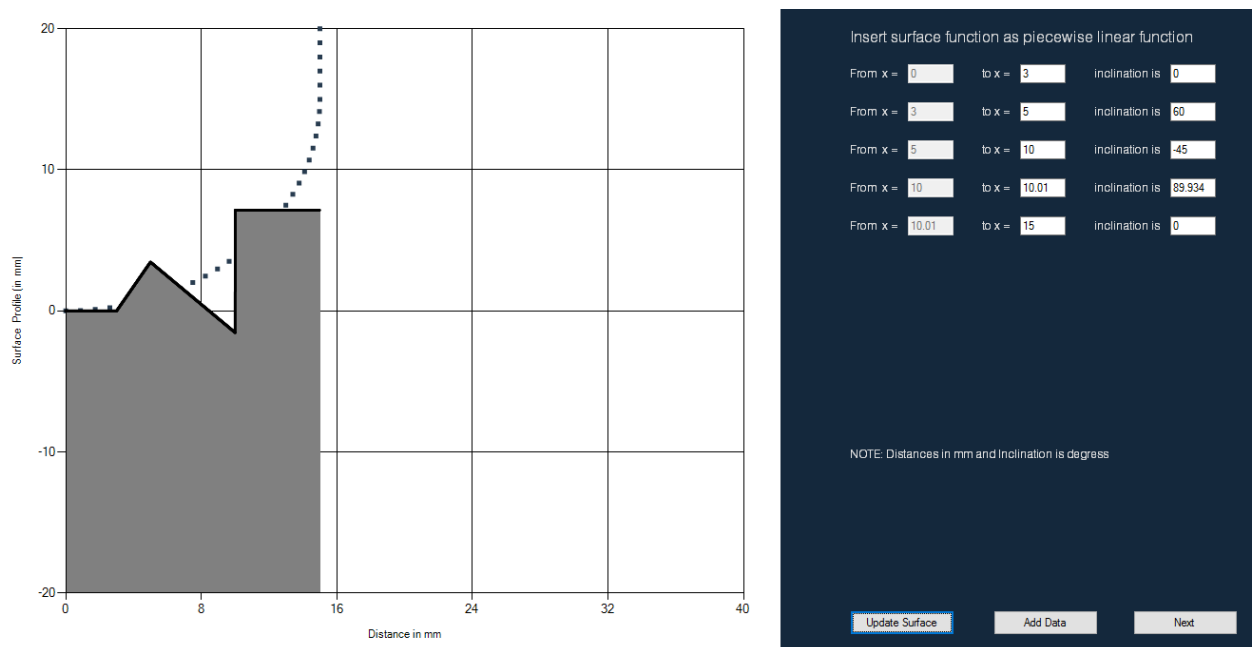


Figure 98: Custom surface as a function of piecewise linear functions

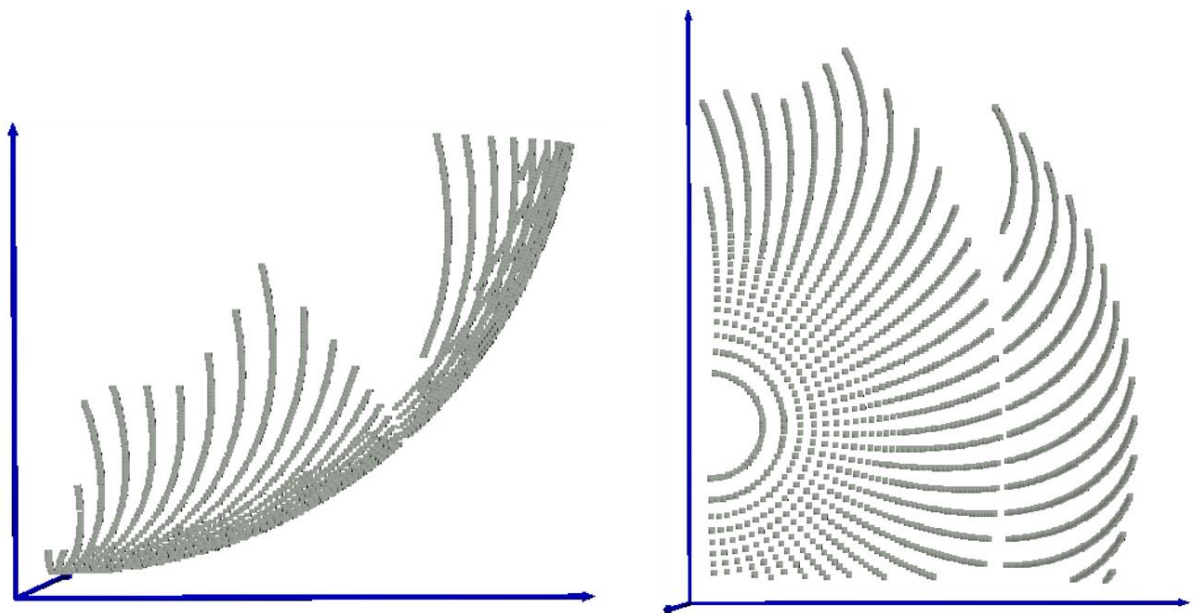


Figure 99; Engagement region for case 14 (a) front view (b) top view

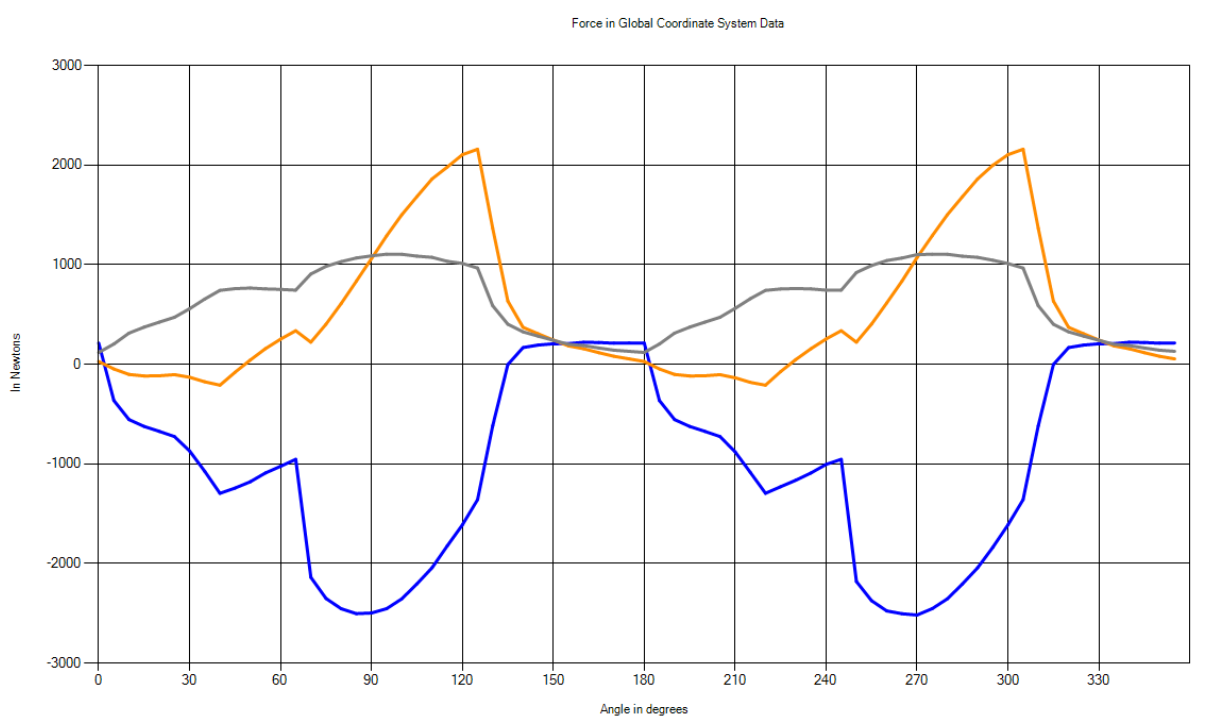


Figure 100: Forces in GCS for case 14

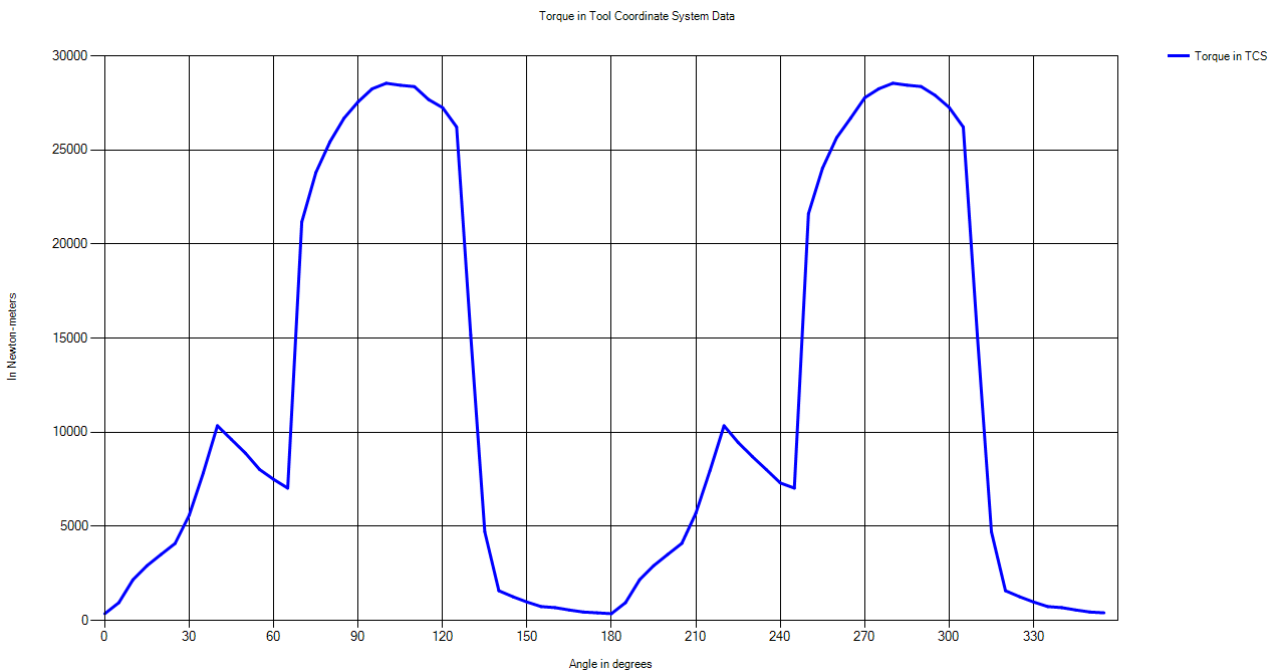


Figure 101: Torque in TCS for case 14

4.3.15 Case 15: Following Cut, Step Over =10, *lead* = 0, *tilt* = 0

Input parameters: *Depth of cut* = 10 mm; *Table feed* = 100 mm/sec; *D* = 20 mm; *h* = 20 mm, *planar surface*; *ball end milling tool*; simulation is done for 1 revolution of tool

Output parameter: *Surface roughness* 1.3397 mm

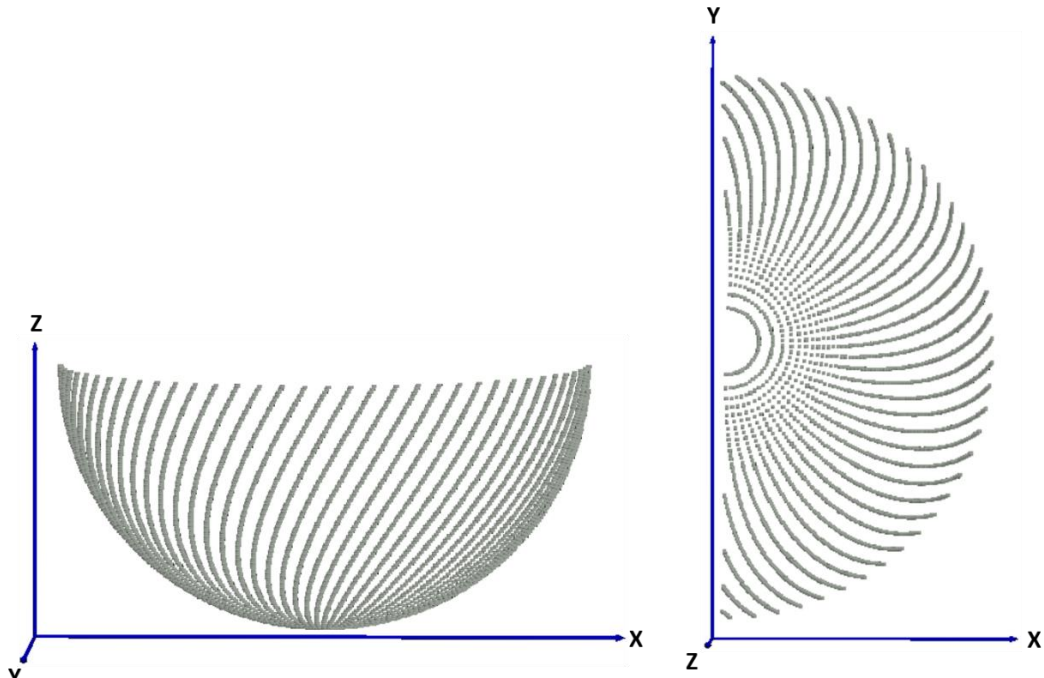


Figure 102: Engagement region for slotting

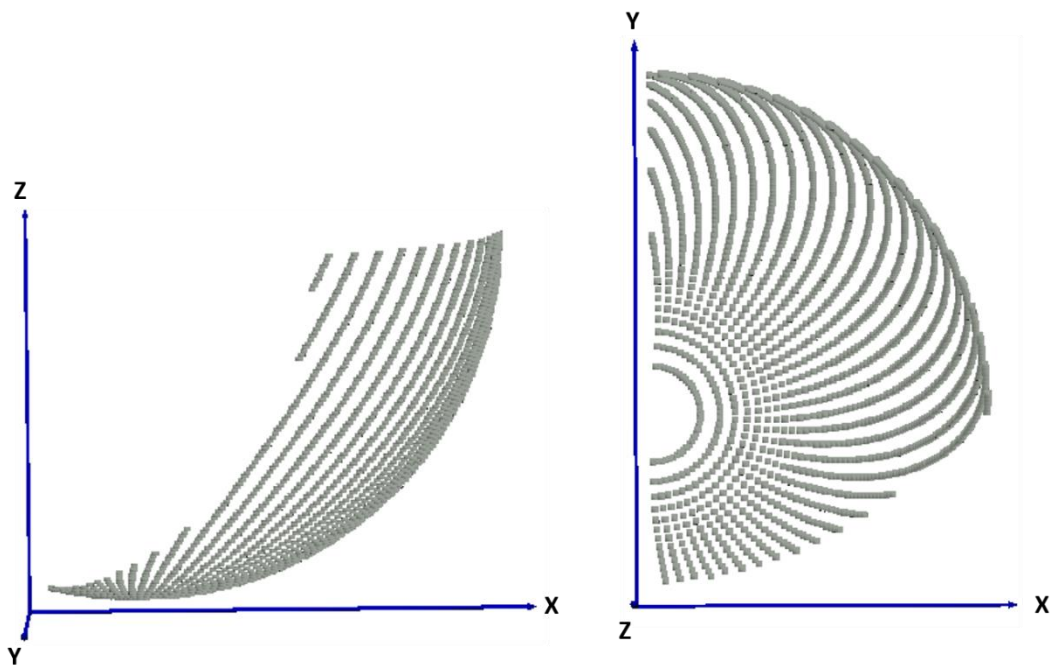


Figure 103: Engagement region for following cut for step over = 10 mm

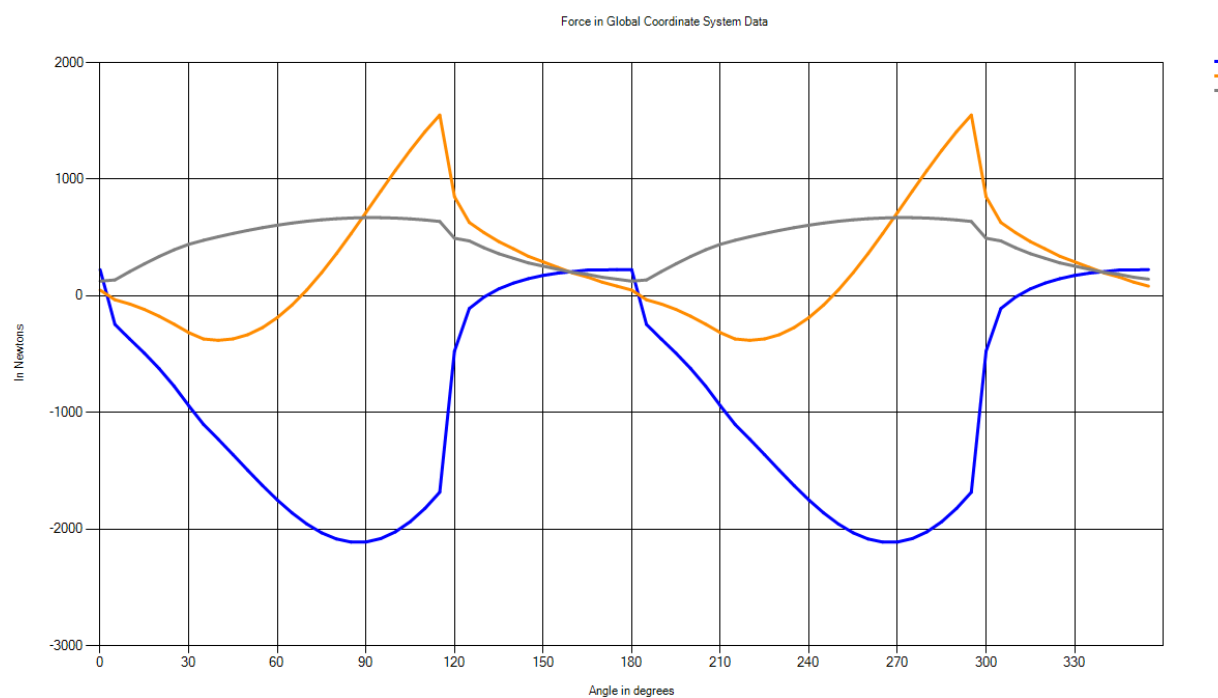


Figure 104 : Forces in GCS for case 15

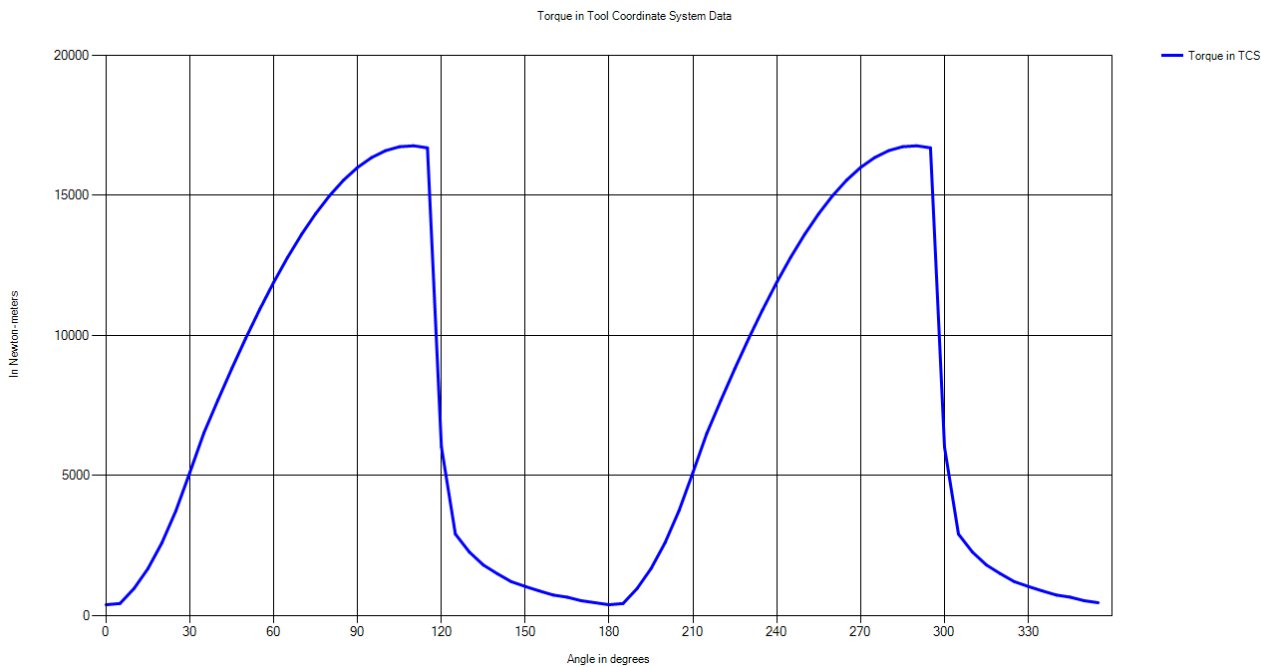


Figure 105: Torque in TCS for case 15

4.3.16 Case 16: Following Cut, Step Over =10, $lead = 0^0$, $tilt = 70^0$

Input parameters: *Depth of cut = 10 mm; Table feed = 100 mm/sec; D = 20 mm; h = 20 mm, planar surface; ball end milling tool; simulation is done for 1 revolution of tool*

Output parameter: *Surface roughness 1.2415 mm*

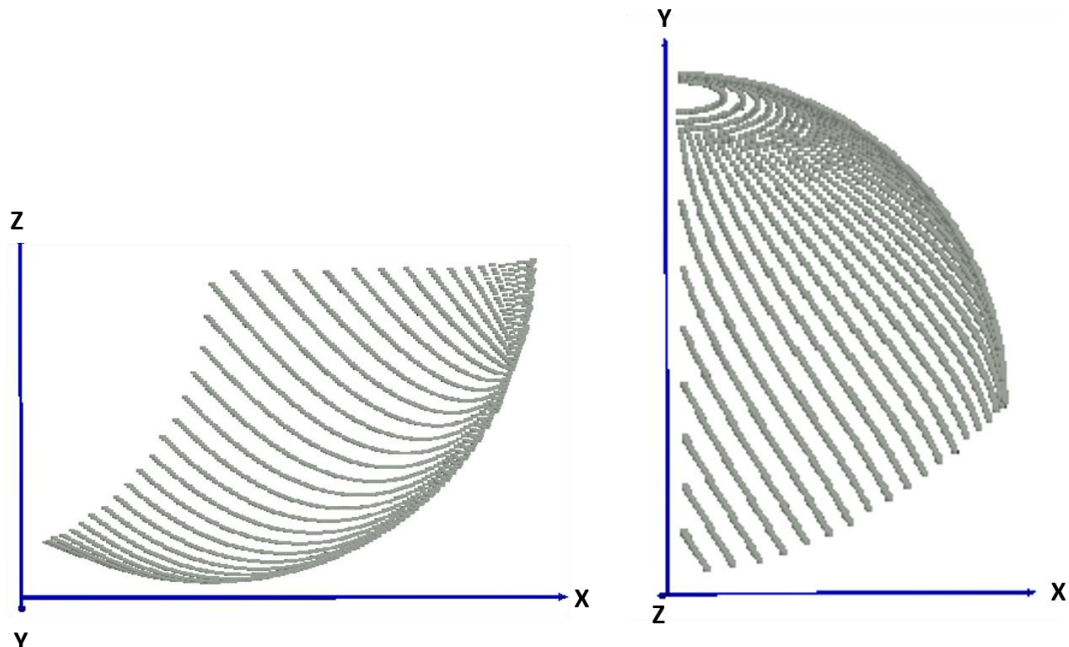


Figure 106: Engagement region for following cut with step over 10 mm and non-zero tilt

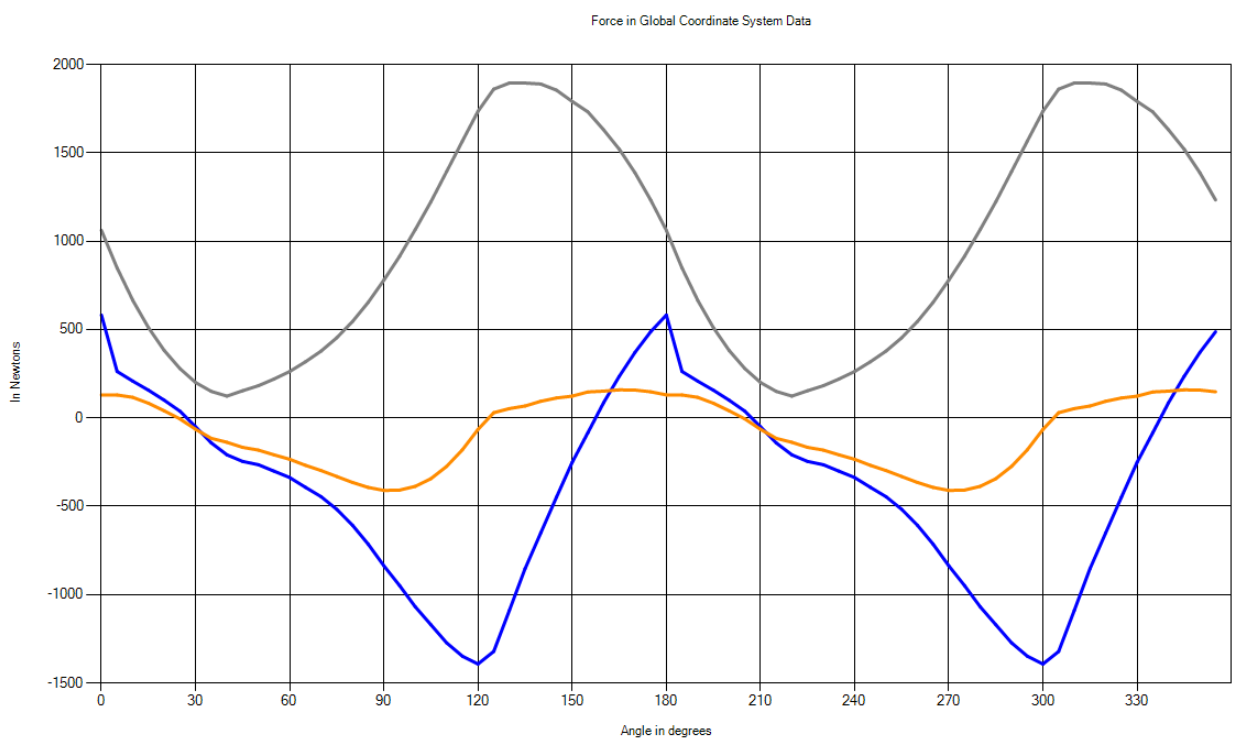


Figure 107: Forces in GCS for case 16

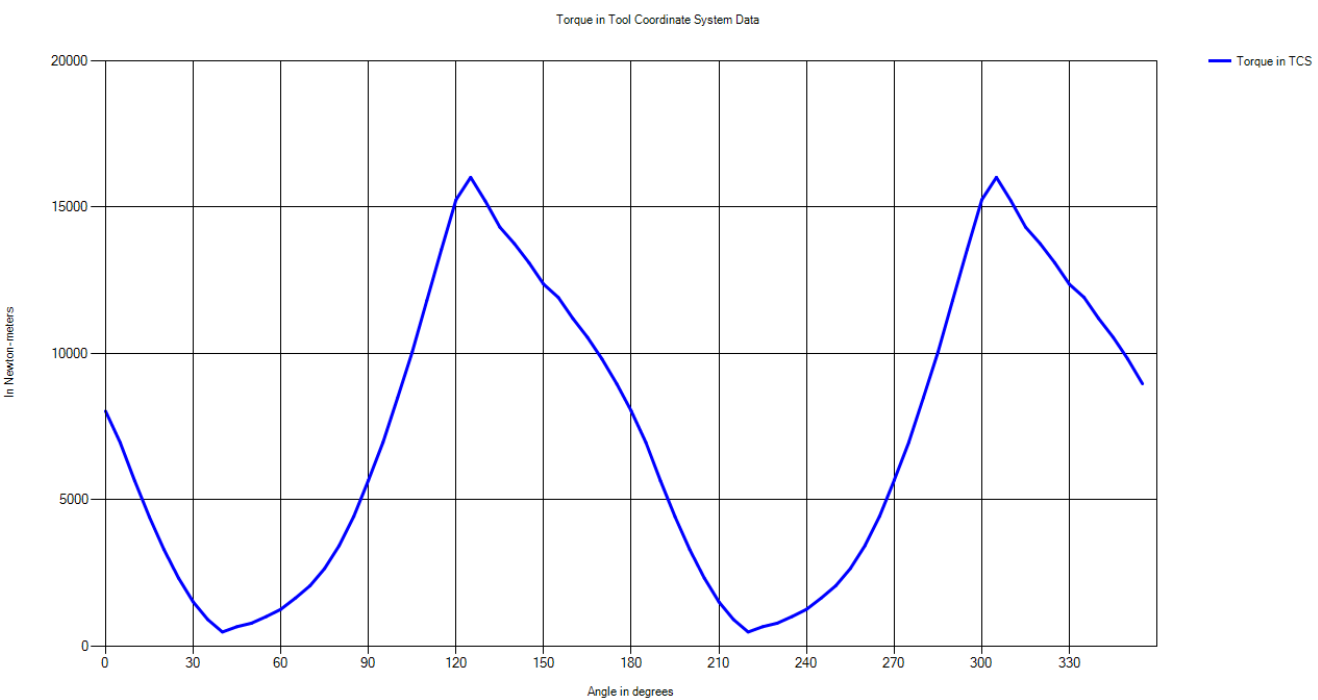


Figure 108: Torque in TCS for case 16

CHAPTER 5

CONCLUSIONS AND PLAN FOR FUTURE WORK

5.1 Shortcomings of the Current Model

The current model has multiple shortcomings and limitations as mentioned below

- i. Orthogonal Cutting Data is based on empirical results obtained after conducting experiments and then fitting a regression model, Hence the results obtained from OCD are not necessarily accurate.
- ii. The model has been developed only for Titanium alloy.
- iii. The model considers the tool is always ideal, rigid, edges are always sharp and does not wear while machining, whereas in real life tool wears out due the cyclic force. Since tool is not completely rigid and deflects under forces which creates vibrations in the tool. The depth of cut changes due to chatter in the machining process.
- iv. Chips are considered to be in most ideal form also known as undeformed chips. In reality, chips dimensions are different and chips interfere in cutting process.
- v. The axial discretization is based on taking constant values of axial increment which results in unequal chip widths. For example, in case of ball-end mill chip width is defined as:

$$db = \frac{dz}{\sin K}$$

For angles, which are close to zero degree, the chip width is very large and hence inaccurate.

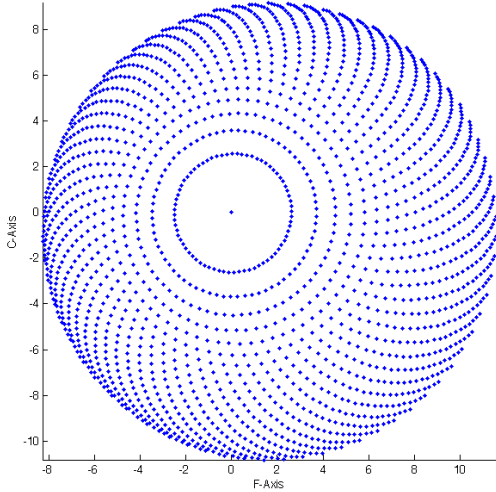


Figure 109: Discretization of cutting tool

5.2 Conclusions

As discussed earlier, the objective of this project was to analytically model the forces generated during the 5-axes milling process. The model is based on an empirical mechanistic approach in which basic orthogonal cutting parameters of the shear-zone are determined by using a regression curve fitting of numerous experimental results. The methodology follows a modular approach to model the forces in which the tool surface is discretized and forces are calculated considering each element undergoing orthogonal cutting. The results are benchmarked against data from published literature.

The variation of cutting forces in tool coordinate system and FCN coordinate system with angular position of the tool as well as the Torque required at any time has been determined. The lead and the tilt angles for the minimization of the cutting forces are predicted using the model. The previous model has been extended to incorporate general milling cutters and multiple non-planar surfaces. Aspects of surface finishing parameters have been added to the model to optimize the machining time as well as cost incurred by adjusting the values of tilt and step over.

The following conclusions were made from the simulated results:

- i) Simulations were performed for nine different tool geometries. Keeping all the machining parameters constant inverted cone end mill experiences the maximum amount of resultant force and torque. (refer section 4.3.1 to 4.3.8)

- ii) Force and torque simulations were performed for ball-end milling tool when it hits a step (refer section 4.3.12), the rate of change of forces in the starting zone is much compared to later zone i.e. more forces are required in just entering a step surface, once entered additional force requirement decreases.
- iii) Forces and torque required in the case when tool has horizontal as well as vertical feed of is much larger when the case when tool has only horizontal feed i.e. forces required in the case of plunging is much more than in case of slotting keeping the same machining parameters (refer section 4.2).
- iv) As the number of flutes increase the force and torque experienced by the tool are more evenly distributed while considering a revolution and the value of maximum force or torque experienced by the tool reduces keeping the same machining parameters (refer section 4.1.1 and section 4.1.2).
- v) In the case when tool has vertical feed and the engagement zone is increasing with time the normal forces and torque increases in a parabolic fashion. The normal force increases at a much rapid rate and reaches the maximum then the torque experienced by the tool (refer section 4.2.2).
- vi) Surface roughness is a function of radius of tool, step over and tilt angle. Better surface finish (less scallop height) can be achieved with altering the tilt angle i.e. machining time can be reduced for a particular surface roughness by changing the tilt angle.

5.3 Future Scope

Futures work can include making the model more generic, accurate and generate more empirical results. The current model can be extended to incorporate these aspects in future:

- i. Further aspects of surface finishing can be added. The tool tip cannot cut the material and should not be present in the cutting region. The current model can be extended to automate the selection of tilt angle and step over to optimize the machining time and surface roughness.

- ii. Using this model, the energy lost in cutting ($power = \omega \times torque$) and energy dissipated as heat can be known, the model can be extended to incorporate lubrication and cooling aspects.
- iii. CAM/CAD models can be integrated with the current model. Workpiece surface can be dynamically updated and the combination of the lead and tilt angles can be obtained at each point of time to optimize the entire process in terms of machining time, while maintaining the surface roughness within the tolerance limit.
- iv. Automation can be done in terms of path selection of the tool given the initial and final workpiece model cutting within the surface tolerance limit. The entire cutting process can be simulated visually to display the cutting region dynamically as the tool moves.
- v. Experimental validation of the data generated by the proposed model can be performed. The current model has been benchmarked against published literature data.
- vi. Orthogonal Cutting Data (OCD) for other materials can be developed based on experimental results.
- vii. The tool undergoes cyclic loading and can go fatigue failure. Tool wearing aspects can be added to the model, and both models can communicate back and forth/

CHAPTER 6

REFERENCES

- [1] E. Ozturk, T. Tunc and E. Budak, "INVESTIGATION OF LEAD AND TILT ANGLES EFFECT IN 5-AXIBALL-END MILLING PROCESSES," *International journal of machine tools and manufacture*, pp. 1053-1062, 2009.
- [2] Ozturk, E., and Erhan Budak. "Modeling of 5-axis milling processes." *Machining Science and Technology* 11.3 (2007): 287-311.
- [3] P. Budak and Y. Altintas, "Predicetion of Milling Force Coefficients From Orthogonal Cutting Data," *Department of Mechanical Engineering, The University of British Columbia, Canada*.
- [4] P. Lee and Y. Altintas, , "PREDICTION OF BALL END MILLING FORCES FROM ORTHOGONAL CUTTING DATA," *International journal of machine tools and manufacture*, pp. 1059-1072, 1996.
- [5] B. Li, H. Yujin, X. Wang and C. Li, "AN ANALYTICAL MODEL OF OBLIQUE CUTTING WITH APPLICATION TO END MILLING," *Machining Science and Technology, An International Journal*, pp. 453-484, 2011.
- [6] Y. ALTINTAS, "METAL CUTTING MECHANICS, MACHINE TOOL VIBRATIONS, AND CNC DESIGN," in *MANUFACTURING AUTOMATION Second edition*, p. Chapter 2.
- [7] Budak, Erhan. *Mechanics and dynamics of milling thin walled structures*. Diss. University of British Columbia, 1994.
- [8] D. K. Pawar and T. S. Khot, "TRACTION MODEL DEVELOPMENT FOR MULTI_AXIS BALL END MILLING PROCESSES," 2015.
- [9] B. Li, X. Wang and a. et, "ANALYTICAL PREDICTION OF CUTTING FORCES IN ORTHOGONAL CUTTING USING UNEQUAL DIVISION SHEAR-ZONE MODEL," *International Journal of Advanced Manufacturing Technology*, pp. 431-443, 2011.
- [10] E. Ozturk and E. Budak, "MODELLING OF 5 AXIS MILLING PROCESSES, MACHINING SCIENCE AND TECHNOLOGY," pp. 287-311, 2007.
- [11] Y. Altintas, "Manufacturing Automation: Metal Cutting Mechanics, Machine Tool Vibrations, and CNC Design," *Cambridge University Press*, Second edition 2012.

[12] Engin, S., and Y. Altintas. "Mechanics and dynamics of general milling cutters.: Part I: helical end mills." *International Journal of Machine Tools and Manufacture* 41.15 (2001): 2195-2212.

[13] Engin, S., and Y. Altintas. "Mechanics and dynamics of general milling cutters.: Part II: inserted cutters." *International Journal of Machine Tools and Manufacture* 41.15 (2001): 2213-2231.